ATR

AUSTRALIAN TELECOMMUNICATION RESEARCH

Volume 12, Number 2, 1978

ATR is published twice a year (in May and November) by the Telecommunication Society of Australia. In addition special issues may be published.
ATR publishes papers relating to research into telecommunications in Australia.

CONTRIBUTIONS: The editors will be pleased to consider papers for publication. Contributions should be addressed to the Secretary, ATR, c/- Telecom Australia Research Laboratories, 22 Winterton Rd., Clayton, Vic., 3168.

RESPONSIBILITY: The Society and the Board of Editors are not responsible for statements made or opinions expressed by authors of articles in this journal.

SUBSCRIPTIONS: Subscriptions for ATR may be placed with the General Secretary, Telecommunication Society of Australia, Box 4050, G.P.O., Melbourne, Victoria, Australia, 3001. The subscription rates are detailed below. All rates are post free. Remittances should be made payable to the Telecommunications Society of Australia, in Australian currency and should yield the full amount free of any bank charges.

The Telecommunication Society of Australia publishes the following:

1. **The Telecommunication Journal of Australia** (3 issues per year)

Subscription — Free to Members of the Society* resident in Australia
Non-members in Australia $6
Non-members or Members Overseas $9

2. **ATR** (2 issues per year)

Subscription — To Members of the Society* resident in Australia $4
Non-members in Australia $9
Non-members or Members Overseas $12
Single Copies — To Members of the Society resident in Australia $3
Non-members within Australia $6
Non-members or Members Overseas $7

* Membership of the Society $3

All overseas copies are sent post-free by surface mail.

Enquiries and Subscriptions for all publications may be addressed to:
The General Secretary, Telecommunication Society of Australia, Box 4050, G.P.O. Melbourne, Victoria, Australia, 3001.

ATR

AUSTRALIAN TELECOMMUNICATION RESEARCH

ISSN 0001-2777

Volume 12, Number 2, 1978

Contents

Challenge . . .

The future of the electronics and telecommunications industries in Australia has been the subject of considerable debate and anxiety in recent times. There is very little R. and D. currently being conducted in the electronics industry, which is now little better than a group of assemblers of components and sub-assemblies which have been designed, developed and manufactured overseas. The telecommunications industry is heavily dependent on orders from Telecom Australia, the Defence Department and the Department of Transport.

The future of these industries was discussed by The Institution of Engineers, Australia in March this year; it is interesting to note that The Institution has now published the proceedings of that conference, including some guidelines for government and industry aimed at promoting a recovery (National Conference Publication 78/1). One of these guidelines is that:

> "The local electronics industry should be supported by an onshore LSI (large scale integration) silicon technology rather than by developing a local discrete components industry."

This guideline is interesting in its scope; it comes from a national body, with national interests and national security at heart. However, the great majority of the Australian electronics and telecommunications industries are owned by overseas interests; naturally, the overseas owned companies will have a major interest in their own corporate developments, which are mainly oriented to their major markets, with design and support facilities relatively close to those major markets on the other side of the world. How will these companies react to the suggestion that they should utilise a local facility, which would not have the thru-put of those overseas facilities servicing the large international groups, and which will therefore almost certainly be less efficient and more costly.

It is predictable that the only way such a scheme could work would be for a completely Australian owned Company to control the facility, with government policies to ensure that that facility is used. Australian owned companies are not large enough to fully establish and operate such a facility without government support. However, the government has already gone a long way towards providing a semiconductor facility in an Australian owned company through the Defence Department, but there is still a long way to go. How will the government react to the provision of more funds, at a time when it is trying to cut down expenditure? It should be realised that such expenditure is highly beneficial towards the economy due to the multiplier effect; provision of the facility will create jobs and stimulate cash circulation. Will other groups like Telecom Australia and the Department of Transport, who obviously have considerable market clout, also support such a policy and facility by ensuring that their suppliers must use such a facility?

A further guideline that The Institution has laid down is that:

> "A firm statement from Government regarding future policies concerning the electronics and telecommunications industries should be issued. This should be independent of party policies and should desirably have a time horizon of fifteen years."

Such a challenge is timely, particularly in regard to such a significant underpinning of the local electronics and telecommunications industries, it will also afford an opportunity for some cooperative interparty statesmanship rather than interparty political points scoring, which is all too frequent these days. Such an exercise would be a novel and welcome innovation in Australian party politics.

Can our Leaders meet the challenges handed down by The Institution of Engineers Australia?

Diagnosis of Telephone Exchange Equipment Faults by Collation of Abnormalities in Real Traffic

A. WILLIS
BPO Research Centre
England

Many events that could be symtomatic of equipment faults are detected during the operation of the control programs in SPC exchanges. Often these are not used in the diagnosis of faults because they cannot, on their own, specify which item used by the call was faulty, and because their numbers make manual analysis laborious.

This paper describes a system for automatically analysing these events to detect faulty equipment and shows how detection and diagnosis of shared equipment faults can be improved by monitoring calls in the exchange more closely. Effects of the approach are wide-ranging, impinging on the partitioning of equipment, the way it is described in control system records, the degree of supervision applied by the control programs and the distribution of processing between the exchange and a maintenance centre. The system could obviate the use of special test equipment for routine diagnosis of shared equipment faults.

The work described was carried out at the Telecom Australia Research Laboratories between January and May 1977 as part of an engineer exchange scheme with the British Post Office Research Centre.

1. INTRODUCTION

The advent of stored program control (SPC) offers the prospect of better quality communications not just because of the high reliability of the electronic components used in SPC exchanges but also thanks to the power of SPC to quickly diagnose and avoid equipment faults. Hitherto automatic fault diagnosis has required large amounts of processor store to hold fault dictionaries and the like, or complex test equipment. This paper describes the basis of an automatic fault diagnosis technique which promises to be more economic in application. The technique is already in use on the Pathfinder experimental SPC exchange (Ref.1) at the British Post Office Research Centre, and has been applied experimentally to the Integrated Switching and Transmission (IST) exchange (Ref.4) of Telecom Australia Research Laboratories.

In a telephone exchange a large part of the equipment is shared between subscribers in the form of switch crosspoints, digit receivers, tone senders and receivers, etc. When one of these items develops a fault it affects only a proportion of calls handled by the system, because no one item of this type of equipment is used by every call. Consequently it is not essential to rectify the situation as rapidly as in the case of equipment which is common to all calls, but it is desirable that the system detects and avoids the faulty equipment, and that a procedure exists for its eventual repair.

Modern exchange systems aim to perform detection and diagnosis automatically, to the extent of identifying a faulty unit and perhaps removing it from service. Automation of this process reduces the maintenance work load and facilitates the centralization of the maintenance task so that skilled personnel may be shared over many exchanges. The technique to be described is designed to diagnose faults in shared equipment and is well suited to a centralized maintenance environment.

2. DETECTION AND DIAGNOSIS OF SHARED EQUIPMENT FAULTS

The type of exchange equipment being considered presents to the outside world two interfaces; one to the control system over which it sends data and receives instructions, and another to the subscriber who uses the telephone exchange. Most fault detection schemes check for correct operation at these interfaces.

The interface to the control system is generally monitored using a standard error protection scheme, requiring acknowledgement or checking of data passed, the failure of which can be taken as an unambiguous indication of faulty equipment. However, success at this interface by no means guarantees the unit is operating properly, so it is necessary to monitor the second interface, the one to the subscriber. This is more difficult since it requires access to signals which are normally monitored by the control system only through the equipment under test. Two techniques have been used to check correct operation here. The first is the provision of special test equipment, perhaps con-

trolled by the exchange control system, in the form of routiners for particular equipment types or test call generators testing the exchange as a whole. The second technique is to allot maximum times to certain transactions with the subscriber. These time-outs ensure that equipment isn't held needlessly when a subscriber behaves 'irresponsibly' by, for example, lifting his handset but not dialling, and have the effect of forcibly terminating the call if the time-out expires. Although primarily a protection mechanism, applications have shown that increased incidence of such time-outs can be indicative of equipment faults (Ref.2). Other systems (Ref.3) have monitored average hold time or use rate and have associated distortion of these figures with faults in the equipment.

The success of systems such as those just described suggests that information may be gained about the success or failure of a call, and hence about the correct operation of exchange equipment, by monitoring users' reactions. When a call encounters faulty exchange equipment, some deviation from the normal pattern of events is inevitable. For example; if the caller does not receive dial tone he will usually clear without signalling; if there is no transmission when the called party answers he will abandon the call, so a high incidence of clear before signalling, or short holding time calls associated with a particular equipment unit could indicate that it is faulty. This sort of 'abnormal behaviour' is in fact an implied complaint on the part of the subscriber (it is asking too much to expect him to complain every time a call attempt fails) but it would normally go unnoticed by the system. However the application of SPC gives the control system the power to closely supervise the progress of calls, to detect instances of abnormal behaviour, and to relate these to the equipment involved. It should be possible, therefore, by treating these instances of abnormal behaviour in a similar manner to fault reports from a test call generator, to detect and diagnose equipment faults.

It is a characteristic of this indirect type of fault report, and of the indications given by routining and test call generation, that they cannot be specific about which item of equipment used by the call was faulty. For example, failure to receive dial tone could be due to a faulty dial tone sender, or a fault in any of the crosspoints used to connect the sender, or the customer's line or telephone. All units associated with the call must be suspected even though only one is faulty. Furthermore, abnormal behaviour during a call does not guarantee that an equipment fault exists at all. However, enough information would exist to allow identification of a faulty unit, since false reports, occasioned by either legitimate abnormal behaviour or association of working units with the faulty one, will be shared over correctly working units. Only the faulty unit will occur systematically in fault reports.

A collation technique has been devised, to automatically extract the significant data from such fault reports which have a high level of redundant information. It parallels the actions of the maintenance engineer when analysing the reports by looking for items of equipment that appear more often than pure chance would dictate. It is applicable to ordinary system fault reports and particularly to a centralized maintenance system where it would greatly reduce the redundant information presented to staff for manual analysis. However, it is crucial to the use of abnormal behaviour type fault reports that this analysis be automated, since the quantity of data involved would defy a manual approach.

To summarize, collation is a technique for extracting the significance from fault reports containing redundant information. The increased analysis capacity arising from automated collation, coupled with the ability of SPC systems to closely monitor subscribers' reactions, makes it possible to suspect all equipment associated with a call that deviates from the normal, and identify as faulty the particular item of equipment associated repeatedly with such calls.

The complex test equipment normally used to detect exchange equipment faults is expensive and limited in the variety of tests and conditions it can apply. The technique described does not require this additional hardware, and uses every call switched as a test. It takes advantage of the wide variety of conditions applied to the system by live users, and so could be more thorough than the ad hoc provision of special test equipment.

3. SIMPLE COLLATION

3.1 The Technique

Collation is basically integration, for each item of equipment, of the fault reports minus the successful uses. Practically, a 'leaky bucket' count is kept for each item and is incremented when the item is implicated by a fault report and decremented when it is used successfully. If the bucket 'overflows', by reaching some predetermined maximum, the equipment can be considered faulty because the ratio of successful to unsuccessful uses dropped below the acceptable level for a significant time.

The technique is well suited to the treatment of 'uncertain' faults, where there are false fault reports because the event considered to be symptomatic of a fault can also be produced by legitimate subscriber action (eg. short holding time calls), or because the system cannot tell which particular unit is responsible for a call's failure and so reports all units used. These false reports implicate correctly functioning units in a random fashion so that if their average rate of occurrence can be predicted the collation count parameters may be fixed such that they will not cause overflow. True fault reports will repeatedly implicate the same unit, and eventually cause its count to overflow.

3.2 Count Parameters

The collation count simulates a random walk with reflecting barriers at 0 and M, the overflow level (Ref.5). The counter is incremented by an amount, a, when its associated equipment is implicated in a fault report, and decremented by one when used successfully. If the counter reaches the value M an alarm is raised and the counter reset to a starting value, i, in this case 1. The counter is also reset to i whenever it reaches 0.

False fault reports represent a source of continuous 'background noise' in the face of

which the average level of the counter must not rise. If p is the probability of a fault report, then the average change in the counter value for each report is:-

$$\mu = pa - (1-p)$$

Consequently the average counter level will not rise providing:-

$$a \leq \frac{1 - p}{p}$$

When no fault exists then the probability, p, is the probability of a false fault report and this relationship gives a guide to a suitable value for the increment amount, 'a'.

When a fault exists the fault report probability increases by Δp so that:-

$$p + \Delta p > \frac{1}{a + 1}$$

and the counter level rises, on average, to eventually reach M and raise an alarm.

One important characteristic of the system is the mean time taken to detect a fault, which, in the language of the counter, is the mean number of steps in a run that starts when it is reset to i and ends when it reaches the maximum, M. After the first step of the run the count will have a probability p of being at i+a (because there was a fault report) and a probability q (q = 1-p) of being at i-1 (because there was a successful use report). If $1 < i < (M-a)$ the run continues. If i = 1 there is a probability q that the run will reach 0 and hence end at this step, and a probability p that the run will continue from 1+a. If $M - a \leq i < M$ there is a probability p that the run will reach M and hence end at this step, and a probability q that it will continue from i-1. If V_i is the probability that the run ends with the counter at M when the starting value was i, and M_i is the mean number of steps in a run when the starting value is i, then:-

$$V_1 = pV_{a+1}$$

$$V_i = qV_{i-1} + pV_{i+a} \qquad 1 < i < M - a$$

$$V_i = qV_{i-1} + p \qquad M - a \leq i < M$$

$$M_1 = 1 + pM_{a+1}$$

$$M_i = 1 + qM_{i-1} + pM_{i+a} \qquad 1 < i < M - a$$

$$M_i = 1 + qM_{i-1} \qquad M - a \leq i < M$$

By specifying the boundary conditions for V_i and M_i:

$$V_i = 0 \quad \text{for } i \leq 0$$

$$V_i = 1 \quad \text{for } M \leq i$$

$$M_i = 0 \quad \text{for } i \leq 0$$

$$M_i = 0 \quad \text{for } M \leq i$$

the equations may be simplified to:

$$V_i = qV_{i-1} + pV_{i+a} \qquad 0 < i < M$$

$$M_i = 1 + qM_{i-1} + pM_{i+a} \qquad 0 < i < M$$

In each case we have M-1 equations in M-1 unknowns, so the equations may be solved for V_i and M_i.

Now the mean interval between resetting the counter, M_i, includes cases of the counter reaching 0 as well as M, so the mean interval between alarms is therefore

$$T_i = \frac{M_i}{V_i}$$

For large values of M the solution is time consuming so a numerical approximation method has been developed which yields results of the form shown in Fig.1. This example depicts the relationship between the probability of a fault report, p, and the mean, or expected, number of uses of a unit between count overflows, T, for a count with maximum, M, of 100 and increment, a, of 3.

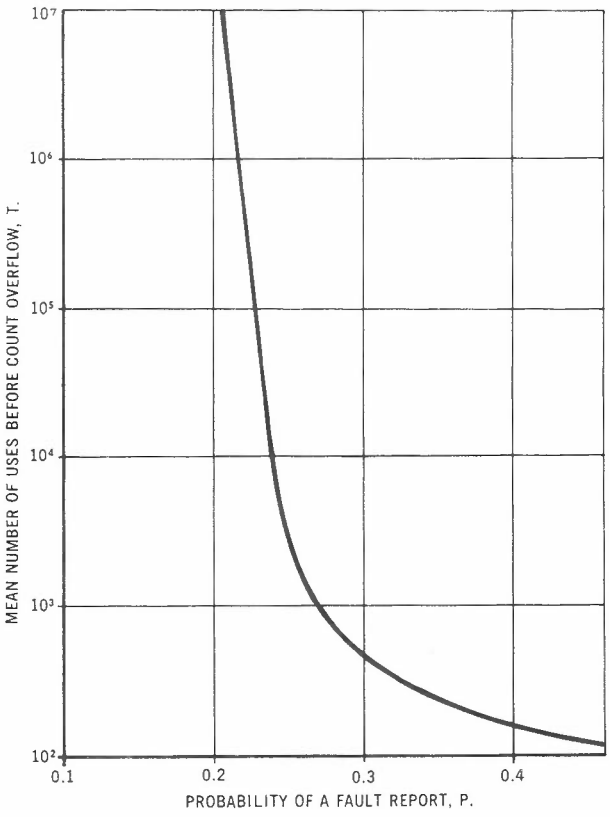

Fig.1 - Graph of the relationship between the mean number of uses between alarms, T, and the fault report probability, p, for a collation count with increment, a, = 3 and maximum, M, = 100.

3.3 Discussion

The example of Fig.1 shows that it is not satisfactory simply to choose a value for the increment amount, a, that would result in no rise of average counter level when no fault exists, because the random nature of false fault reports creates an unacceptably low mean time between count overflows. Inspection of Fig.1 suggests that a count with these parameters would perform satisfactorily in the face of a false report probability of about 0.2. In this case the mean number of uses between false alarms would be of the order of a million which, even in the case of short holding time equipment such as multi-frequency signalling receivers, represents a mean time between false alarms of about a year.

Figure 1 also emphasizes the sensitivity of the collation system since, with these parameters, a doubling of the fault report probability from the no-fault level of 0.2 results in a reduction of the mean time to overflow by almost 5 orders of magnitude. If the equipment concerned developed a fault that increased the fault report probability to 0.4, then it would be detected within an average of 150 uses of the equipment. This relationship between time to detect and fault report probability ensures that the greater the degredation of service caused by a fault, the faster it is detected.

A family of curves can be drawn covering a range of values of increment, a, which would be shifted along the x-axis but have similar shape, provided the maximum to increment ratio (M/a) was held constant. Increasing the count maximum increases the mean time between false alarms at the expense of slower response to genuine faults.

4. EXCHANGE AND CONTROL SYSTEM DESIGN IMPLICATIONS

4.1 Repair Philosophy

A successful fault diagnosis technique must be linked to the repair philosophy of the system. The unit replacement approach is commonly adopted in telecommunications systems, whereby a faulty unit is replaced by a spare and repaired elsewhere. Consequently the resolution of the diagnostic system at the exchange must extend to the replaceable unit level, so a collation count is associated with each replaceable unit.

However, the choice of replaceable unit boundaries cannot be taken in isolation. The collation technique can only resolve between units that are alloted independently to a call, because only in this way can it be assured that the count for a faulty unit will rise faster than those of the units with which it interworks. Therefore replaceable units must coincide with units that are capable of separate control and use on calls.

Such a limitation is a reasonable one since there is nothing to be gained, as far as continued operation of the exchange is concerned, from diagnosing a fault to a particular card in a digit receiver, for example, when the entire unit is rendered inoperative by the fault anyway.

4.2 Hidden Equipment

Some equipment units are never allotted explicitly by the control programs and so their identities do not appear in the records analysed by collation. For example, power supply units and waveform generators which are often separate entities serving several equipment units. Failure of a common unit will appear as failure of all the units it serves. To avoid this confusion collation counts should be kept separately for these hidden units, and fault reports for the dependent unit treated as implied fault reports for the hidden unit. If the count maximum for the hidden unit is fixed slightly lower than for its dependants, collation will detect the faulty hidden unit first.

To operate such a scheme some representation of the dependency of one unit on another is required by the diagnostic process.

4.3 Non Random Events

Collation can handle false fault reports because they should implicate equipment on a random basis. There are certain situations where this may not be true. If two units are always used together, collation will be unable to identify a fault in one of them. This can occur if units are selected sequentially and there are the same number of two different types of unit, which are always allotted to a call at the same stage. Dial pulse receiver and dial tone sender, if they were realised as separate units, could be an example of such a pair. Fortunately, it is unlikely that a real system would satisfy all these conditions. Truly random selection of equipment would be a complete solution.

At the terminals of the exchange, where equipment is shared less, we enter an area less amenable to the collation approach. Particular differences become dominant, so that, for example, collation might report as faulty the telephone of a subscriber who frequently makes short holding time calls for quite legitimate reasons. As individual differences become relevant in this way, collation can only work if its parameters are fixed on a more individual basis.

The problem of non random selection can also arise between groups of equipment units if an item of equipment is common to one of the groups. For example, consider two groups of equipment units, A and B, each group consisting of several units that perform the same function, and any unit in group B being available for selection for use in conjunction with any unit in group A. Furthermore, suppose that group B units are only ever used with group A units as illustrated in Fig.2. Faults in any of the units are still detectable as long as units are selected randomly. Now, if either group of units has an item in common, such as the power supply to the A units in Fig.2, and that common unit fails, then the collation counts for A units and B units will overflow. In other words collation will give a completely false indication that B units have failed.

The problem could be overcome by setting the count maximum for the power supply lower than that for the units, as suggested when considering hidden equipment in Section 4.2. A more elegant solution would be to carefully control the de-

pendency of one device upon another at the design stage, so that no functional group of equipment units is completely dependent upon any single unit. Functions should be shared over common equipment as illustrated in Fig.3 for power supply units and signalling senders.

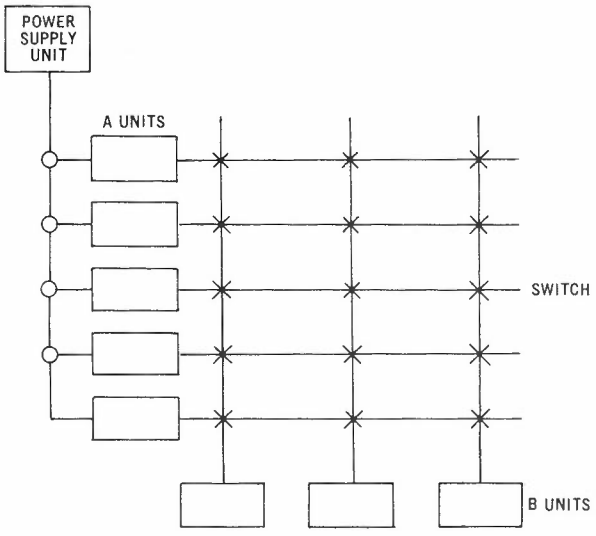

Fig.2 - Example of units dependent upon common equipment.

The correct arrangement shown in Fig.3 may seem obvious, but the same distribution should occur for all other interfaces between equipment units and their external environment; for connections to the control system and to subscribers' lines the dependencies on common equipment may not be so obvious.

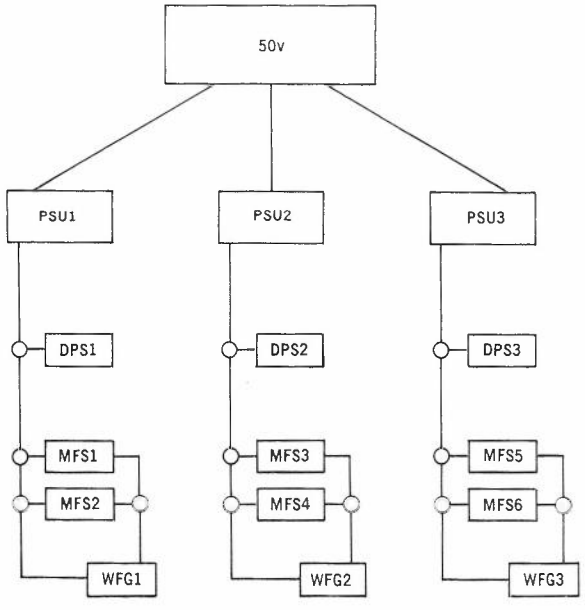

PSU = POWER SUPPLY UNIT
DPS = DIAL PULSE SENDER
MFS = MULTI FREQUENCY SENDER
WFG = WAVE FORM GENERATOR

Fig.3 - Correct grouping of equipment.

4.4 Information Flow

The reports of failed and successful calls that are required to pass between the call control programs and the diagnosis program represent a significant flow of data within the system. It has already been suggested that advantages may be gained by performing diagnostic processing at a maintenance centre remote from the exchange. Diagnostic reports would pass to the centre by data-link, and it can be shown that the data rate required is not excessive. Based on the report structure used for experiments on Telecom Australia's Integrated Switching and Transmission (IST) exchange, and assuming a report is generated for every call, a data rate of 740 bits/s is generated for 1000 Erlangs of traffic.

A reduction in this figure could be achieved by not reporting successful use of equipment, but decrementing collation counts at a rate proportional to traffic.

The extent to which the data can be shared by other processes might also be important. The information required at the maintenance centre may, with only a few additions, be the same as that required for equipment usage statistics and for charging customers, for example.

5. CONCLUSIONS

Experience with collation on Pathfinder exchange, and the experimental application to Telecom Australia's Integrated Switching and Transmission exchange, suggest that it is a viable means of diagnosing faults. Not only can it be used to automate the analysis of fault reports that were originally produced for manual treatment, but also, by means of the abnormal behaviour type of fault, the fault detection and diagnosis powers of the system may be greatly enhanced.

Little has been said about what might constitute abnormal behaviour other than the examples quoted of clear-before-signalling and short holding time. A good starting point might be to define the limits of normal behaviour. There is scope for both analysis and observation of calls to select those deviations from normal that might reasonably be monitored for.

The trend in maintenance schemes is towards a cost effective approach in which action is taken only for faults that affect service. Collation is well suited to this approach because detection of a fault is directly related to its effect on service. Furthermore, it offers diagnosis at low cost, because large fault-dictionaries are avoided and collation counts need only be stored when they rise to a value greater than one. Special test equipment is not required and artificial test traffic is unnecessary because every call switched through the exchange is used as a test.

6. ACKNOWLEDGEMENTS

Acknowledgement is made to the Director of Research of the British Post Office for permission to publish this paper, and to the Director and staff of the Telecom Australia Research Lab-

oratories for their assistance and use of their facilities. Also to D.J. Bond of the BPO Research Centre and R.G. Addie of the Telecom Australia Research Laboratories for their assistance with Section 3.

7. REFERENCES

1. Smith, C.S.A. and Park, I.D.C., "Pathfinder : An Experimental Telephone Exchange using Stored-Program Control", The Post Office Elect. Engrs. Journal, Vol.70, Part 2, (July 1977), pp.68-75.

2. Petterson, A.D., "Automatic Disturbance Recording Equipment for Crossbar Exchanges", Telecom Journal of Australia, Vol.17, No.1, (Feb. 1976).

3. Lewis, J.W., "ICUP Tracks 'Killer Trunks', Nips Traffic Troubles in the Bud", Telephone Eng. and Management, March 15, 1975.

4. Crew, G., "The IST Project", Telecom Australia Research Laboratories Report No.6931.

5. Feller, W., "An Introduction to Probability Theory and its Applications", Third Edition, Vol.1, Wiley.

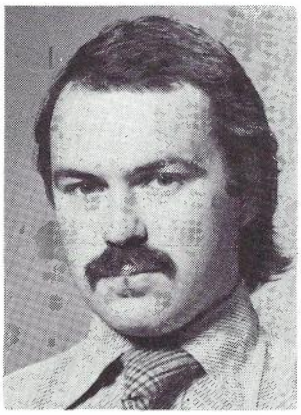

BIOGRAPHY

ALAN WILLIS joined the British Post Office as a technician in 1968. He obtained a BPO scholarship to study for a Degree in Computers and Communications Engineering at the University of Essex, England, and graduated in 1973 with First Class Honours. Since then he has worked at the BPO Research Centre on various projects concerning stored program control of telephone exchanges. His interest in diagnostic techniques led to a visit to the Research Laboratories of Telecom Australia in 1977. Mr. Willis is a Chartered Engineer and a Member of the Institution of Electrical Engineers.

Earth-Space Path Rain Attenuation at 11 and 14 GHz — Darwin, Australia

R.K. FLAVIN
Telecom Australia Research Laboratories

Rain attenuation measurements at 11 and 14 GHz, at a fixed elevation angle of 60°, have been made at Darwin through the 1977/78 "wet season". The results allow a fairly reliable estimate to be made of rain margin for earth stations located in Australian tropical areas. The availability of attenuation statistics measured simultaneously at 11 and 14 GHz permits a reasonably accurate extrapolation to other frequencies in the 10-15 GHz range. The Darwin results are compared with other 11 GHz radiometric measurements made at Innisfail, Queensland at fixed elevation angles of 30° and 45°.

1. INTRODUCTION

With the increased use of satellite communications systems there is a growing pressure to operate at higher frequencies because of saturation of the lower bands. In addition to accommodating greater traffic capacities the use of frequencies above 10 GHz minimize potential interference with existing terrestrial systems and thereby facilitate the siting of earth stations.

While signal attenuation by rain is not a problem at lower frequencies, above 10 GHz this effect becomes the dominant loss mechanism after free-space transmission loss. Any communication system which involves some form of free-space transmission must have a fading or attenuation margin built into the design which is directly related to the required system availability, or maximum time the system is inoperative. Proper earth station design in a satellite communication system requires at least a knowledge of the rain statistics in the area. If one has a measure of the associated microwave attenuation, not only will the fading or rain margin be determined for that area, but also a more comprehensive evaluation can be made of other sites where rain statistics provide the only available data.

The ideal method of determining rain attenuation statistics on an earth-space path is to monitor the direct transmissions of a satellite. In the absence of such a source one can resort to radiometric techniques whereby an antenna-receiver-recorder system is used to measure thermal noise radiation from the sun and/or the sky. Since the sky can be considered a lossy absorbing medium a knowledge of thermal radiation from that medium can be used to predict attenuation through the medium.

Since late 1972, the Telecom Australia Research Laboratories have been actively engaged in radiometric measurements of rain attenuation on earth-space paths in tropical climates. The results reported so far (Refs.1,2) have been associated with 11 GHz measurements at Innisfail, Queensland. A second radiometer system installed at Darwin (Latitude 12° 27' S, longitude 130° 50' E) has recently been providing reliable attenuation data at both 11 and 14 GHz. This data not only complements the Innisfail results but also allows one to gain insight into the frequency dependence of attenuation by rain on earth-space paths.

Originally, the Darwin radiometer was designed as a dual-beam dual-frequency system capable of operating in a sun-tracking mode (Ref.3). Because of the problems of converting variable-elevation sun-tracking data to attenuation statistics for fixed elevation earth-space paths, it was decided to operate the Darwin radiometer at a fixed elevation angle, continuously monitoring "sky noise temperature". Even though this mode of operation has limitations which will be discussed later, its use has gained wide acceptance as a convenient method of measurement.

It was an important consideration in picking a site for these studies that the attenuation statistics for the area represent a worse case condition for an Australian Satellite System. Now, it has been well established that rain attenuation is directly associated with rain intensity and not directly with rain accumulation. For these reasons radiometer studies in Australia have been carried out in tropical climates where the probability of high rain intensities is also high. The choice of sites is also based on the fact that rain attenuation data for earth-space paths in such regions is rather scarce.

2. GENERAL CONSIDERATIONS

2.1 Propagation Geometry

In establishing the fixed azimuth and elevation angle for the Darwin radiometer, practical use of the data was the predominant consideration. Since any Satellite System for Australia would probably involve an intermediate to large earth station located in Darwin, the data should be directly applicable to that

siting. Potential geostationary satellite orbit positions suggest a high viewing angle from Darwin.

The Innisfail, Queensland studies have used fixed elevation angles of 30° and 45° for 11 GHz rain attenuation measurements. It was decided to use a 60° elevation angle in Darwin in order to best complement the Innisfail results, while at the same time acquire realistic data for a Darwin earth station design.

As part of the measurement system a series of five tipping-bucket raingauges were installed throughout Darwin. These raingauges were kindly provided by the Bureau of Meteorology for these investigations. The approximate location of each raingauge is shown in Fig.1. Each location was picked for its security and accessibility and three of them (including one located at the radiometer site) were aligned along the propagation path. As shown in Fig.1 the propagation path azimuth is approximiately 30° with respect to true north.

2.2 Radiometer Limitations

In discussing the technique of radiometric measurements of rain attenuation there will be frequent reference to temperature. In all cases it should be understood that these are noise temperatures T as defined in the well known relationship for available noise power from a resistance or blackbody source - P = kTB, where k is Boltzmanns' constant and B is the bandwidth for measurement of power P. The units of noise temperature are absolute and are given in kelvin (K).

If the sky is considered a lossy absorbing medium the atmospheric attenuation is given by,

$$A(dB) = 10 \log \left[\frac{T_a}{T_a - T_s} \right] \qquad (1)$$

where T_s is a measured sky temperature, and T_a is an effective temperature of the absorbing

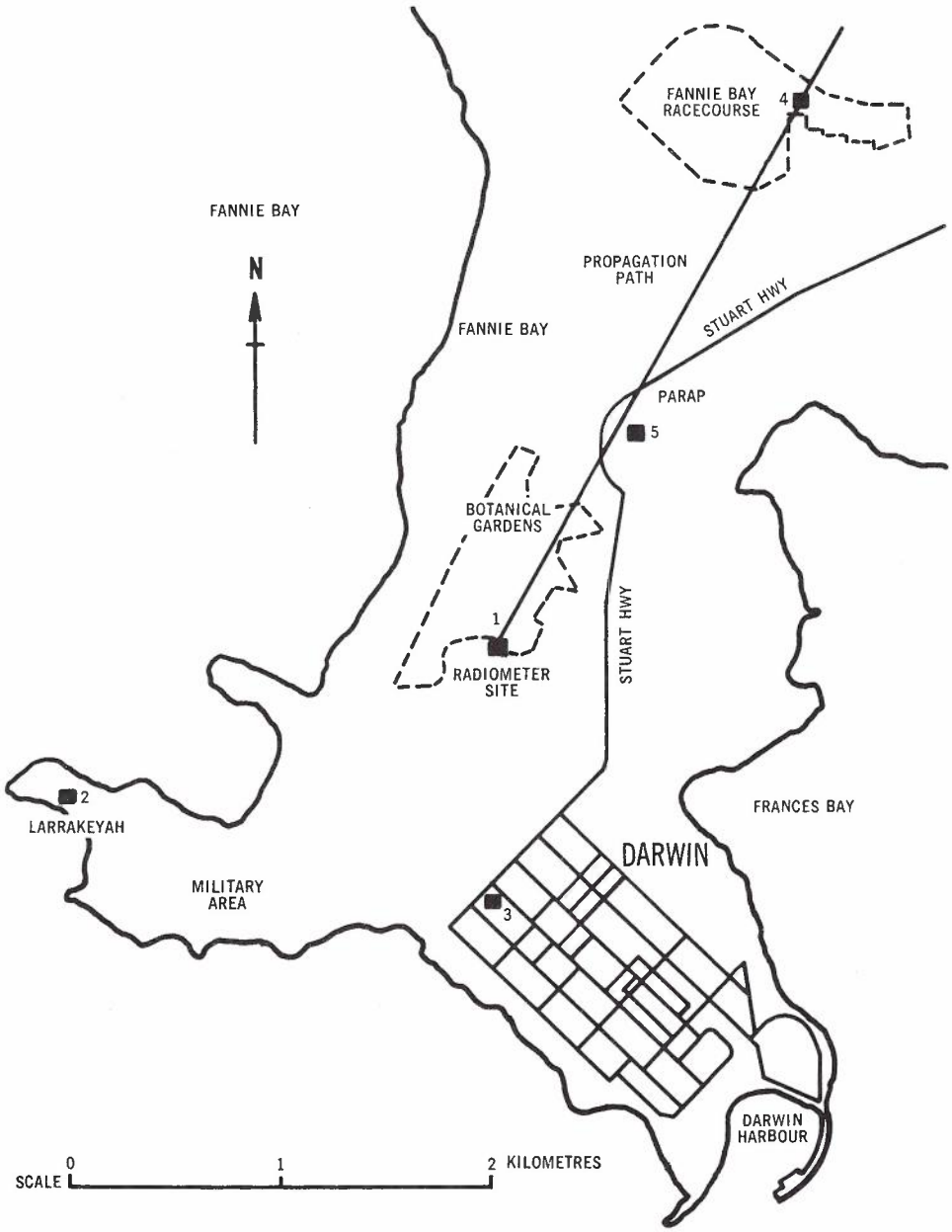

Fig.1 - Radiometer and raingauge location in Darwin.

medium corresponding to the sky temperature limit for which there is infinite attenuation. The T_a value is closely related to an average physical temperature over the path length for which the lossy medium is attenuating. In practice, it is very difficult to accurately determine the value of T_a in any particular case, because it depends on a number of various factors.

For a true attenuation level of 12 dB and an effective temperature T_a of 290K, there is approximately $\pm$ 10% error (in dB) in the estimated attenuation value for a T_a uncertainty of $\mp$ 5K, and the largest error is associated with a lower T_a value. In evaluating the radiometer data the assigned value of T_a can never be lower than that value which would predict infinite attenuation. In other words very high attenuation events, where the recorded sky noise temperature approaches the ground temperature, can be used to determine a lower limit for the T_a value. From 14 GHz radiometer data accumulated at Darwin so far, there are several events which placed that lower T_a value at 290K. This effective noise temperature of the sky as an infinitely attenuating medium is higher than that value used by most other investigators, but is not surprising if one considers the tropical climate of Darwin. Examination of records provided by the Bureau of Meteorology showed that the average height for a 290K temperature level in Darwin during January 1978 was two kilometers. An effected path length for rain attenuation can be defined as that distance which would predict the attenuation if there were uniform rain and drop size distribution over the path. Considering that the predicted effective path length for high rain rates and high elevation angles is approximately 2-3 km (Ref.4), the assumption of a minimum effective temperature T_a of 290K is most plausible for Darwin.

Another error which can be significant in radiometric measurements is the omission from the simple theory of the effects due to scattering. Consider, for example, the sky as a lossy medium which can scatter energy from an incoming signal out of the propagation path as well as absorb it. If the scattering coefficient is small compared to the absorption coefficient there is a negligible correction to the simple theory discussed so far. In any event, the attenuation predicted from radiometric measurements is always underestimated if scattering effects are omitted, and the error increases with increasing frequency (Ref.5). The magnitude of this error has been recently measured (Ref.6) and the results show reasonable agreement with the theory. The general conclusion that one may draw from those studies is that at frequencies of 11 and 14 GHz and high elevation angles the effect of scattering on radiometric measurements is small, and for all intents and purposes may be neglected.

Having established a minimum effective noise temperature of the sky as an infinitely attenuating medium, and operating at frequencies where scattering effects are minimal, it is felt that the Darwin radiometer results are reasonably accurate up to a maximum attenuation reading of 12 dB. This assumption is based on the fact that any small error due to scattering is in an opposite sense to any error due to a higher true T_a value.

3. FIELD INSTRUMENTATION

3.1 Radiometer Design

The present radiometer design is an evolution of a previous design (Ref.3) which was installed in the field before Cyclone Tracey (December 1974). A complete upgrading of the radiometer has been performed producing a stable system whose performance is well within the theoretically predicted sensitivity.

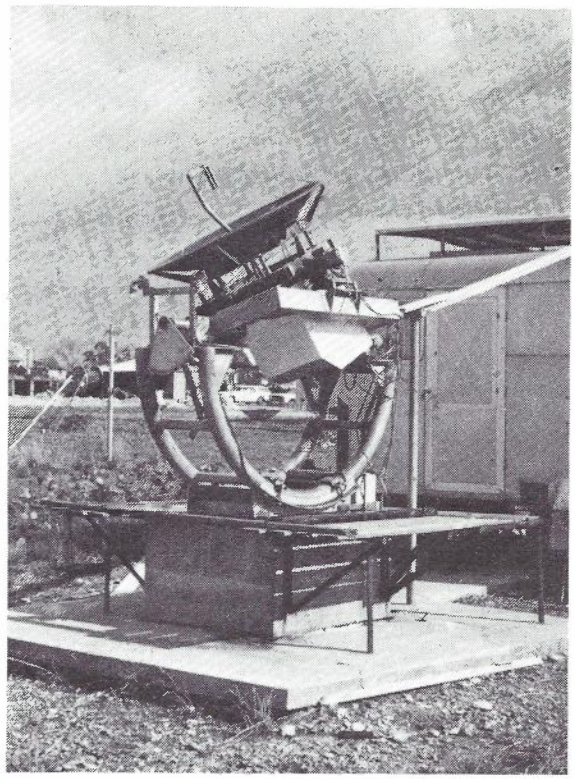

Fig.2 - Darwin radiometer system.

A picture of the Darwin radiometer is shown in Fig.2. The equatorial antenna mount is the result of the original sun-tracking design and is seen holding the antenna at a fixed azimuth of 30° and elevation of 60°. Two horn feeds provide a dual-beam configuration with a beam separation of 3.65°. The four foot (1.22 meter) antenna dish provides a beamwidth of 1.67° at 11.075 GHz and 1.30° at 14.25 GHz. Both the center beam and offset beam inputs are diplexed to provide two 200 MHz bands centred at 11.075 GHz and 14.25 GHz, and each frequency is fed to its corresponding receiver.

The two receivers are identical and the design is based on a concept used at the Communications Laboratory of the Japan Telegraph and Telephone Corporation (Ref.7). The receiver design is shown in block diagram form in Fig.3. Two switchable ferrite circulators are used to modulate the dual-beam input. The first one driven at 1170 Hz compares the two beams with respect to each other. The second circulator compares that output with an ambient temperature termination at a 433 Hz rate. The output is then

processed in a conventional superheterodyne receiver and then synchronously detected in such a way as to recover independently voltages proportional to the noise temperature as seen by the main beam, the offset beam, and the difference between the two.

Each hour the radiometer is calibrated with an avalanche diode which has proven to be a very stable noise source. During the calibration cycle the second switchable ferrite circulator (driven at 433 Hz) is clamped to the ambient termination for a period of 30 seconds, establishing a reference noise temperature for all recordings. Then the noise diode is turned on at either a 433 Hz or 1170 Hz rate (alternating between the two conditions on each hour) for another period of 30 seconds, thereby establishing a second temperature level which is accurately known. In this way the error in data reduction due to long term gain variations is reduced to a negligible value. A typical data recording is displayed in Fig.4. In actual operation there are six different coloured traces (three for each frequency). The calibration tracings are also shown.

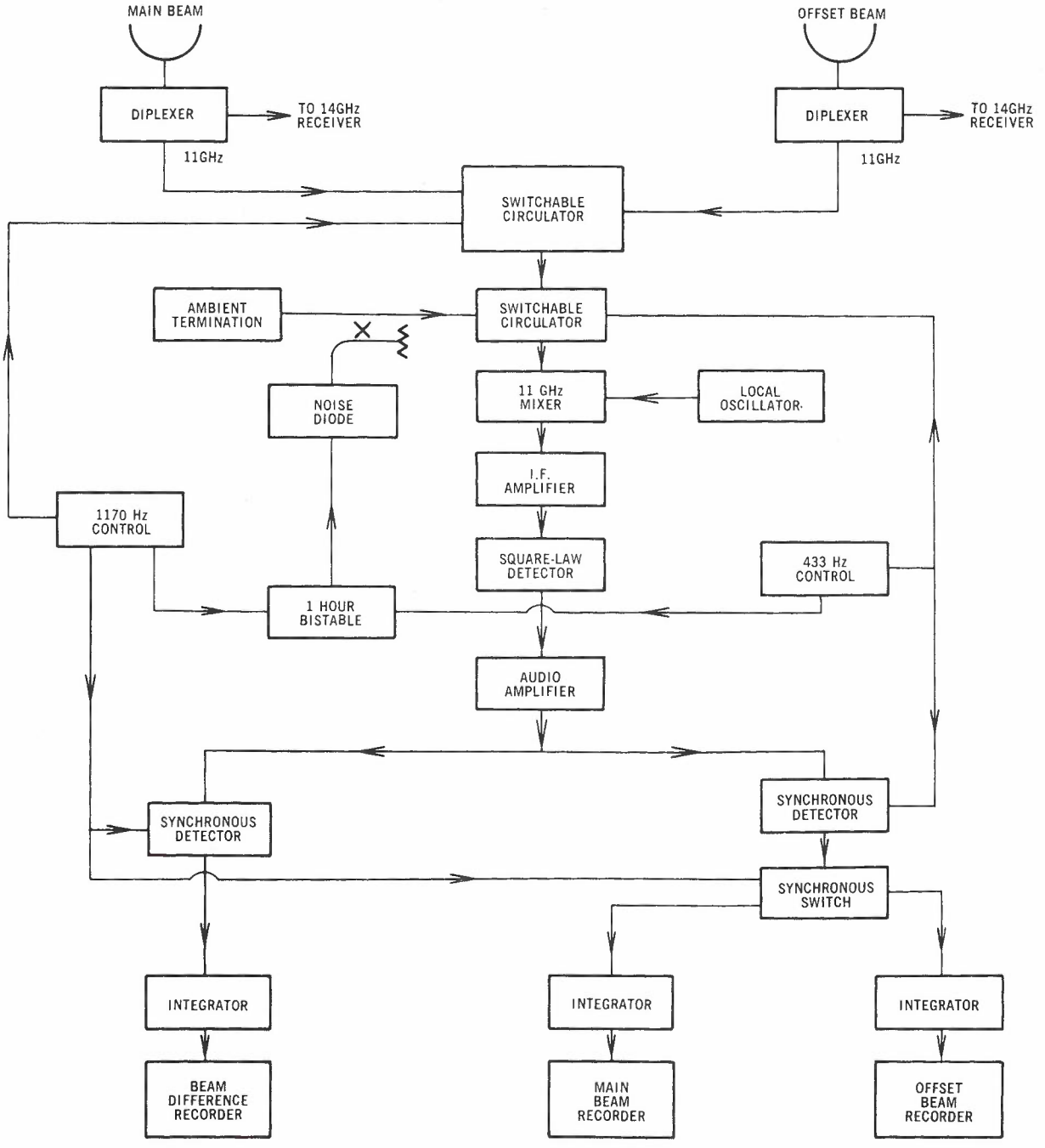

Fig.3 - Darwin radiometer receiver.

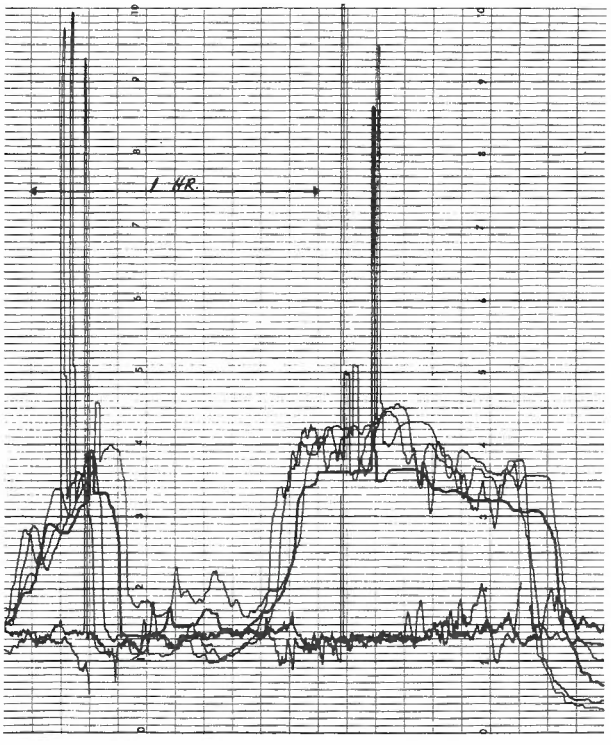

Fig.4 - Typical radiometer data.

3.2 Raingauge Network

As explained previously there are five tipping bucket raingauges three of which (including the one at the radiometer site) are aligned along the propagation path. Each site has a transmitter which is activated for each tip of the bucket corresponding to 0.2 mm of rain. A coded tone pulse is transmitted by telephone line to the radiometer site and detected by a receiver system which discriminates against false signals.

The various channels of the raingauge receiver are sampled every 30 seconds by a dotting-pen multichannel recorder, and every minute by a digital data logger system. Time markers and ambient temperatures are also recorded, which are important in the data reduction.

4. RESULTS

Because of system faults early rain attenuation data was compromised to the point where it could not be correctly evaluated, and for that reason all radiometer results prior to November 1977 have been excluded from the present analysis. Raingauge data has been reliable since the 1975/76 "wet season" and some results are included for the corresponding times of operation.

Total results which have been analysed can be broken down for convenience into four categories. The first includes the rain statistics for the Darwin area and the rain intensity results measured over a three year period. The second includes the normal rain attenuation probabilities (i.e. cumulative distributions) for 11 and 14 GHz and the correlation of these results with rain intensity statistics. The third category involves the comparison of the previous results with the 11 GHz data from Innisfail, Queensland where radiometric measurements were taken at two elevation angles different than Darwin. Finally, the frequency dependence of the Darwin data is analysed with the intent of comparing the results with classical theory for rain attenuation.

4.1 Darwin Rain Statistics

Information about point rainfall intensities in the Darwin area is contained in a Bureau of Meteorology Bulletin (Ref.8). Darwin is unique in that the major rainfall occurs during the "wet season" which for all intents and purposes covers the seven month period from mid-October to mid-May. The total average annual rainfall accumulation in Darwin is 1.62 meters. Of that amount less than 2% is contributed from the five "dry" months. Figure 5 shows a plot of the average rain intensity statistics for Darwin airport covering an 18 year period. For illustration purposes the average "wet season" was taken from November through May.

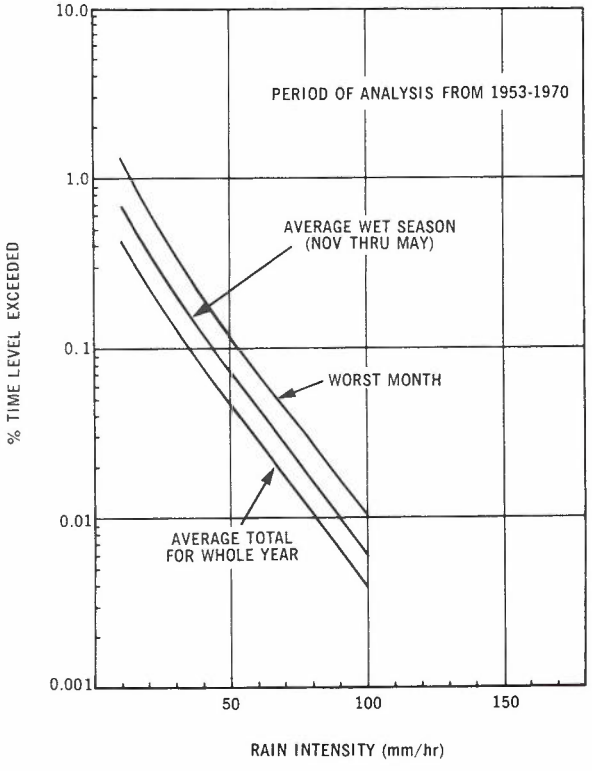

Fig.5 - Average rain intensity statistics for Darwin.

The measured rain intensity probabilities for three "wet seasons" are illustrated in Fig.6. It would appear that the 75/76 season was dry to average, the 76/77 season extremely wet, and the 77/78 season slightly above average as far as the rain intensity distribution is concerned. The data for 75/76 was relatively sparse and might not represent the true condition. Nevertheless, the potential seasonal variation is very much in evidence. The 76/77 data shows rain intensity statistics for the whole season higher than the average worst month! The fact that there were flooding conditions that year strengthens the validity of these observations.

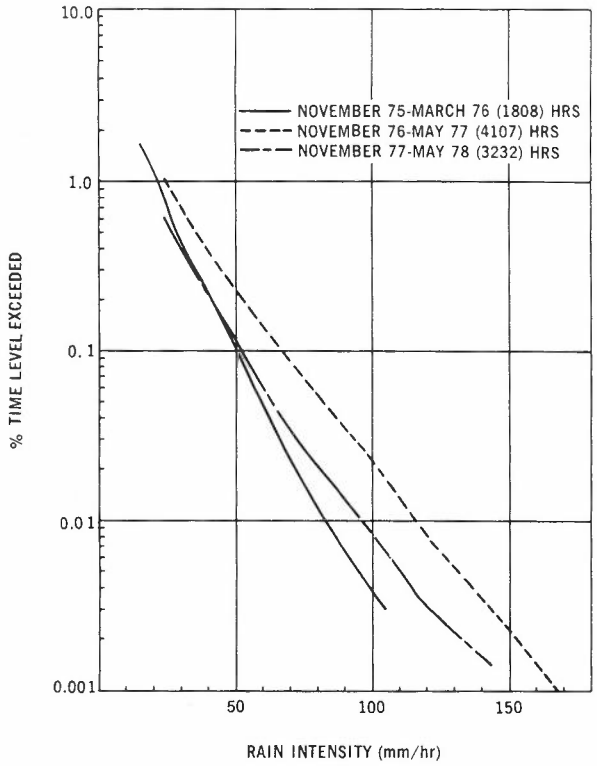

Fig.6 - Rain rate data for Darwin.

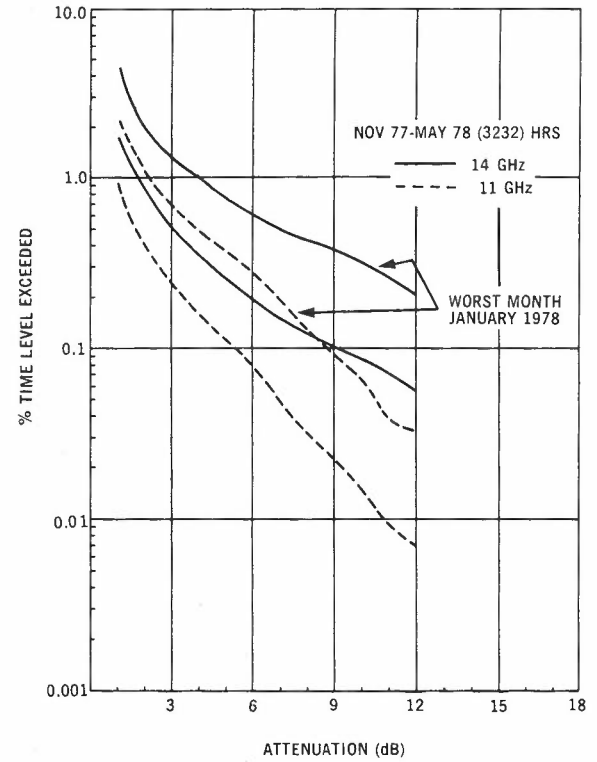

Fig.7 - Attenuation probability at 11 and 14GHz.

4.2 Rain Attenuation at 11 and 14 GHz

In order to properly compare the radiometer attenuation results at both 11 and 14 GHz, and also to relate attenuation to rain intensity statistics, only those times were analysed where the attenuation at both 11 and 14 GHz and the on-site raingauge measurements were simultaneously valid. This restriction reduced the number of hours of valid measurements to 3232 hours for the period November 1977 through May 1978. The attenuation statistics for 11 and 14 GHz are shown in Fig.7. The percentage time that a level is exceeded is plotted versus attenuation for both the seasonal data and the worst month condition. For the 77/78 wet season the results show that levels of 5.3 dB attenuation at 11 GHz and 9 dB attenuation at 14 GHz are exceeded for 0.1% of the time. There is a substantial increase for the worst month condition with that same probability level corresponding to 9.0 dB and >15 dB for 11 and 14 GHz respectively.

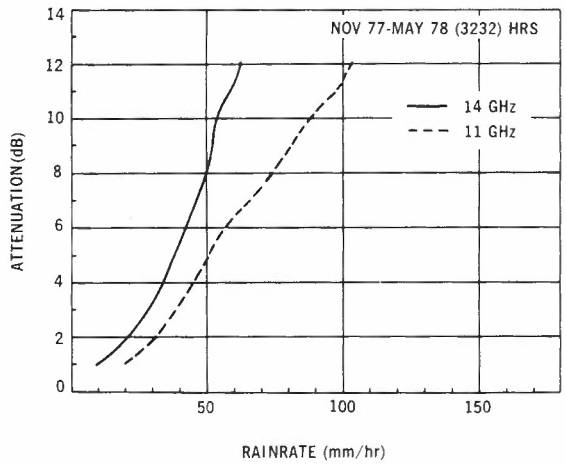

Fig.8 - Coincident rain attenuation versus point rain intensity.

Figure 8 shows the relationship between 11 and 14 GHz attenuation and the local on-site rain intensity corresponding to the same probability level. There are essentially no differences between the curves shown and the same curves for the worst month condition, and for that reason the latter curves have been omitted. Because the cumulative distribution for rain intensity is different for the two cases, we apparently have a firm relationship for the area and its climate. More data will need to be analysed to reinforce that conclusion. As we shall see later, the relationship between attenuation and point rain intensity as determined experimentally in tropical climates also appears to be independent of the propagation geometry.

4.3 Comparison of Darwin and Innisfail Data

Having accumulated radiometric data in Darwin at a fixed elevation angle of 60°, it was logical to compare these results with different fixed angle 11 GHz measurements taken at Innisfail, Queensland. The cumulative distributions for attenuation and point rain intensity are shown in Figs.9 and 10 respectively. For each elevation angle only that attenuation and rainrate data was used which was simultaneously valid.

It should be pointed out here that no special meaning should be attached to the various elevation angle data shown in Figs. 9 and 10. The curves represent results from two diff-

erent areas with different rain statistics, and in the case of Darwin the results are not extensive enough to represent an annual average.

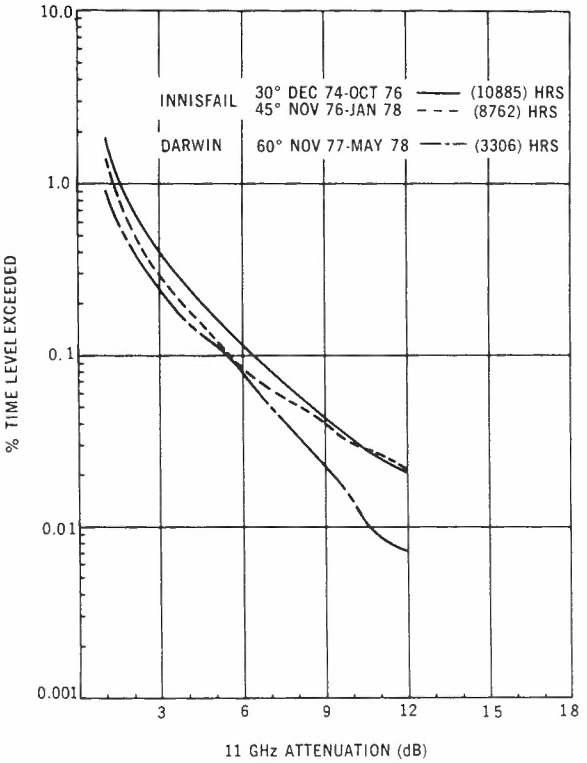

Fig.9 - Attenuation probabilities for Darwin and Innisfail, Queensland.

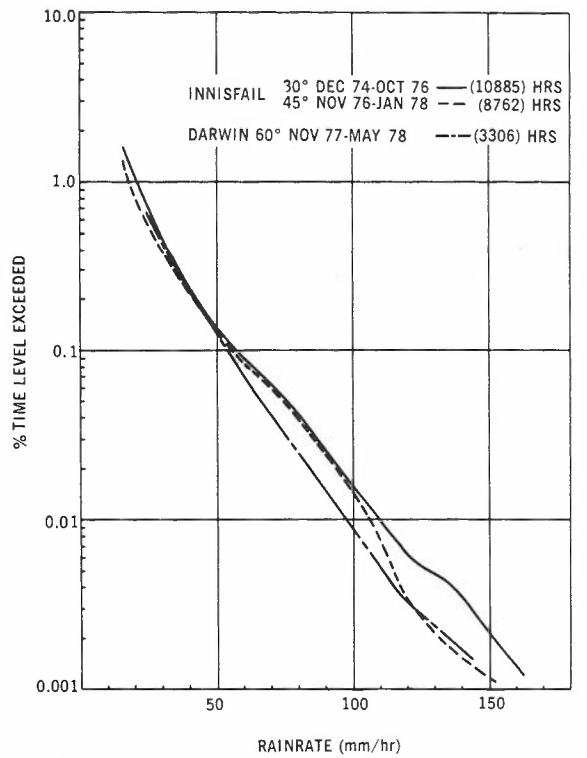

Fig.10 - Rain rate probabilities for Darwin and Innisfail, Queensland.

The data, however, can be used to come up with an interesting result. If we again correlate attenuation at 11 GHz with point rain intensity taken at the same probability level we are essentially by-passing any temporal dependencies. The results of such a correlation are shown in Fig.11. One can see that the relationship is fairly independent of elevation angle and location. More Darwin data will need to be analysed to reinforce that conclusion but the Innisfail results by themselves look fairly convincing. Classical theory would predict a propagation angle dependence between attenuation and point rainrate correlations if the attenuating medium were stratified and homogenous with a uniform raindrop size distribution. This angular dependence is evidently reduced in tropical climate conditions where the rain intensity probabilities are relatively high and the average rain cell size relatively small.

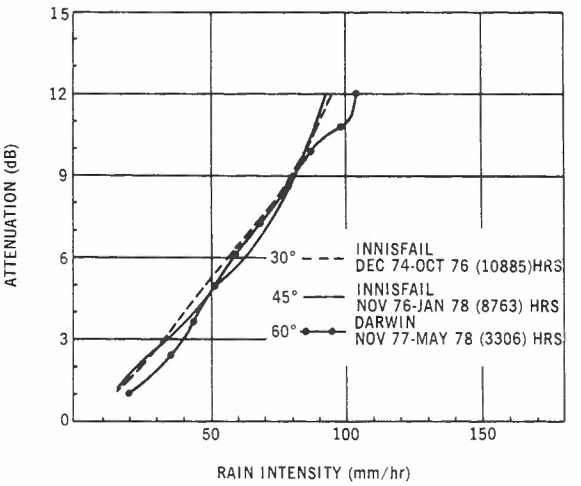

Fig.11 - Comparison of 11GHz attenuation versus point rain intensity for different elevation angles.

4.4 Frequency Dependence

Numerical results for the total attenuation coefficient of microwave signals propagating through rain have been reported by several authors (Refs.9,10). These results are based on the classical theory of propagation through a uniform rainfall along the path, and a Laws and Parsons raindrop size distribution. If one examines the frequency dependence predicted by these results for the frequency range 10-15 GHz, one can get an estimate of the non-linearity that might be expected for data measured in that same frequency range. For various fixed rainfall rates the numerical results were curve fitted with a power law relation. The most nonlinear frequency dependence occurred at the lower rain rates and the maximum departure from a best linear approximation for attenuation coefficient (in dB/km) was found to be about 2% for the frequency range of 10-15 GHz. Because of this negligible departure from linearity over the frequency range of interest it was decided to analyse the present Darwin results in a fashion similar to that used in the analysis of 30 months running of the ESRO radiometer experiment in Europe (Ref.11). By analysing the attenuation difference between 11 and 14 GHz as a

function of the attenuation at 11 GHz, with each set of points occurring at the same probability level, one can get an indication of the frequency dependence. This has been done in Fig.12.

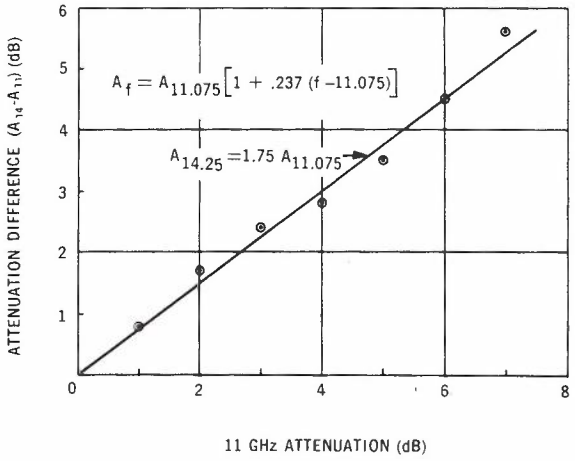

Fig.12 - Attenuation difference versus attenuation at 11GHz.

A linear regression curve fit of the data was performed showing a negligible non-zero intercept. The attenuation data at 14.25 GHz was found to be a factor 1.75 higher than attenuation data at 11.075 GHz taken at the same probability level. If put into a general linear equation it is easy to show the relation for attenuation A_f at any other frequency as being

$$A_f = A_{11.075}\ [1 + 0.237\ (f - 11.075)] \qquad (2)$$

where f is the frequency in GHz. Considering the small departure from linearity predicted by the classical theory of propagation through rain for the frequency range 10-15 GHz the above equation should allow a fairly accurate extrapolation to other frequencies in that range given a value of rain attenuation at 11 GHz. Again, more Darwin attenuation data will be needed to validate this empirical relation. The results reported in (Ref.11) show the same relation except for the normalization frequency, which is 11.5 GHz in that report.

One can also analyse the ratio of attenuation data obtained simultaneously at two frequencies to get an estimate of the extent of rain or effective path length (Ref.12,13). This approach uses the fact that for a Laws and Parsons dropsize distribution the classical Mie theory predicts a particular rain rate for a given ratio of attenuation for two specific frequencies. If one knows this apparent rain rate, the attenuation coefficient from theory, and the absolute value of attenuation, then one can calculate an effective pathlength for that attenuation level.

According to Olsen et al (Ref.14) the attenuation coefficient can be described effectively by the empirical relation $A = aR^b$ (dB/km), where R = rainrate (mm/hr) and a and b are constants for a particular frequency and rain temperature. Using their tables for a rain temperature of 20°C and a Laws and Parsons dropsize distribution, and extrapolating to the desired frequencies, the values for a and b were found to be 0.0130, 1.257 for 11.075 GHz, and 0.0286, 1.187 for 14.25 GHz. The ratio of attenuation values taken at the same probability level has already been shown to be fairly constant with a value of 1.75, and not decreasing with increasing attenuation as shown in (Ref.12). If the effective path length is the same at both frequencies the apparent rainrate corresponding to that attenuation ratio is 26.3 mm/hr. This fixed apparent rainrate corresponds to an increasing effective path length of approximately 1 to 9 km for the attenuation range at 11 GHz of 1 to 7 dB respectively.

These attenuation ratio results are at variance with the trends predicted in (Ref.12) and cannot be explained at present. There are differences which might negate the direct comparison - two of them being the different climate in Darwin which suggests a different raindrop size distribution, and the use of a fixed elevation angle rather than a sun-tracking radiometer to obtain the data. One might also ask whether the assumption of a constant effective path-length with frequency is valid for the measurements performed in Darwin.

5. CONCLUSIONS

In the tropical regions of Australia rain attenuation for frequencies above 10 GHz can be severe. If an earth station design in Darwin were based on a 99.9% availability for the worst month condition, the rain margin for attenuation only could be greater than 9.0 dB at 11 GHz, and greater than 15 dB at 14 GHz. If the availability were based on a worst wet season condition the corresponding rain margins would be approximately 5 and 9 dB respectively. These results are similar to those achieved with radiometric measurements at Innisfail, Queensland.

The difference in rain attenuation measured simultaneously at 11 and 14 GHz is a fairly linear function of the absolute level of attenuation. For this reason a simple relationship can be empirically determined which will allow extrapolation of attenuation data to any frequency not too far removed from the data frequencies. From the 11 and 14 GHz attenuation statistics measured at Darwin this relation is given by equation (2) in this paper for the frequency range 10-15 GHz.

The radiometric rain attenuation measurements carried out in Australia have provided data from two different locations with different climates at fixed elevation angles of 30°, 45° and 60°. The relationship between coincident rain attenuation at 11 GHz and point rain intensity (taken at the same probability level) does not appear to be a function of elevation angle for these climates. This same relationship also seems to be fairly constant at both 11 and 14 GHz for the Darwin area and similar climates.

One season's data is insufficient to establish reliable average statistics. The Darwin area can have a pronounced seasonal variation in its rainrate cumulative distribution. More data is needed from the Darwin area to reinforce the results so far, especially the esti-

mated frequency dependence of attenuation statistics.

6. ACKNOWLEDGEMENTS

The contributions from a number of Sections of the Telecom Research Laboratories is gratefully acknowledged.

Special thanks are extended to all the Darwin Telecom personnel associated with the effort, and in particular to the Blake Street personnel who carried out the daily maintenance of the radiometer system.

7. REFERENCES

1. Jenkinson, G.F., "Tropical Rain Attenuation at 11 GHz - A Study of 18 Months Measurements at Innisfail, Queensland", Australian Telecommun. Res., 1975, Vol.9, No.1, pp.45-53.

2. Jenkinson, G.F, "Tropical Rain Attenuation at 11 GHz on Earth-Space Paths - Radiometric Measurements in Australia", Proc.IEEE, March 1977, Vol.65, No.3, pp.480-481.

3. Flavin, R.K., "Radiometer Microwave Receiver for the Measurement of Atmospheric Attenuation at 11 and 14 GHz", Proc.IREE, November 1975, Vol.36, No.11, pp.353-358.

4. "Propagation Data Required for Space Telecommunications Systems", CCIR Report 564-1 (1978).

5. Zavody, A.M., "Effect of Scattering by Rain on Radiometer Measurements at Millimetre Wavelengths", Proc.IEE, April 1974, Vol.121, No.4, pp.257-263.

6. Chadha, R., and Lane, J.A., "Effect of Scattering in Measurements of Rain Attenuation by Passive Radiometry", Electronics Letters, March 1977, Vol.13, No.7, pp.177-178.

7. Morita, K., Akeyama, A., and Kuramochi, K., "Measurements of Attenuation in the 11 GHz Band due to Rainfall in Propagation Paths at High Angles of Elevation", Japan Telegraph and Telephone Corporation, Material No.A.P. 70-3 (1970-04) April 1970.

8. Pierrehumbert, C.L., "Point Rainfall Intensity - Frequency - Duration Data", Dept. of Science Bureau of Meteorology Bulletin No.49, August 1974, Australian Government Publishing Service.

9. Medhurst, R.G., "Rainfall Attenuation of Centimeter Waves: Comparison of Theory and Measurement", IEEE Trans. Antennas Propagat., July 1965, Vol.AP-13, No.4, pp.550-564.

10. Setzer, D.E., "Computed Transmission Through Rain at Microwave and Visible Frequencies", B.S.T.J., October 1970, Vol.49, pp.1873-1892.

11. Galante, F.M., "Results of 30 Months Running of the ESRO Radiometer Experiment", Problems of Space and Terrestrial Microwave Propagation Symposium, 7-9 April 1975, Graz Austria.

12. Hogg, D.C., "Intensity and Extent of Rain on Earth-Space Paths", Nature, June 1973, Vol.243, pp.337-338.

13. Hogg, D.C., and Chu, T., "The Role of Rain in Satellite Communications", Proc. IEEE, Sept. 1975, Vol.63, No.9, pp.1308-1331.

14. Olsen, R.L., Rogers, D.V., and Hodge, D.B., "The aR^b Relation in the Calculation of Rain Attenuation", IEEE Trans. Antennas Propagat., March 1978, Vol.AP-26, No.2, pp.318-329.

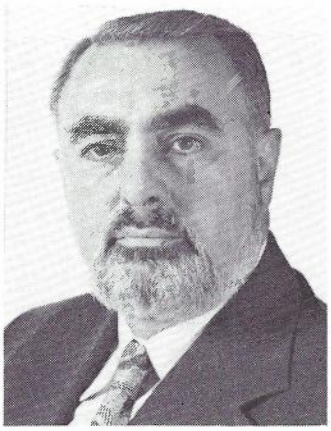

BIOGRAPHY

RICHARD K. FLAVIN graduated in 1958 from Tufts University, U.S.A., with the qualification B.Sc. (Physics) and received the M.Sc. (Physics) Degree from the University of Connecticut, U.S.A., in 1964. Between 1958 and 1964 he was engaged in basic research of plasma physics at the United Aircraft Corporation Research Laboratories in Connecticut. From 1964 to 1971 he worked as a senior microwave engineer in such American companies as Raytheon, Hewlett-Packard, and Control Data Corporation. During this time he was mainly involved with the research, design and development of parametric amplifier systems and various microwave component subsystems.

Mr. Flavin joined the Telecom Research Laboratories in December 1971. Since that time he has worked as an Engineer on the design and development of microwave receivers for radiometers, studies of earth stations for an Australian Satellite Communication System, and the design of low cost parametric amplifiers for small earth stations. He is currently an Engineer Class 4 (acting) in the Satellite Section of the Advanced Techniques Branch.

On the Peakedness of Primary and Secondary Processes

C.E.M. PEARCE
University of Adelaide
South Australia

Some basic properties of peakedness are found and proved for offered, overflow and carried traffics.

1. INTRODUCTION

The standard model of teletraffic theory is that of a finite or infinite trunk group with negative exponential holding times (of mean $1/\mu$, say) fed by a renewal stream (Palm Ref.1, Takács Refs.2,3, Cohen Ref.4). Palm and Takács have shown that in the finite trunk group case the overflow is also a renewal stream, so that the above studies may be used for the analysis of overflow traffic. We regard the carried and overflow traffics as secondary stochastic processes induced by the original offered renewal stream.

Practical probabilistic calculations for more complicated systems are most commonly carried out via Wilkinson's Equivalent Random method (Ref.5) and its extension to smooth traffic (Brettschneider Ref.6, Nightingale Ref.7), although some alternative techniques have been proposed (Jensen Ref.8, Rubas Ref.9, Freeman Ref.10). Here we categorise traffic as being smooth (smoother than pure chance traffic) if its peakedness factor z is less than unity and rough (rougher than pure chance) if z exceeds unity, where z is defined as the variance to mean ratio v/m for the trunk occupancy distribution resulting when the traffic is offered to a hypothetical infinite trunk group. In practice, of course, infinite trunk groups are idealisations of large finite trunk groups (Heffes and Holtzman Ref.11). Accordingly we shall also define a peakedness factor z_N for a finite group of N trunks as the variance to mean ratio v_N/m_N of the actual steady-state trunk occupancy distribution induced on that group. In this we follow Wilkinson (Ref.5) and diverge from Heffes and Holtzman (Ref.12), who employ the variance to mean ratio of the traffic load that would be carried on an infinite trunk group to which the carried arrival process were offered, with holding times distributed identically to but independently of those of the finite group.

In the case of a renewal input, z is given by the formula

$$z = \left[1-\phi(\mu)\right]^{-1} + \left[\mu\phi'(0)\right]^{-1} \qquad (1)$$

where

$$\phi(s) = \int_0^\infty e^{-sx}\, dF(x), \quad \text{Re. } s \geq 0$$

F being the distribution function for time intervals in the renewal stream (Heffes and Holtzman Ref.11). It is easily seen that a knowledge of z and the mean traffic $m = \left[-\mu\phi'(0)\right]^{-1}$ does not completely characterise the carried traffic (Holtzman Ref.13).

Despite its central role in the Equivalent Random method and its extension, no systematic study of the mathematical properties of peakedness appears to have been published, possibly because it is deemed a less soundly-based mathematical concept than the dimensionless and statistically standard coefficient of variation v/m^2 (Palm's "form factor"). In view of the nonlinear trunk occupancy response to offered traffic, the appropriateness of such a view is questionable. On the contrary, we hope in this paper to make a case for the mathematically "nice" properties of peakedness, at least in the context of renewal offered traffic and negative exponential holding times. Apropos the choice of peakedness, analogous properties for the coefficient of variation are considered briefly in Section 8. Some isolated exact results appear in the literature. Wilkinson (Ref.5) notes the formula

$$z_N = 1 - \text{load on last trunk} \qquad (2)$$

and Heffes and Holtzman (Ref.11) show that for a given renewal input

$$z \to 1 \quad \text{as} \quad \mu \to \infty \qquad (3)$$

The best-known result, that the overflow arising from Poisson offered traffic has $z > 1$, is frequently quoted but does not appear to have received an explicit proof in the literature, although it is given as an exercise by Cooper (Ref.14).

In Section 2 we determine some properties of peakedness for a renewal stream of traffic. Sections 4 and 5 look at the two associated secondary processes, the carried and overflow traffics, resulting when the primary traffic is offered to a finite group of trunks. Finally, in Sections 6 and 7, we consider asymptotic results holding in the context of light or heavy traffic.

In the following we shall assume that the primary offered traffic has $F(0+) = 0$, that is, with probability one two calls do not occur simultaneously. This implies in particular that the

mean inter-arrival time for calls, $-\phi'(0)$, is non-zero. We shall assume for convenience that it is also finite. Our results modify in an obvious way if it is not.

2. BOUNDS FOR z

The following special case of Jensen's inequality (Ref.15, p.110) has been found useful. This we shall prove from first principles, as we wish to note that strict inequality can occur only for one particular distribution.

Lemma 1:

For given values μ, $r = -[\phi'(0)]$, the transform $\phi(\mu)$ is minimised by taking the underlying distribution as the degenerate distribution with probability mass unity at the value r.

Proof: We have

$$\int_0^\infty e^{-\mu x} F(x)dx =$$

$$\int_r^\infty e^{-\mu x}\, dx + \int_0^r F(x)\, e^{-\mu x}\, dx - \int_r^\infty [1-F(x)] e^{-\mu x}\, dx$$

$$\geq \int_r^\infty e^{-\mu x}\, dx + e^{-\mu r}\left[\int_0^r F(x)dx - \int_r^\infty (1-F(x))dx\right] \qquad (4)$$

Also

$$\int_0^\infty [1-F(x)]dx = r = \int_0^r dx$$

so that

$$\int_0^r F(x)dx = \int_r^\infty [1-F(x)]dx.$$

By virtue of this condition relation (4) reduces to

$$\int_0^\infty e^{-\mu x} F(x)dx \geq \int_r^\infty e^{-\mu x}\, dx ,$$

so that

$$\mu\int_0^\infty e^{-\mu x} F(x)dx \geq e^{-\mu r}$$

$$= \int_0^\infty e^{-\mu x}\, dH(x),$$

where H is the distribution function of the degenerate distribution with unit probability mass at r. Since $F(0+) = 0$, the left hand side of the inequality is just $\int_0^\infty e^{-\mu x}\, dF(x)$, and the result is proved.

In fact it is clear from the inequality (4) that the minimum is realised for no distribution function other than H. By the lemma, equation (1) leads immediately to

Theorem 1:

For renewal traffic with mean $m = [-\mu\phi'(0)]^{-1}$, the peakedness z satisfies the inequality

$$z \geq [1-\exp(-m^{-1})]^{-1} - m \quad , \qquad (5)$$

with equality subsisting only for deterministic traffic of mean m.

Corollary:

By elementary calculus, the right hand side of (5) can be shown to approach a global infimum of 1/2 as $m \to \infty$ and a global supremum of 1 as $m \to 0$. Thus renewal traffic always has peakedness exceeding 1/2 and a deterministic stream is smooth at all intensities.

By contrast, there is no finite upper bound on z. We have

Theorem 2:

Renewal streams presenting any given mean offered traffic m exist for which z is arbitrarily large.

Proof by Construction:

For $t = (\mu m)^{-1}$ and $a < t < b$, suppose that inter-arrival times X for calls are given by

$$P(X = a) = (b-t)/(b-a) = 1 - P(X = b)$$

so that $EX = t$ and the mean offered traffic is m. We have

$$\phi(\mu) = e^{-\mu a}\,(b-t)/(b-a) + e^{-\mu b}\,(t-a)/(b-a).$$

By taking 'a' sufficiently small and 'b' sufficiently large we can insure that $\phi(\mu)$ is arbitrarily close to unity. The required result follows from (1).

3. A CHARACTERISATION OF POISSON STREAMS

In conjunction with Theorem 1, the following result underlines the basic dependence of peakedness on traffic intensity.

Theorem 3:

The Poisson stream is the only renewal stream of given functional form for which the peakedness z has a constant value, independent of the intensity of the stream.

Proof:

Variation of the intensity of a stream presented to a trunk group is equivalent, as far as the steady-state trunk occupancy of the group is concerned, to leaving the offered traffic unaltered and varying the parameter μ of the holding times, large μ corresponding to low input intensities and small μ to high input intensities. Thus z is constant, if and only if the μ-derivative of the right hand side of (1) vanishes identically, that is,

$$[1-\phi(\mu)]^2 - \mu^2\phi'(0)\phi'(\mu) = 0$$

holding for all $\mu > 0$. This relation may be treated as a differential equation for ϕ. With the requirement $\phi(\infty) = 0$, we may solve to derive

$$\phi(s) = \lambda/(\lambda+s) \qquad (6)$$

for all $s \geq 0$, where $\lambda = -[\phi'(0)]^{-1}$. By analytic continuation, the same formula must hold in the region Re. $s \geq 0$ of the complex s-plane. Since $\phi(s)$ has the form (6) for Poisson arrivals, the desired result follows from the uniqueness theorem for Laplace-Stieltjes transforms.

Substitution from (6) into (1) yields the familiar result that the constant value z for Poisson traffic is unity.

4. OVERFLOW TRAFFIC

Theorem 4:

Suppose a renewal stream with peakedness z is presented to a single trunk. Then the overflow is also a renewal process, with peakedness z' satisfying

$$z' > \min(1,z) \qquad (7)$$

Proof:

The renewal character of the overflow is well-known (Palm Ref.1), (Takács Ref.3).

Suppose the inter-event times of the offered and overflow traffics have respective distribution functions F(x), G(x), and let

$$\phi(s) = \int_0^\infty e^{-sx}\, dF(x), \quad \text{Re. } s \geq 0,$$

$$\psi(s) = \int_0^\infty e^{-sx}\, dG(x), \quad \text{Re. } s \geq 0.$$

Our starting point is the relation

$$z'-1 = \frac{\psi(\mu)}{1-\psi(\mu)} + [\mu\psi'(0)]^{-1}, \qquad (8)$$

which is simply equation (1) applied to the overflow stream. From Takács (Ref.3) or the author (Ref.16) we have

$$\psi(\mu) = \frac{\phi(2\mu)}{\phi(2\mu)+1-\phi(\mu)}$$

and

$$\psi'(0) = \phi'(0)/\phi(\mu),$$

so that (8) may be written as

$$z'-1 = \phi(\mu)\left[\frac{\phi(2\mu)}{\phi(\mu)\{1-\phi(\mu)\}} + \{\mu\phi'(0)\}^{-1}\right].$$

Holtzman (Ref.13) notes that

$$\phi(j\mu) \geq [\phi(\mu)]^j, \qquad j \geq 1 \qquad (9)$$

and Winsten (Ref.17) has shown for the case $j = 2$ that strict inequality obtains unless the underlying distribution function is degenerate. Thus we have

$$z'-1 \geq \phi(\mu)\left[\frac{\phi(\mu)}{1-\phi(\mu)} + \{\mu\phi'(0)\}^{-1}\right]$$

with strict inequality unless F is degenerate. Comparison with (1) gives us

$$z'-1 \geq \phi(\mu)[z-1].$$

As $0 < \phi(\mu) < 1$, the desired result is immediate for $z \neq 1$. For the remaining case $z = 1$, we have $z' \geq 1$, with strict inequality unless F is degenerate. The possibility of equality here is eliminated by the corollary to Theorem 1, and the proof is complete.

Theorem 4 generalises at once to overflows from an arbitrary number of trunks as

Theorem 5:

If renewal traffic with peakedness z is offered to a finite group of L trunks, the peakedness Z of the overflow satisfies

$$Z > \min(1,z). \qquad (10)$$

Proof:

This result follows from Theorem 4 by the principle of mathematical induction applied to the number of trunks. We can regard the L trunks in sequence, the overflow from each being a renewal stream presented to the next. Theorem 4 then gives both the basis for the induction and the general step.

Theorem 5 shows that the overflow from chance or rougher than chance offered traffic is rough, while that from smooth traffic is less smooth. In the particular case of Poisson offered traffic $z = 1$ and Theorem 5 establishes the well-known result that $Z > 1$ for the overflow.

We observe in passing the following slightly surprising proposition.

Theorem 6:

The Poisson stream can occur as the overflow traffic from a single trunk.

Proof:

With notation as in Theorem 4, we have

$$\psi(s) = \frac{\phi(s+\mu)}{1+\phi(s+\mu)-\phi(s)}$$

(c.f. Takács Ref.3). The overflow traffic will be Poisson if $\psi(s) = \lambda/(\lambda+s)$ for some $\lambda > 0$, that is, if ϕ satisfies

$$\phi(s+\mu) = [1-\phi(s)]\lambda/s .$$

The theorem is proved if $\phi(s)$ is the Laplace-Stieltjes transform of some honest distribution

function F. On inversion of the transforms, we have that

$$e^{-\mu t} F'(t) = \lambda[1-F(t)]$$

which solves, with the initial condition F(0)=0, as

$$F(t) = 1-\exp\left[-\frac{\lambda}{\mu}(e^{\mu t}-1)\right], \quad t \geq 0. \qquad (11)$$

F(t) is clearly an honest distribution function as required.

It might be hoped that our results could be strengthened in some way; such possibilities as

(i) $Z \leq \max(1,z)$

(ii) $Z \geq \max(1,z)$

suggest themselves naturally. No such simple inequality seems to hold generally. In fact, both (i) and (ii) occur in particular instances, so that neither can be generally true. Suppose a renewal stream characterised by (11) is offered to a group of trunks. As in Theorem 5, we may consider the overflow as resulting from a sequence of overflows from single trunks. By Theorem 4 we have on considering the first of these that $z < 1$ for the offered traffic. If the first overflow is offered to a second trunk, the peakedness Z of the overflow must satisfy $Z > 1$, again by Theorem 4. This provides an example of (ii).

On the other hand, suppose our second overflow is regarded as an offered traffic for a further N trunks (so that $z > 1$). By a result of Belyaev (Ref.18) the resultant overflow is asymptotically Poisson as $N \to \infty$, so that for N sufficiently large $Z < z$. This provides an instance of (i).

Although both of these examples have $Z > 1$, values of Z less than unity can occur (c.f. Ref. 16, where it is shown that Z can be arbitrarily close to 1/2).

5. CARRIED TRAFFIC

The following preliminary result has been found useful. For a given functional form ϕ and fixed positive integer N, define

$$[r,s] = \left[\sum_{m=r}^{N} \binom{N}{m} h_m^{-1}\right] \Big/ \sum_{m=s}^{N} \binom{N}{m} h_m^{-1},$$

with

$$h_n = \begin{cases} \prod_{j=1}^{n} \dfrac{\phi(j\mu)}{1-\phi(j\mu)}, & n \geq 1 \\ 1, & n = 0 \end{cases}$$

so that $0 < [r,s] < 1$ for $0 \leq s < r \leq N$. We have

Lemma 2:

$$[2,1] < [1,0] \qquad (12)$$

Proof:

It is easily verified that each term of the series $\sum_{\ell=0}^{n-1} \binom{n-1}{\ell}(-1/N)^{\ell}$ is numerically less than the preceding one if $1 \leq n \leq N$, so that

$$1-(n-1)/N \leq (1-1/N)^{n-1} < y^{n-1}, \quad 1 \leq n \leq N,$$

for any y satisfying

$$N/(N+1) < y < 1. \qquad (13)$$

Hence for y as above

$$\left[1-(n-1)/N\right] \sum_{m=0}^{n-1} y^m < n y^{n-1}, \quad 1 \leq n \leq N$$

and so

$$0 \leq \frac{\left[1-(n-1)/N\right]}{n} \cdot \frac{1-y^n}{y^n} < \frac{1-y}{y}, \quad 1 \leq n \leq N.$$

Multiplication of these inequalities yields

$$\binom{N}{n} \prod_{m=1}^{n} (1-y^m)/y^m < N^n(1-y)^n/y^n \qquad 1 \leq n \leq N. \qquad (14)$$

Relation (13) implies $N(1-y)/y < 1$, so that we may sum (14) over n to derive

$$\sum_{n=0}^{N} \binom{N}{n} \prod_{m=1}^{n} (1-y^m)/y^m < \left[1-N(1-y)/y\right]^{-1}, \qquad (15)$$

where the empty product is taken as unity. From equation (9)

$$\left[1-\phi(m\mu)\right]/\phi(m\mu) \leq (1-\left[\phi(\mu)\right]^m)/\left[\phi(\mu)\right]^m$$

Hence on setting $y = \phi(\mu)$, we have by comparison with (15) that

$$\sum_{n=0}^{N} \binom{N}{n} h_n^{-1} < \left[1-N h_1^{-1}\right]^{-1} \text{ if } 1 > \phi(\mu) > N/(N+1).$$

Simple algebraic rearrangement of this formula, employing the relation

$$\sum_{0}^{N} \binom{N}{n} h_n^{-1} = 1+\sum_{1}^{N} \binom{N}{n} h_n^{-1} = 1+N h_1^{-1}+\sum_{2}^{N} \binom{N}{n} h_n^{-1}$$

gives (12) for $1 > \phi(\mu) > N/(N+1)$. On the other hand (12) can also be written as $[1,0] < N h_1^{-1}$,

which is trivially satisfied if $h_1 \leq N$, that is, if $\phi(\mu) \leq N/(N+1)$. The desired result (12) thus holds for all values of $\phi(\mu)$.

Lemma 2 has done the work to allow us to deduce a carried traffic version of Theorem 5:

Theorem 7:

The peakedness Z_N of the carried traffic is related to the peakedness z of the offered traffic by the inequality

$$Z_N < \max(1,z).$$

Proof:

From (Ref.16) we have

$$Z_N = 1 - M_N + h_1 - N\pi_N/(1-\pi_N) ,$$

where π_N is the blocking probability. Substitution for M_N and π_N from the formulae given in (Ref.16) yield

$$Z_N - 1 = -m[1,0] + h_1[2,1] \qquad (16)$$

$$< (-m+h_1)[1,0]$$

$$= (z-1)[1,0],$$

from equation (1) and the definition of h_1. As $0 < [1,0] < 1$, the theorem follows at once.

Theorem 7 shows us that rough offered traffic becomes less rough carried traffic, while smooth offered traffic leads to smooth carried traffic. The first part of the result is as we might expect intuitively: the overflow "clips off" the peaks of the rough offered traffic. This extends to arbitrary renewal traffic with $z \geq 1$ the known result (2) of Wilkinson, which tells us that $Z_N < z = 1$ for Poisson offered traffic. The second part of the theorem behooves a caution with this sort of intuition, since it does not claim that offered smooth traffic results in smoother carried traffic. Indeed, the results of the following section make it clear that this need not be the case, as any sufficiently light offered traffic produces carried traffic with $Z_N \sim 1$.

6. LIGHT TRAFFIC

Suppose we take μ very large. Then $[1,0]$, $[2,1] \sim 1$, m, $h_1 \sim 0$, so that $Z_N \sim 1$, regardless of the structure of the offered traffic. This result also holds in the limit as $N \to \infty$, giving a result of Heffes and Holtzman already noted as (3). With the interpretation of $\mu \sim \infty$ as light traffic we see that the Heffes-Holtzman result follows as a corollary of the theorem of Belyaev noted earlier. This asymptotic result depends on the traffic being of low intensity, as no finite renewal traffic is reproduced (with suitable scale change) on overflowing (c.f. Ref. 16). In fact, any sufficiently light traffic has some resemblance to Poisson traffic in the trunk occupancy distribution induced.

Suppose the inter-arrival time distribution has a finite density $d \neq 0$ at the origin. Then $s\phi(s) \to d$ as $s \to \infty$, so that $h_n \sim (d/\mu)^n/n!$ for μ large. Both with offered and carried traffic, the steady-state probability π_j that an arriving call finds j trunks occupied can be expressed as a simple function of the h_n (see Ref.16). It follows that, to the term of lowest order, each probability π_j is the same as for Poisson traffic with parameter $\lambda = d$. Perhaps unfortunately for practical consequences, the correspondence breaks down for the continuous time occupancy distribution $\{q_j\}$. The relevant formulae in this case involve the mean offered traffic as well as the h_n. The agreement of the q-distribution thus holds only for those renewal streams for which the probability density of the inter-arrival times at the origin is numerically equal to the mean arrival rate.

7. HEAVY TRAFFIC

First consider offered traffic. In accordance with our method of representing variations in the offered traffic intensity by variations in μ, we write $z = z(\mu)$. As Heffes and Holtzman have noted (Ref.11), in most practical trunking situations we are operating with heavy traffic, so that z may be taken approximately as $z(0)$. We have by an elementary mean value theorem that

$$\phi(\mu) = 1 + \mu\phi'(0) + (\mu^2/2)\phi''(\xi) \quad \text{for } \mu \text{ small},$$

for some ξ on $(0,\mu)$. Substitution of this expression in (1) gives

$$z(\mu) = \frac{\phi''(\xi)}{2\phi'(0)[\phi'(0)+(\mu/2)\phi''(\xi)]}$$

On letting $\mu \to 0$, we derive an asymptotic formula for peakedness in heavy traffic, viz.

$$z(0) = \frac{\phi''(0)}{2[\phi'(0)]^2} = (1+c)/2 \text{ , say,} \qquad (17)$$

when $\phi''(0)$ exists, and $z(\mu) \to \infty$ as $\mu \to 0$ otherwise. The constant c in (17) is the coefficient of variation of the inter-event time distribution function for the renewal stream, that is, the ratio of the variance of inter-arrival times to the square of their mean. In particular $c = 0$ for deterministic arrivals, giving the asymptotic result $z(0) = 1/2$ already noted for deterministic traffic.

We turn now to carried traffic. The expansion

$$\phi(n\mu) = 1 + n\mu\phi'(0) + O(\mu^2) \quad \text{for } \mu \text{ small}$$

leads to $h_n^{-1} = n!\, x^n + O(x^{n+1})$ for x small,

where $x = -\mu\phi'(0)$ is the reciprocal of the mean offered traffic. Hence

$$[1,0] = Nx + O(x^2)$$
$$[2,1] = (N-1)x + O(x^2)$$

and we deduce from (16) that

$$Z_N = O(x) \qquad (18)$$

for heavy traffic, as we would expect. This makes it clear that, for carried traffic, smoothness is an indication of the intensity of the offered traffic as much as of its structure.

8. COEFFICIENT OF VARIATION

Analogously to (1), the coefficient of variation $w = v/m^2$ of the offered traffic is given by

$$w = -1-\mu\phi'(0)/[1-\phi(\mu)] \qquad (19)$$

The corresponding quantity w' for the overflow from a single trunk is

$$w' = -1-\mu\psi'(0)/[1-\psi(\mu)]$$

in the notation of Theorem 4, which can be re-expressed as

$$w' = -1- \frac{\mu\phi'(0)}{1-\phi(\mu)} \cdot \frac{\phi(2\mu)+1-\phi(\mu)}{\phi(\mu)}$$

Since $\phi(2\mu) \geq [\phi(\mu)]^2 \neq 1$, the latter term in the product in the preceding equation is greater than unity, so that

$$w' > -1- \frac{\mu\phi'(0)}{1-\phi(\mu)} = w.$$

By an inductive argument we have, paralleling Theorem 5, that the coefficient of variation W of the overflow from any finite number of trunks exceeds that of the offered traffic:

$$W > w . \qquad (20)$$

The coefficient of variation W_N for the traffic carried on N trunks is given by

$$W_N = [-\mu\phi'(0)]\left[1/(1-\phi(\mu)) - \sum_{n=1}^{N} \binom{N}{n} h_n^{-1}\right]$$
$$< w , \qquad (21)$$

that is, the carried traffic always has coefficient of variation less than that of the offered traffic (c.f. Theorem 7).

Relations (20) and (21) are simpler than the corresponding results for peakedness. Further, consider the derivative formed from equation (19):

$$dw/d\mu = \frac{-\phi'(0)}{1-\phi(\mu)} \left[1+\mu\phi'(\mu)/(1-\phi(\mu))\right].$$

With the use of a mean value theorem, we have

$$1 = \phi(\mu) - \mu\phi'(\mu) + (\mu^2/2)\phi''(\eta)$$

for some η on $(0,\mu)$. Substitution of this value shows that

$$dw/d\mu = \frac{-\phi'(0)}{1-\phi(\mu)} \cdot \frac{\mu^2\phi''(\eta)}{2[1-\phi(\mu)]} > 0 ,$$

so that w is strictly monotone increasing with μ. It follows from (19) that $w \to 0$ as $\mu \to 0$ while $w \to \infty$ as $\mu \to \infty$. This shows that the coefficient of variation of any offered traffic as measured by trunk occupancy decreases monotonically from ∞ to 0 as the intensity of the offered traffic increases from 0 to ∞. It may also be shown simply that W, $W_N \to 0$ as $\mu \to 0$ and W, $W_N \to \infty$ as $\mu \to \infty$. These results make clear that the variance and the square of the mean tend to be of different orders of magnitude both for primary and secondary traffics. By contrast it is implicit in our results on peakedness that variance and mean tend more to be of like magnitude, which makes mean and peakedness a more natural pair of working parameters than mean and coefficient of variation.

9. REFERENCES

1. Palm, C., "Intensitatsschwankungen im Fernsprechverkehr", Ericsson Technics, Vol.44, pp.1-189, 1943.

2. Takács, L., "On the Generalisation of Erlang's Formula", Acta Math. Acad. Sci. Hung., Vol.7, pp.419-433, 1956.

3. Takács, L., "On the Limiting Distribution of the Number of Coincidences Concerning Telephone Traffic", Ann. Math. Stat., Vol.30, pp. 134-142, 1959.

4. Cohen, J.W., "The Full Availability Group of Trunks with an Arbitrary Distribution of the Inter-arrival Times and the Negative Exponential Holding Time Distribution", Simon Stevin Wis-en Natuurkundig Tijdschrift, Vol.26, pp.169-181, 1957.

5. Wilkinson, R.I., "Theories for Toll Traffic Engineering in the U.S.A.", Bell System Tech. J., Vol.35, pp.421-514, 1956.

6. Brettschneider, G., "Extension of the Equivalent Random Method to Smooth Traffics", Seventh International Teletraffic Congress, Stockholm, pp.411/1-9, 1973.

7. Nightingale, D.T., "Computations with Smooth Traffics and the Wormald Chart", Aust. Tele. Res., Vol.11, No.1, pp.45-52, 1977.

8. Jensen, E., "On Arrival Processes for Overflow Calls", Seventh International Teletraffic Congress, Stockholm, pp.416/1-7, 1973.

9. Rubas, J., "Dimensioning of Alternative Routing Networks Offered Smooth Traffic", Aust. Tele. Res., Vol.11, No.1, pp.38-44, 1977.

10. Freeman, A.H., "The Accuracy of Overflow Traffic Models", Aust. Tele. Res., Vol.11, No.1, pp.98-101, 1977.

11. Heffes, H. and Holtzman, J.M., "Peakedness in Switching Machines: its Effect and Estimation", Eighth International Teletraffic Congress, Melbourne, pp.343/1-8, 1976.

12. Heffes, H. and Holtzman, J.M., "Peakedness of Traffic Carried by a Finite Trunk Group with Renewal Input", Bell System Tech. J., Vol.52, pp.1617-1642, 1973.

13. Holtzman, J.M., "The Accuracy of the Equivalent Random Method with Renewal Inputs", Seventh International Teletraffic Congress, Stockholm, pp.414/1-6, 1973.

14. Cooper, R.B., "Introduction to Queueing Theory", Macmillan, New York, 1972.

15. Royden, H.L., "Real Analysis", Collier-Macmillan, Toronto, second edition, 1968.

16. Pearce, C.E.M. and Potter, R.M., "Some Formulae Old and New for Overflow Traffic in Telephony", Aust. Tele. Res., Vol.11, No.1, pp.92-97, 1977.

17. Winsten, C.B., "Geometric Distributions in the Theory of Queues", J. Roy. Statist. Soc. B. Vol.21, pp.1-35, 1959.

18. Belyaev, Yu. K., "Limit Theorem for Dissipative Flows", Theory of Prob. and its Applications, Vol.8, pp.165-173, 1963.

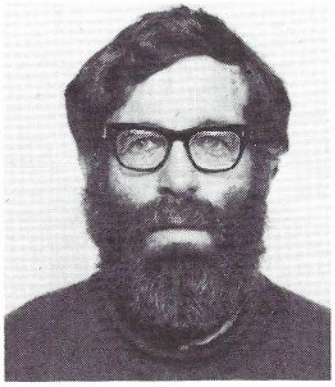

BIOGRAPHY

CHARLES PEARCE received his early training in New Zealand in Mathematics and Physics. He subsequently came to Australia where he completed a Ph.D. in the area of Stochastic Processes at Canberra in 1965. After a period lecturing in Britain he returned to Australia and joined the University of Adelaide in 1968 as a Senior Lecturer in Mathematics.

He is interested generally in the area of Applied Probability and has recently been working on some problems in telephone traffic.

Structural Characteristics of Optical Fibres

E. JOHANSEN
Telecom Australia Research Laboratories

P.V.H. SABINE
Telecom Australia Research Laboratories

The first part of this paper outlines the modified chemical vapour deposition fibre fabrication process. Various inherent structural characteristics of the fibres are related to particular manufacturing operations and techniques for investigating these characteristics are discussed. The scanning electron microscope, and in particular the secondary electron imaging and microprobe modes, is shown to provide a powerful analytical tool for examining the physical and compositional properties of fibres. Measurement of the near-field intensity distribution is found to be a rapid and convenient technique for investigating some important optical transmission properties of the fibre - most notably, for determining the refractive index profile. The primary purpose of this paper is to show that a greater understanding of the fibre can be obtained by correlating results from all three techniques. Practical results illustrating this correlation procedure are presented. The particular fibres described are experimental step index and step index - barrier layer fibres manufactured at the AWA Research Laboratory under contract to Telecom Australia.

1. INTRODUCTION

Optical fibre communications is advancing rapidly from the realm of laboratory experiments towards practical systems applications. The main stimulus for this progress has been the development of very low loss optical fibres. Improvements in materials purification and fibre fabrication techniques (Refs.1,2) have resulted in a dramatic reduction of transmission loss. An attenuation of less than 1dB/km over the wavelength range 0.95 - 1.37μm, with a minimum of 0.47dB/km at 1.2μm, has been reported (Ref.2). This is very close to the theoretical lower limit of optical attenuation imposed by Rayleigh scattering in the fibre core material. Considerable effort is now being directed towards the control of other fibre parameters, such as circularity, strength and refractive index profile. This profile describes the variation of refractive index along a diameter of the fibre cross-section.

The most common forms of optical fibre consist of a circular core of transparent, high refractive index material, surrounded by a concentric cladding of lower refractive index material. Light is guided within the fibre core by total internal reflection at the core-cladding interface. When the refractive index is uniform across the core region, the fibre is of the step-index type. The refractive index profile for a step-index fibre is shown in Fig.1(a) and can be described as;

$$\left.\begin{aligned} n(r) &= n(o) && r < a \\ n(r) &= n(o)\,[1 - \Delta n_m] && r \geq a\ . \end{aligned}\right\} \quad (1)$$

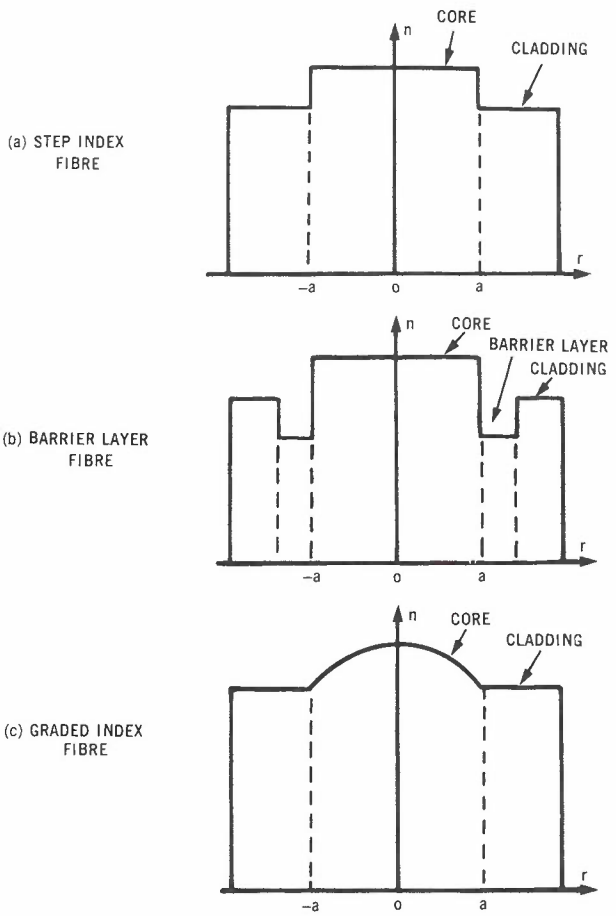

Fig.1 - Ideal refractive index profiles of significant fibre types.

Here r is a variable distance measured from the centre of the fibre core, a is the core radius and Δn_m is the (maximum) relative refractive index difference between the core and the cladding. For typical multimode optical fibres the core radius and cladding thickness are approximately equal and within the range 25-50μm. The core-cladding refractive index difference is generally small, so that typically $\Delta n_m \leq 0.015$ in fibres designed for telecommunications applications. An important fibre parameter is the numerical aperture,

$$NA = \sin \theta_c = \left[n(o)^2 - n(a)^2\right]^{\frac{1}{2}}$$

$$\doteq n(o) \left[2\Delta n_m\right]^{\frac{1}{2}} \qquad (2)$$

where θ_c is the maximum angle, measured in air, at which an off-axis meridional ray incident upon the core region at a fibre end-face, will undergo total internal reflection at the core-cladding interface and so will be guided by the fibre. Thus the numerical aperture is a measure of the light coupling ability of the fibre when illuminated by a wide-angle source, such as a light emitting diode.

The step-index barrier layer fibre is a doubly-clad fibre with a low refractive index region between the core and cladding. As indicated in the refractive index profile of this fibre, Fig. 1(b), the barrier layer has a refractive index lower than the cladding. Inclusion of this barrier layer makes possible fibres of large numerical aperture, optically isolates the core from the external cladding and eases fabrication requirements (Ref.3).

Multimode step-index fibres are a suitable transmission medium when only moderate bandwidths are needed (Ref.4). Much higher bandwidths are attainable with graded index fibres, in which the refractive index decreases from a maximum at the core centre to a lower value at the core-cladding interface. Theoretical considerations (Ref.5) show that there exists an optimum near-parabolic refractive index profile for which the transit time of all rays is very nearly equalised, resulting in maximum bandwidth utilization. However, the refractive index profile must be controlled accurately to achieve this optimum condition. Thus there is a great deal of interest in the particular class of graded index profiles defined by

$$\left.\begin{aligned} n(r) &= n(o)\left[1 - \Delta n_m (r/a)^{\alpha}\right] \qquad r < a \\ n(r) &= n(o)\left[1 - \Delta n_m\right] \qquad r \geq a \end{aligned}\right\} \qquad (3)$$

where $1 < \alpha < \infty$. Note that $\alpha=2$ describes a parabolic refractive index profile, illustrated in Fig.1(c), while $\alpha=\infty$ describes a step index profile.

The refractive index profiles depicted in Fig.1 are ideal. Many different techniques have been developed to manufacture glass optical fibres (Ref.6). Fibres of the lowest transmission loss (Ref.2) have been fabricated by the modified chemical vapour deposition (MCVD) process (Refs.6,7). However the cores of practical MCVD fibres generally contain small-scale structural characteristics and inhomogeneities due to the particular operations involved in the manufacturing process. These structural characteristics may perturb the refractive index profile from the desired step or graded index variation. This, in turn, may influence the transmission performance of the fibre.

An outline of the MCVD process is presented in the next section of this paper. Emphasis is placed upon the process used at the AWA Research Laboratory (Refs.6,8,9). The inherent structural characteristics of MCVD fibres are then described. Various techniques for studying these characteristics are considered briefly in Section 4. More detailed discussion is devoted to two techniques that prove particularly informative. These are the examination of prepared fibre end-faces with a scanning electron microscope and scanning of the near-field intensity distribution to deduce the fibre refractive index profile. Practical results from investigations of step-index (phosphosilicate core) and step-index barrier layer (borosilicate clad-phosphosilicate core) multimode MCVD fibres are reported. These experimental fibres were fabricated during the development of the manufacturing facility at the AWA Research Laboratory.

2. MODIFIED CHEMICAL VAPOUR DEPOSITION PROCESS

Detailed descriptions of the MCVD process for fabricating phosphosilicate-core glass fibres have been published (Refs.6,7,8,9). Only a brief summary is presented here to emphasize relationships between various stages of the manufacturing process and the nature of the structural characteristics observed in the fibres.

The apparatus used in MCVD fibre manufacture is shown diagramatically in Fig.2. For step or graded index fibres, the starting materials are the liquids phosphorus oxychloride, $POCl_3$, and silicon tetrachloride, $SiCl_4$. Pure dry oxygen is bubbled through containers of these liquids, becomes saturated with the corresponding vapours and, in combination with excess oxygen, is fed into a silica glass (SiO_2) tube. This tube, typically of 10mm outside diameter and 1mm wall thickness, is held and rotated in the chucks of a glass-working lathe. An oxygen-propane burner mounted on the carriage of the lathe moves along the 80cm length of the tube and locally heats the outside wall to 1500°C. Within the 5cm long hot zone simultaneous oxidation and fusion of the chlorides occur to produce a 10-15μm layer of glass on the inside wall. This glass layer comprises SiO_2 and an admixture of P_2O_5; the refractive index of the composite glass is raised with increasing P_2O_5 concentration (Ref.7). To achieve a fibre diameter to core diameter ratio of 2:1 requires a total deposition thickness of 400μm. Typically 15-30 glass layers must be deposited by successive passes of the burner. To fabricate a step index fibre, all glass layers are deposited with the same nominal P_2O_5 concentration. Graded index fibres are formed, in this case, by intro-

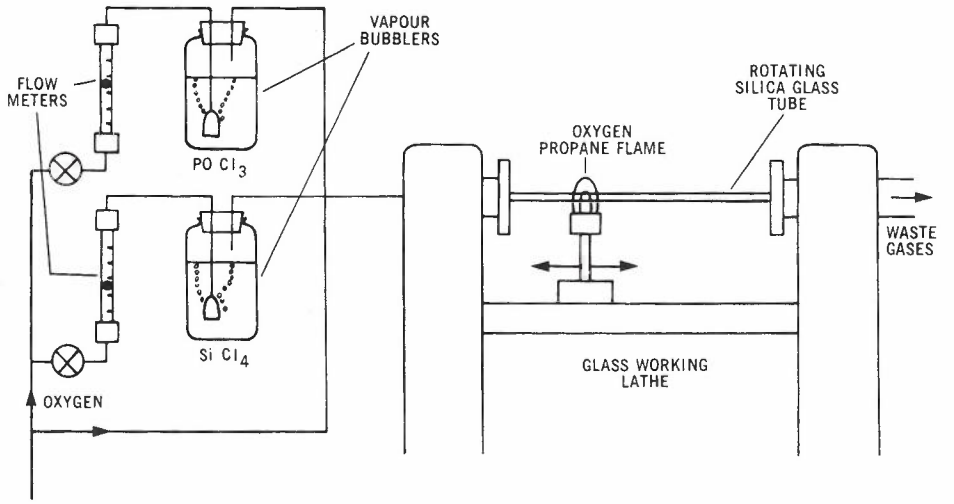

Fig.2 - Diagram of the modified chemical vapour deposition system (after Nicol, Ref.6).

ducing small increases of the P_2O_5 concentration in each successive layer.

When a barrier layer fibre is required, a third bubbler containing the liquid boron tribromide, BBr_3, is added to the system. The initial glass layers deposited comprise SiO_2 and an admixture of B_2O_3 ; the refractive index of this glass is lowered with increasing B_2O_3 concentration. These borosilicate glass layers form the barrier layer of the fibre. Then follows the deposition, in the manner described previously, of the phosphosilicate glass layers to form the core of the fibre.

Upon completion of the deposition stage, the oxygen flow is stopped and the hot zone temperature is raised to 2000°C for a further three-to-six passes. During these passes the SiO_2 containment tube is collapsed, under its own surface tension, into a solid preform.

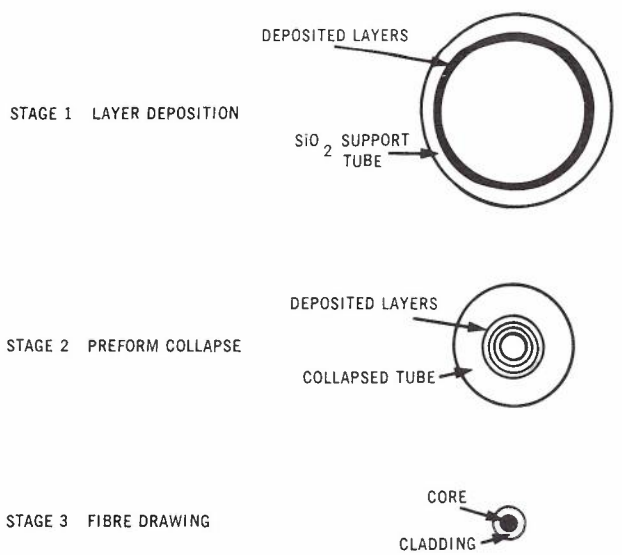

Fig.3 - The MCVD process for fabricating optical fibres.

The final stage is to draw the preform into a fibre. The preform is fed into a spiral flame burner which uniformly heats the end of the preform to over 2000°C. Fibre is drawn from the rear of the burner, through pads which apply a very thin polyurethane coating to protect the fibre from abrasion, and onto a winding drum. The take-up drum speed and the preform feed rates must be controlled carefully to maintain stable fibre dimensions.

Figure 3 summarizes the three stages of the MCVD fibre fabrication process, namely the glass deposition, preform collapse and fibre drawing.

3. INHERENT STRUCTURAL CHARACTERISTICS OF MCVD FIBRES

Optical fibres manufactured by the MCVD process have several inherent structural characteristics. The first is that the fibre core consists of a large number of concentric rings of deposited glass. For most practical situations (Ref.10) the outer radius of the i^{th} core layer can be calculated as

$$r_i = a(i/N)^{\frac{1}{2}} \qquad i=1,2,...N. \qquad (4)$$

In equation (4) N is the total number of core layers deposited, i=1 corresponding to the centremost or last deposited layer, and $a=r_N$ is the core radius. The thickness of the i^{th} layer is

$$t_i = \frac{a\left[i^{\frac{1}{2}} - (i-1)^{\frac{1}{2}}\right]}{N^{\frac{1}{2}}} \qquad i=1,2,...N. \qquad (5)$$

Figure 4(a) illustrates the concentric layer structure of an MCVD fibre core. The variation of layer thickness with layer number is indi-

cated in Fig.4(b) for a typical fibre of core radius a=50μm formed from N=25 deposited layers. For this particular case, the centremost layer has a radius of 10μm and the thickness of the i=25 (or first deposited) layer is 1.0μm.

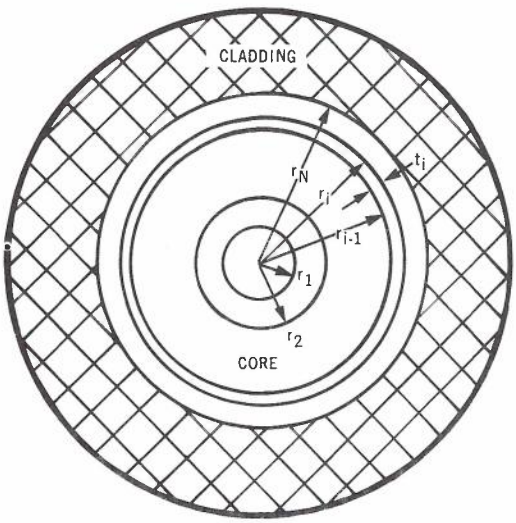

(a) CORE STRUCTURE

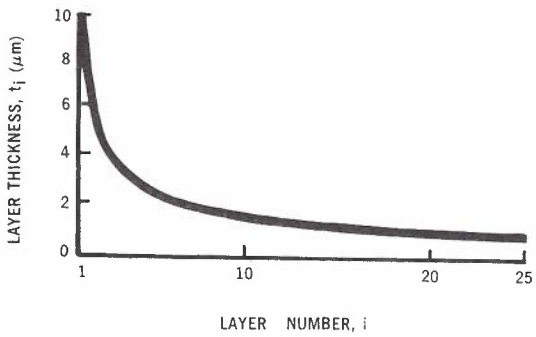

(b) CORE LAYER THICKNESSES FOR A FIBRE WITH $a = 50\mu m$ AND $N = 25$

Fig.4 - The structure of optical fibres manufactured by a MCVD process.

As noted in Section 2, to fabricate an ideal step index fibre all glass layers must be deposited uniformly from glass of the same composition. An ideal graded index fibre is manufactured by gradually increasing the concentration of a suitable dopant in each successive layer, to create a smoothly graded profile. But, in practice, small uncontrolled fluctuations of the glass composition can cause perturbations over a region which may be either within one layer thickness or over several adjacent layers. This can make the ring structure of MCVD fibres apparent, even in nominally step index fibres.

The second characteristic is introduced when the deposited tube is collapsed into a solid preform. During the high temperature collapse, volatilization of P_2O_5 from the innermost phosphosilicate layer leaves a reduced dopant concentration and, consequently, a depressed refractive index. Methods for reducing this effect are known (Refs.7,11).

A third characteristic, also resulting from the preform collapse stage, is observed in highly doped fibres. Glasses of high P_2O_5 content have a very low viscosity and there is a tendency for the tube to collapse into a rod of elliptical cross-section. Preform circularity can be improved by a modified collapse process (Refs.7,9).

The three structural characteristics described above are evident in the preform and are preserved through the fibre drawing stage to appear in the fibre. Dopant diffusion during the preform collapse and fibre drawing stages tends to smooth variations in the dopant concentration from layer to layer (Refs.7,12).

4. TECHNIQUES FOR EXAMINING STRUCTURAL CHARACTERISTICS

A variety of techniques have been developed to measure refractive index profiles and to observe small-scale inhomogeneities in optical fibres (Refs.12,13). At Telecom Australia Research Laboratories the methods used have included optical, interference and scanning electron microscopy as well as near-field and far-field scanning. But the two most informative, particularly for studies of MCVD fibres, have proven to be near-field scanning and scanning electron microscope (SEM) examination.

4.1 SEM Examination

The examination of end-sections of optical fibres with a SEM can provide a variety of valuable information concerning the structural characteristics of the fibres. Small compositional variations in the glass material, the glass dopant profile (which can be related to the refractive index profile), the extent of dopant volatilization from the centre of the fibre core, the results of particular manufacturing techniques such as the inclusion of cladding barrier layers, and the presence of any localized material inhomogeneities can all be observed by this method. Any departure of the fibre from the desired circular symmetry, as evidenced by core and cladding ellipticity or core eccentricity, can be measured with the SEM.

Two different types of fibre samples and measurement techniques are employed. Both initially require a small length of fibre with an optically flat end-face. The polyurethane primary coating of the fibre is first removed by an organic solvent. Suitable end-faces are then achieved by tensioning the fibre over a form, with a carefully chosen radius of curvature, and scoring transversely (Ref.14).

4.1.1 Secondary Electron Imaging The first technique of SEM examination requires that the end-face of the fibre be etched in an acid solution. This approach exploits the different etch rates of pure silica and doped silica (Refs.12,13,15) with etchants such as dilute and buffered hydrofluoric acid and p-etch (Ref.16). The etched fibre is mounted on a metal stub and vacuum coated with gold to permit observation in the SEM without specimen charge-up. Because glasses of different composition are etched at different rates

(Ref.16), examination of the etched fibre end-face in the SEM shows surface height variations that relate primarily to changes in the dopant concentration within the silica glass. In addition, other structural properties, such as regions of stress, can influence etch rates. For this reason it is difficult to deduce a quantitative description of the dopant concentration profile from the etched surface profile. The secondary electron imaging mode of the SEM provides an essentially topographical description of a specimen. This imaging mode permits the characteristics of the etched fibre end-face to be observed at higher magnifications and with a vastly greater depth of focus than can be achieved with an optical microscope.

These two important attributes of the SEM are illustrated by the series of micrographs in Fig.5. All five micrographs are of end-faces of barrier layer step-index fibre 242, fabrication data for which is listed in Table 1. Optical micrographs of unetched and lightly etched fibre end-faces are shown in Figs.5(a) and 5(b) respectively. In each of these micrographs the core region has been highlighted by illuminating the fibre from the far end. Clearly the etching process is of considerable benefit in revealing the structural characteristics of the fibre. But the limited resolution and depth of focus of the optical microscope makes accurate observation of these characteristics quite difficult. The micrographs in Figs.5(c) and 5(d) are of a deeply etched end-face, viewed at oblique incidence via the secondary electron imaging mode of the SEM. The large depth of focus of the SEM, even at this high magnification, is evident. Note also that the structural characteristics of the fibre can be discerned in much greater detail than with the optical micrographs. Figure 5(e) is another secondary electron image taken at normal incidence and showing the barrier layer and core regions. Table 1 indicates that all of the individual glass layers of the barrier and core regions can be distinguished in the SEM micrographs.

(b) OPTICAL MICROGRAPH OF LIGHTLY ETCHED FIBRE END-FACE
50 μm

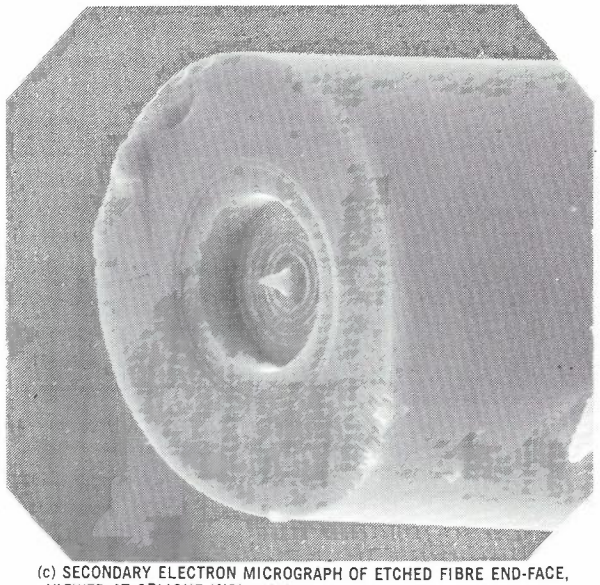

(c) SECONDARY ELECTRON MICROGRAPH OF ETCHED FIBRE END-FACE, VIEWED AT OBLIQUE INCIDENCE
50 μm

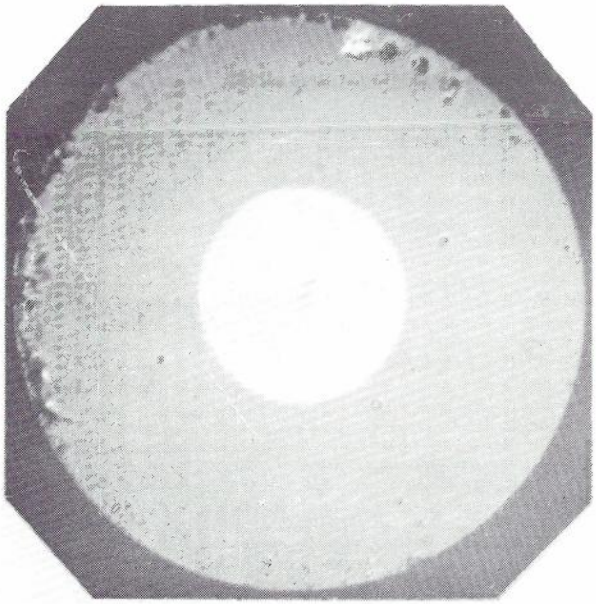

(a) OPTICAL MICROGRAPH OF FLAT FIBRE END-FACE
50 μm

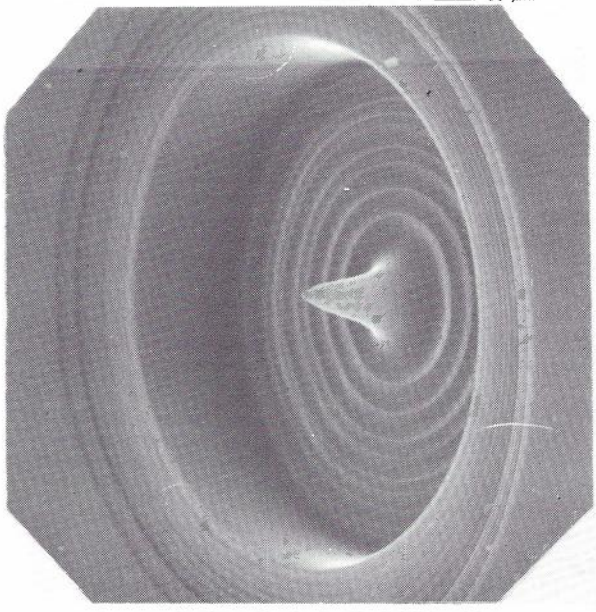

(d) AS FOR (c) BUT WITH INCREASED MAGNIFICATION
10 μm

Fig. 5 (a)-(d)

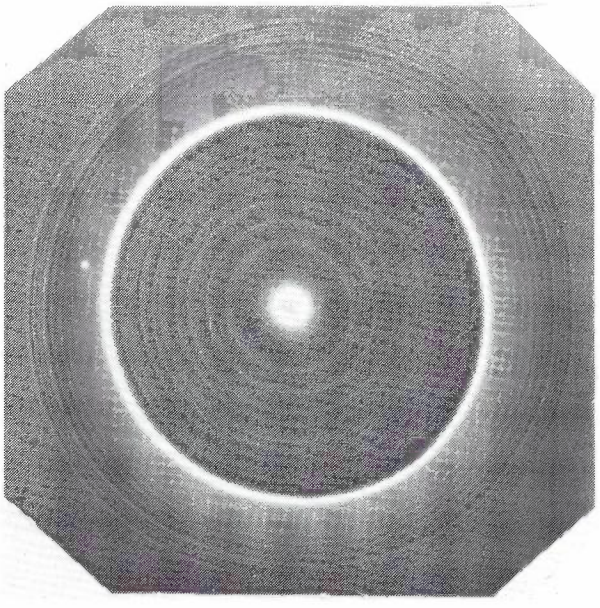

(e) SECONDARY ELECTRON IMAGE OF ETCHED FIBRE END-FACE, VIEWED AT NORMAL INCIDENCE AND SHOWING BARRIER AND CORE LAYERS

10 μm

Fig. 5 (e)

4.1.2 Microprobe Analysis The second technique of SEM examination requires that the unetched end-face of the fibre be coated with carbon, again to prevent specimen charge-up. In response to the incident primary electron beam, the specimen emits x-ray photons. By measuring the wavelengths of these emitted photons the SEM microprobe unit can determine the elemental composition of the specimen. In the case of an optical fibre sample, the microprobe can record the dopant concentrations along a diameter of the fibre end-face. Generally, the relationship between dopant concentration and glass refractive index can be determined empirically (Refs.7,8,9) so that, at least in principle, the microprobe scan can be used to determine the refractive index profile quantitatively (Refs.15,17). In practice, the glass refractive index may show a further dependence upon the method of quenching during fibre manufacture (Ref.18).

The best spatial resolution that can be obtained with the microprobe is approximately 1μm. Other modes of operation of the SEM, such as absorbed electron and backscattered electron imaging, offer greater spatial resolution than the microprobe analysis, without the need for etching the sample as required for the secondary electron image. These additional modes of operation provide results that can be correlated with the microprobe scan, thus ensuring that the measured dopant variations are related to the fibre properties and not to any environmental considerations such as contamination or dust particles.

4.2 Near-Field Scanning

Many different methods have been developed to measure the refractive index profiles of optical fibres (Ref.19). Of these available techniques, near-field scanning is the most rapid and most convenient. This technique relies upon the close resemblance that exists between the near-field intensity distribution of an optical waveguide, with all modes equally excited, and the refractive index profile.

4.2.1 Theory The theoretical basis for the near-field scanning measurement has been well documented (Refs.20,21,22,23) so that only a brief summary is presented here. When a straight length of low-loss, circularly symmetrical optical fibre is illuminated by a Lambertian source, (exciting all modes uniformly), the power distribution at the output face of the fibre due to the contributions of all the guided modes is (Refs.5,19)

$$P(r) / P(o) = \left[n(r)^2 - n(a)^2\right] / \left[n(o)^2 - n(a)^2\right] . \qquad (6)$$

For small values of Δn_m, as encountered in practical fibres, this equation can be re-expressed in the form

$$n(r) - n(a) \doteqdot K.P(r) / P(o) \qquad (7)$$

where $K = \Delta n_m n(o)$ is a constant for any particular fibre. Burrus et al. (Ref.17) employed the above relationship between the refractive index profile and the near-field intensity distribution to obtain qualitative information about the refractive index profiles of several optical fibres. This they did simply by recording the intensity variation across a diameter of the fibre output face.

Because short lengths (typically <1m) of fibres are studied experimentally, the presence of tunnelling leaky modes introduces an additional intensity contribution above that provided by the guided modes alone. This creates an error in the refractive index profile as inferred from the measured near-field intensity distribution. The magnitude of this error decreases with fibre length, z, as the leaky modes attenuate, but may still be significant after 100m. To eliminate this inaccuracy, Payne et al. (Refs.20,21,22,23) introduce a length-dependent correction factor, C(r,z), to equation (7) to determine that

$$n(r)-n(a) \doteqdot K.\left[P(r) / P(o)\right] . \left[1 / C(r,z)\right]. \qquad (8)$$

In its most general form (Refs.21,22) C(r,z) is itself a function of the fibre refractive index profile, so that utilization of the near-field scanning technique would seem to require prior knowledge of the behaviour of the refractive index profile. Fortunately, the correction factor is not a sensitive function of this profile. Thus a single set of curves, C(r,z) has been published (Refs.22,23) as a function of a fibre normalization parameter

$$X = (1/V) \ln (z/a) . \qquad (9)$$

Here

$$V = ak\left[n(o)^2 - n(a)^2\right]^{\frac{1}{2}}$$

$$= ak\,(NA) \qquad (10)$$

is the normalized frequency and $k = 2\pi/\lambda$ is the free space wave vector at the wavelength λ.

The effect of the correction factor is illustrated in Fig.6 for the cases of ideal step and parabolic graded index fibres. In these plots the corrected near-field intensity is a precise description of the fibre refractive index profile.

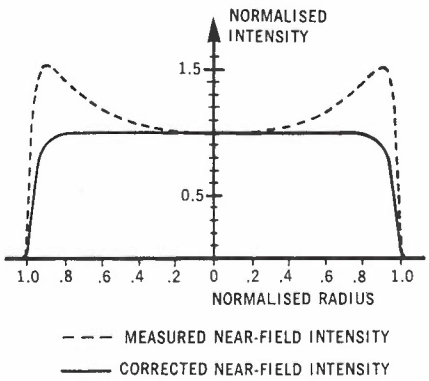

[FIBRE N.A. = 0.26, a = 45 μm, z = 30 cm, λ = 0.93 μm]

(a) STEP INDEX FIBRE

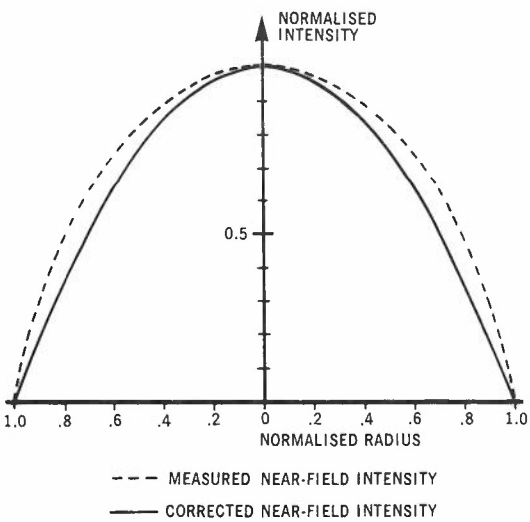

[FIBRE N.A. = 0.31, a = 51 μm, z = 35 cm, λ = 0.8 μm]

(b) GRADED INDEX FIBRE

Fig.6 - Measured and corrected near-field intensity patterns for step index and parabolic graded index fibres (after Sladen et al. Ref.21).

Recent results (Refs.24,25) indicate that the uncorrected near-field intensity profile often agrees better with the actual fibre refractive index profile than does the corrected intensity distribution. This discrepancy arises particularly with graded index fibres of near-parabolic index profile. A theoretical investigation (Ref.26) shows that small deviations from circular symmetry in this type of fibre cause a dramatic increase in the attenuations of the leaky modes. Therefore it is to be expected that the near-field intensity measurement of practical fibres, which generally exhibit a small degree of asymmetry, should not be corrected if the index profile is near-parabolic.

4.2.2 Advantages and Limitations The preceding theoretical discussion highlights several attractive features of the near-field scanning technique. The measurement produces a direct description of the fibre refractive index profile and an accurate value of the index exponent, α, (refer equation (3)) can be determined. Near-field scanning is very sensitive to small index variations. Equation (8) indicates that the optical power distribution is essentially proportional to the index difference; hence in a quartz fibre of NA = 0.2, a 0.1% change in refractive index causes a 10% change in the measured intensity.

The method, however, has the disadvantage that it does not provide absolute values for either n(o), n(a) or Δn_m, which must be obtained by some alternative means. Indeed the above discussion indicates, via equations (9) and (10), that a knowledge of the fibre NA is essential to deduce the near-field intensity correction factor. A convenient technique for establishing the fibre NA is to measure the far-field intensity radiation pattern of a short length of the fibre when excited by an incoherent Lambertian source. Then

$$NA = \sin \theta_c \;\doteqdot\; n(o)\,(2\Delta n_m)^{\frac{1}{2}} \qquad (11)$$

where, by the converse of the argument contained in Section 1, θ_c is the maximum radiation semi-angle in air. Typically θ_c is defined at the -3dB point from maximum intensity (Ref.24).

4.2.3 Spatial Resolution An important consideration is the desired spatial resolution for the near-field scanning measurement. The highest resolution that can be achieved, in theory, is fixed by wave optic considerations (Ref.24). Because a practical fibre can support only a finite number of guided modes (Ref.5), the intensity distribution cannot follow the fine details of the refractive index profile. The optical field cannot vary in the transverse directions faster than $(\sin k_{x_{max}} x)$ where

$$k_{x_{max}} = k\,(NA) \qquad (12)$$

is the maximum value of the transverse wave vector (Ref.24). Hence the minimum distance between nodes and peaks of the intensity distribution is

$$\Delta x = \lambda/4(NA) \qquad (13)$$

This expression provides an estimate of the highest spatial resolution that can be achieved

with near-field scanning; for example, if $\lambda = 0.8\mu m$ and NA = 0.2, then $\Delta x = 1\mu m$. To faithfully resolve these most rapid intensity variations requires a spatial resolution of at least 1:200, assuming a = 50μm. It is interesting to note that this wave-optic imposed resolution limit is comparable to the thickness of the outer layers in a typical fibre, as described in Section 3. A near-field intensity plot should contain information that would indicate any perturbation in the glass composition of the broad inner layers of an MCVD fibre. On the other hand, the wave optic spatial resolution limit may prohibit the observation, in a near-field intensity plot, of a similar perturbation in a narrower outer glass layer.

The wave optic argument emphasizes that the near-field scanning technique for measuring refractive index profiles is based on a geometrical model. For this reason the technique cannot be applied to fibres of low V number (as defined in equation (10)). Such fibres support only a few modes (Ref.5) and modal effects predominate (Ref.27).

4.2.4 System Arrangement A typical near-field scanning arrangement (Ref.21) can be described as follows. A spacially incoherent Lambertian source (generally a tungsten filament lamp with a diffuser and spectral filter) excites a short, straight length of the fibre, which must have flat end faces. A microscope objective, focused on the output face of the fibre, projects an image of that illuminated face into the plane of an apertured photo-detector which scans this field transversely. The projected light beam is chopped, usually at 1 KHz, so that phase-sensitive detection can be used to improve the signal-to-noise ratio. The intensity profile is plotted directly on an x-y recorder.

Figure 7 depicts, in block diagram form, the particular near-field scanning system developed at the Telecom Australia Research Laboratories for the specific purpose of high resolution profiling of MCVD fibres (Refs.28,29). This system incorporates two novel features not found in the typical scanning arrangement described earlier. Firstly, the light source is a pulsed high-intensity flashlamp. Secondly, the entire measurement process is controlled by minicomputer (Ref.30). This versatile system can achieve, simultaneously, spatial and intensity resolutions of better than 0.5% in its normal mode of operation (Ref.29).

5. EXPERIMENTAL RESULTS

Each of the techniques of examination described in Section 4 provides valuable information about the small-scale structural characteristics of optical fibres. But it is frequently difficult to place an accurate physical interpretation upon the fine details observed in each individual measurement. For example, small localized variations in the near-field intensity plot could be due to structural characteristics of the fibre established during the fabrication process. Alternatively, they could result from noise in the measurement system, extraneous factors such as dust particles on the fibre output face, or modal effects due to the fibre possessing only a small or moderate V value. The most effective method of verification is to correlate results from the near-field scan and the various methods

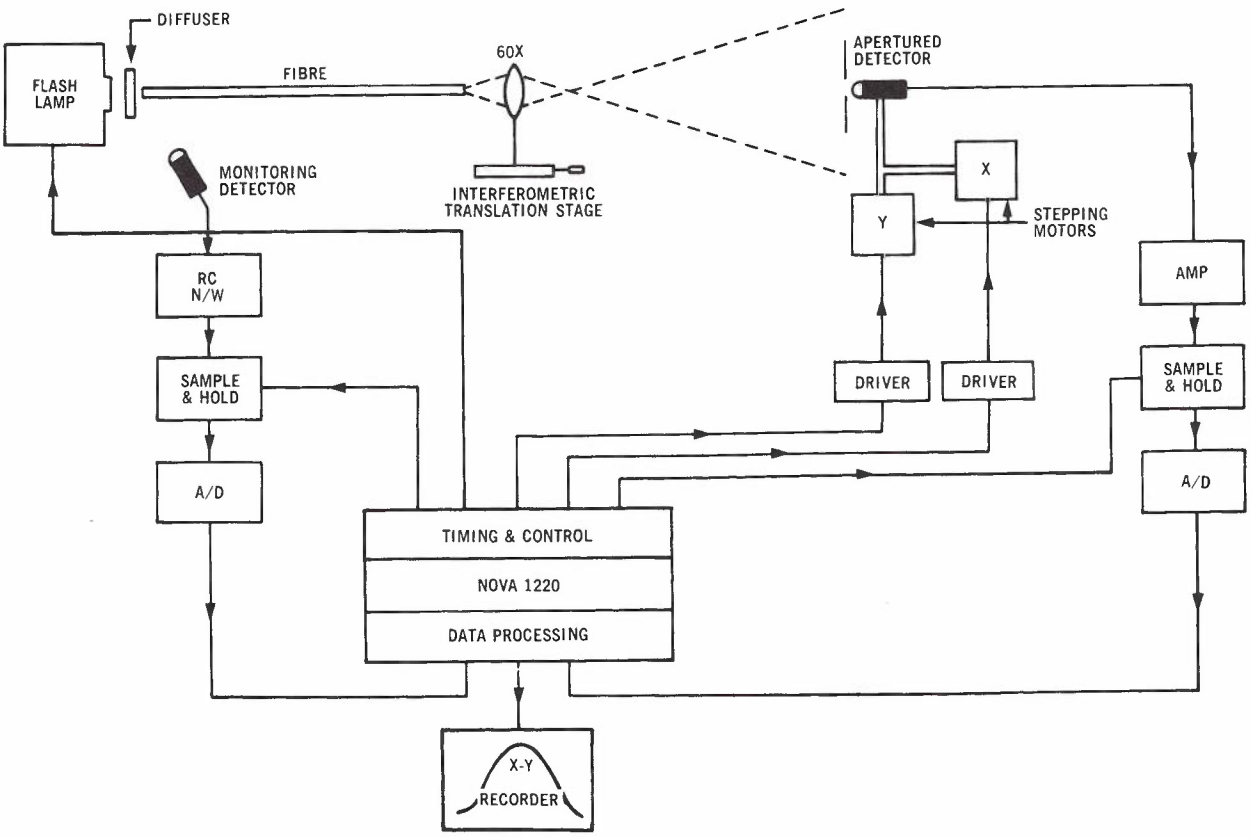

Fig.7 - Near-field scanning system.

of SEM examination (Ref.31). Typical sets of correlated results for a step index and a barrier layer optical fibre, manufactured by AWA, in Sydney, are now presented. Details of the MCVD fabrication process for these two fibres are listed in Table 1.

5.1 AWA Step Index Fibre 121

Secondary electron micrographs of end-faces of AWA step index fibre 121, which have been etched briefly in hydrofluoric acid, are shown in Fig.8. Note that the pure silica cladding is virtually untouched whereas the phosphorus-doped core has been attacked by the acid. Since the etch rate increases with increasing dopant level, the central peak in the core material corresponds to a region of reduced phosphorus concentration, and hence a region of lower refractive index. Obviously this results from the dopant volatilization problem described in Section 3. Smaller perturbations highlighted by the etching process are three rings. Equation (4) and the fabrication data of Table 1 have been used to demonstrate that these rings correspond to the 5th, 7th-8th and 11th deposited layers. The three rings result from small localized decreases in the phosphorus dopant concentration in these layers. However the great majority of the 17 individual core layers in this fibre have not been revealed by the etching process - a fact indicative of a comparatively homogeneous core region. Figure 8 also illustrates the fibre asymmetry introduced in the preform collapse stage (Ref.9).

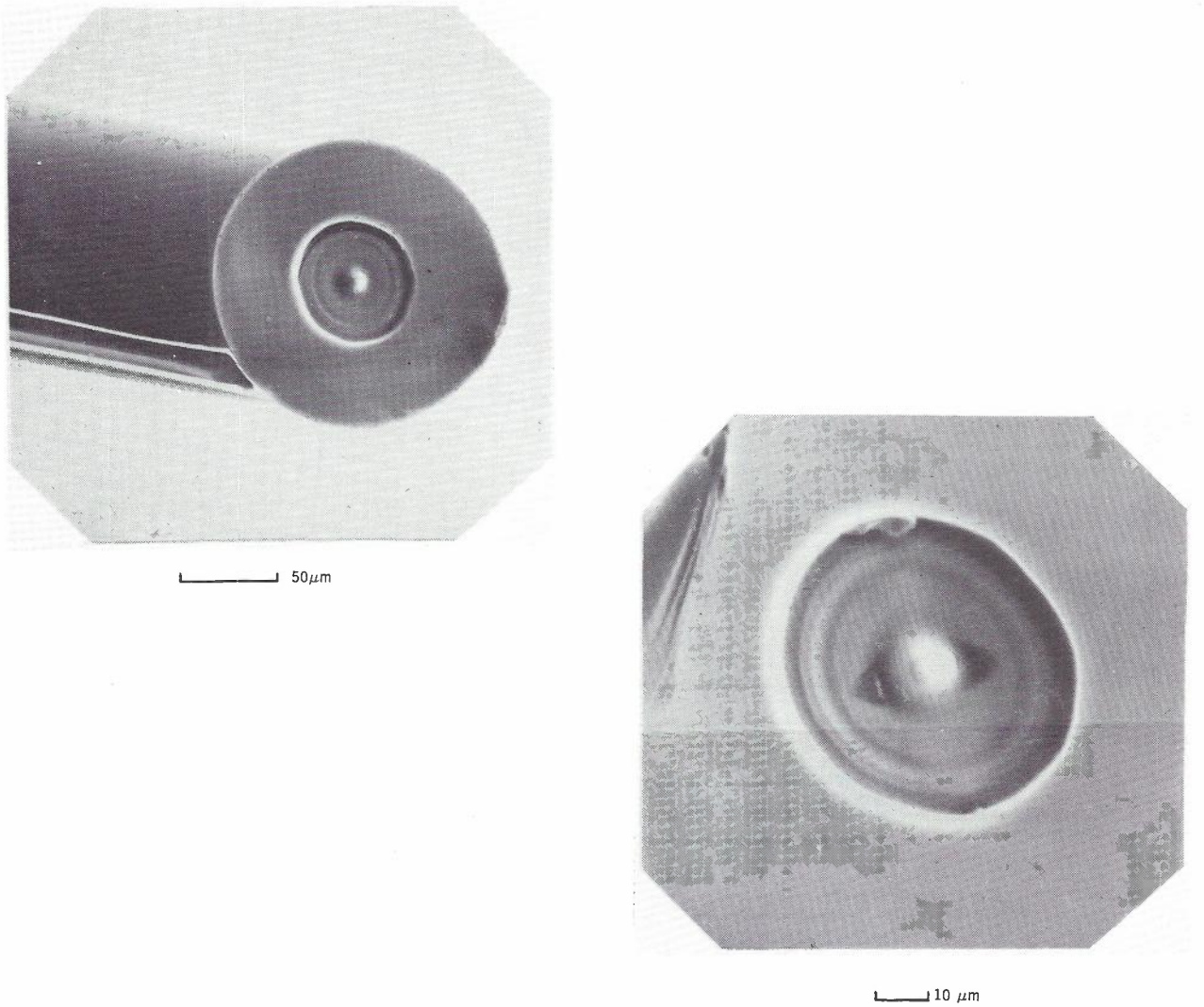

Fig.8 - Secondary electron micrographs of the etched end face of AWA step index fibre 121.

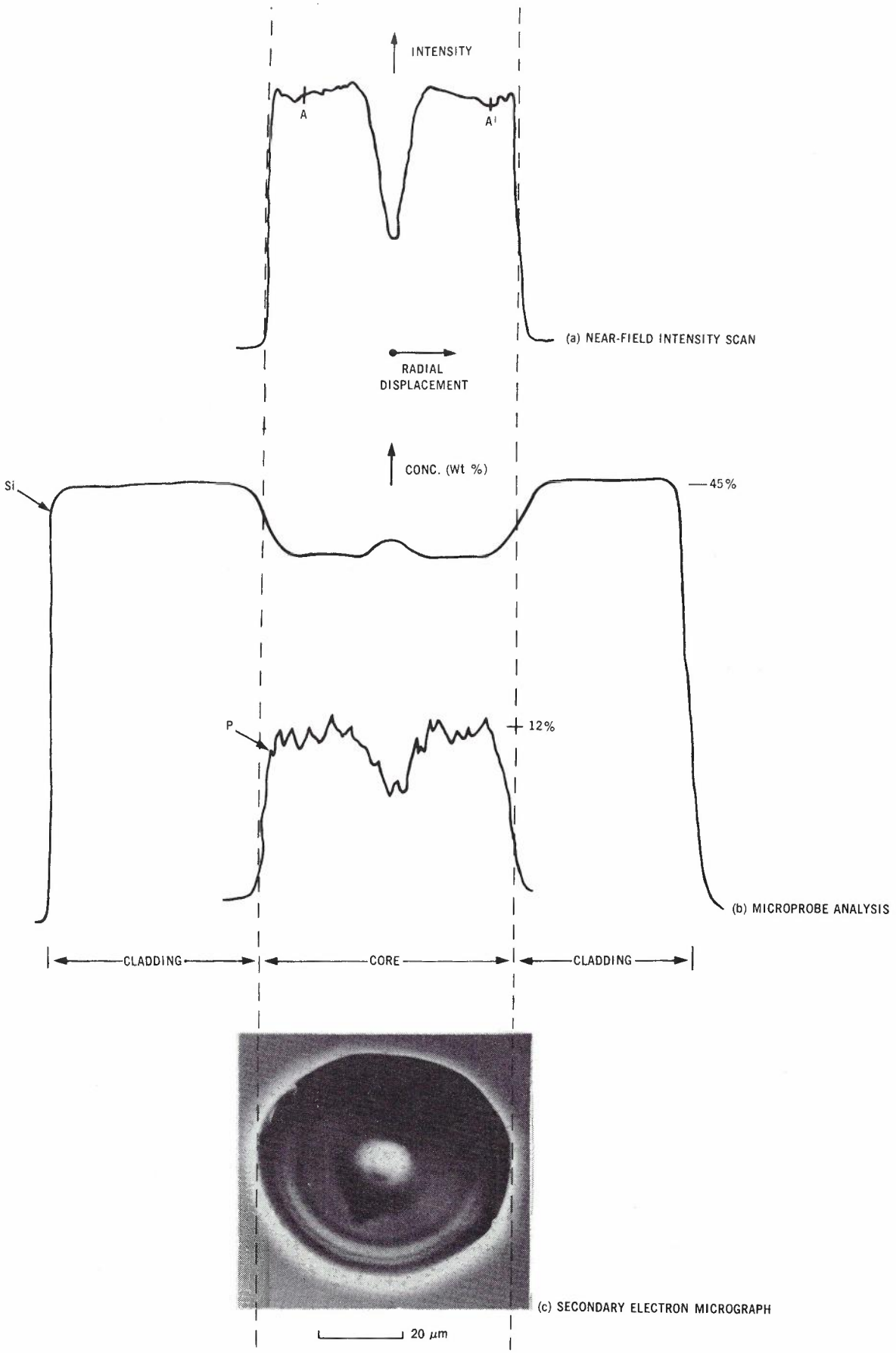

Fig.9 - The near-field intensity scan, microprobe scan and corresponding secondary electron micrograph of AWA step index fibre 121.

The uncorrected near-field intensity scan, Fig.9(a), reveals the region of dopant volatilization as a central dip in the measured intensity. From this graph and equation (4), it can be deduced that dopant volatilization is confined largely to the last deposited layer. The same equation indicates the correspondence between the etched ring structures observed in the secondary electron images and the small deviations in the near-field intensity distribution. For this purpose, the secondary electron micrograph, Fig. 9(c), has been aligned with the direction of the transverse near-field scan. The most prominent of the two etched rings can be correlated with the intensity minimum AA' in Fig.9(a). However, the same scan shows that these two perturbations have little effect upon the near-field intensity distribution.

A comparison of Figs.9(a) and 6(a) emphasizes that the near-field intensity plot of step index fibre 121 exhibits almost no leaky mode contribution in the form of intensity peaks at the core-cladding interface. This is in spite of the comparatively short length, 15cm., of fibre used in this measurement. One possible explanation, in the light of the discussion of Section 4.2.1, may centre upon the comparatively high core ellipticity of 10% (Ref.9).

Fig.9(b) is the SEM microprobe of this fibre. Plots of the silicon and phosphorus concentrations across a diameter of the fibre end-face are presented. Again the central region of phosphorus volatilization is apparent. The microprobe capability is being developed further to improve resolution and to permit an accurate calibration of dopant concentration against refractive index (Ref.18).

5.2 AWA Barrier Layer Fibre 172

Secondary electron micrographs of a cleaved and etched end-face of AWA barrier layer fibre 172 are shown in Fig.10. These micrographs reveal that the pure silica cladding layer remains virtually unaffected by the dilute hydrofluoric acid, while the barrier layer of borosilicate glass has been lightly etched. The phosphosilicate glass core has been attacked more rapidly. Two rings of phosphosilicate glass have etched at a slightly slower rate than the rest of the core material. Once more, equation (4) and the fabrication data of Table 1 can be invoked to disclose that these perturbations arise from a slightly reduced phosphorus concentration in the 9th and 17th deposited core layers. Dopant volatilization is evidenced, as usual, by the central peak in the etched end-faces. Although this fibre is of high numerical aperture, the circular symmetry has been improved considerably in comparison with fibre 121. This improvement was achieved by maintaining a slight positive pressure inside the silica support tube during the preform collapse stage of the manufacturing process (Refs.7,9).

The uncorrected near-field intensity scan, Fig.11(a), of a 15cm. length of fibre, contains evidence of a small leaky mode contribution at the core-barrier layer interface. In comparison with the scan for fibre 121, the central intensity (and hence refractive index) dip is reduced in magnitude. Furthermore, dopant volatilization has been confined entirely to the final deposited glass layer. The two rings of more lightly doped phosphosilicate glass can be correlated with the localized intensity minima A' and B' in Fig.11(a). Clearly the effect of these per-

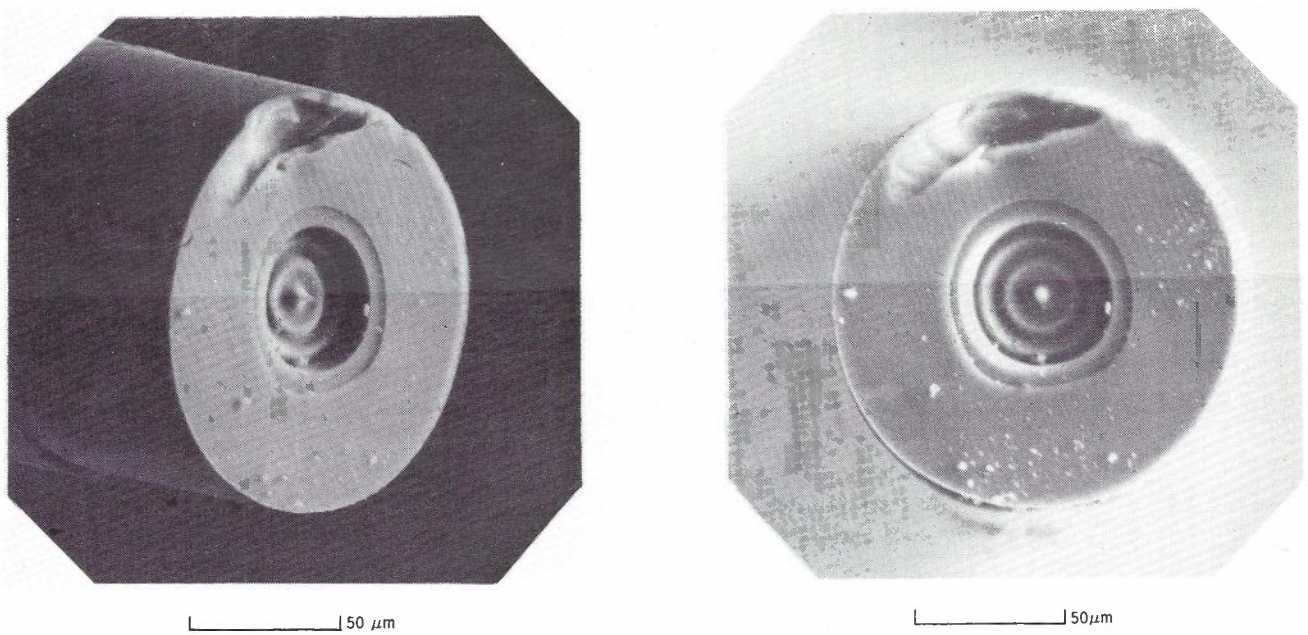

Fig.10 - Secondary electron micrographs of the etched end face of AWA barrier layer fibre 172.

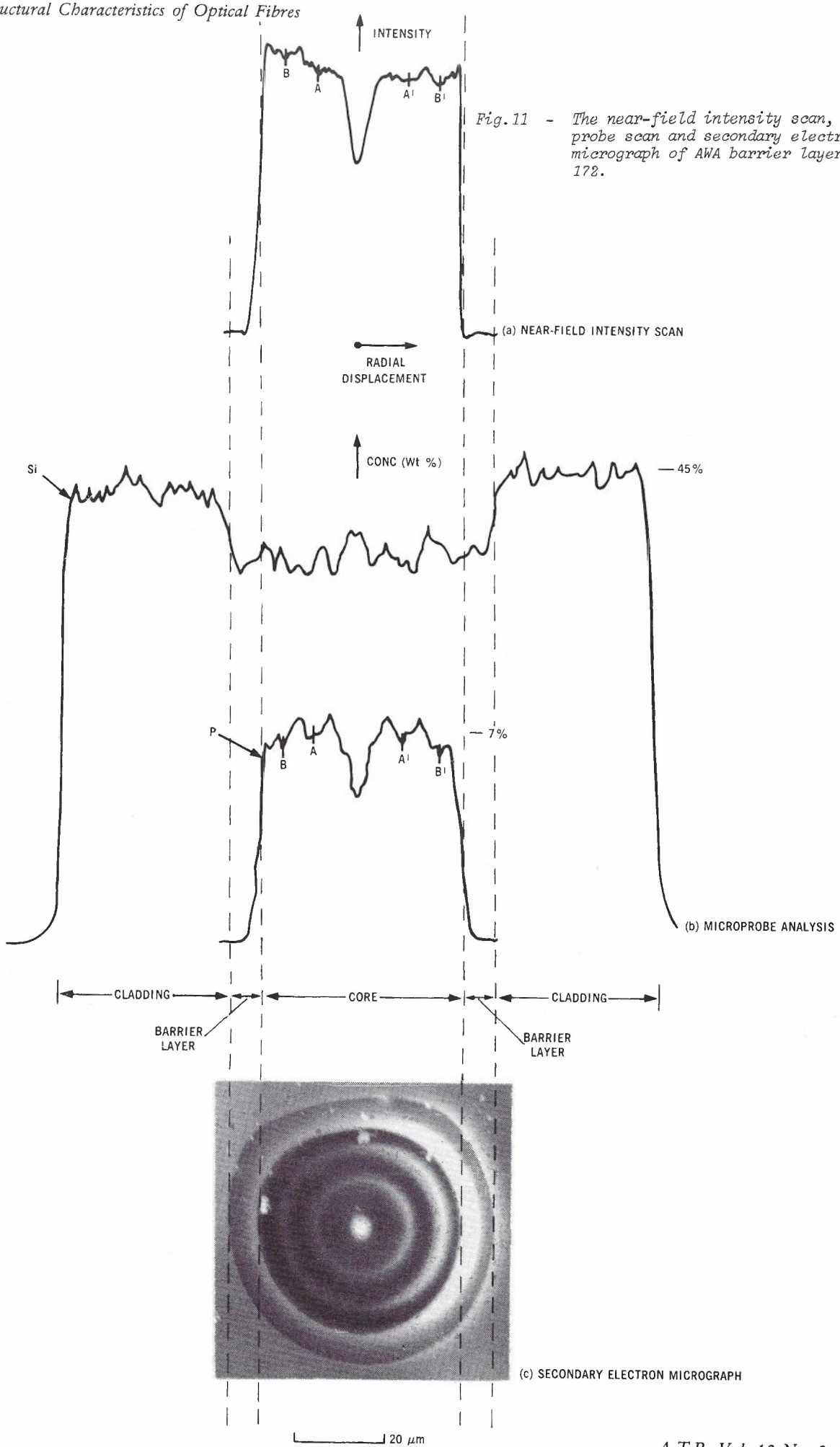

Fig. 11 - The near-field intensity scan, microprobe scan and secondary electron micrograph of AWA barrier layer fibre 172.

turbations upon the near-field intensity distribution, and consequently upon the refractive index profile, has been small. That a similar correlation with localized intensity minima A and B in corresponding locations on the left-hand side of the near-field plot is not so evident, may be due to either of two possible factors. Firstly, in preparing the flat fibre end-faces, there is a tendency for the fibre to break along a plane that is not perfectly normal to the fibre axis (Ref.32). The microscope objective that projects the fibre image for near-field scanning must be of high magnification, and hence small depth of focus. These factors combine to make uniform focus over the entire fibre end-face difficult to achieve. Secondly, the fibre possesses a small degree of asymmetry. Unless the exact scanning paths across the fibre face are known, the complete correlation of results is a formidable task.

Silicon and phosphorus microprobe scans of this fibre are provided in Fig.11(b). The extent of phosphorus volatilization can be observed. The two rings evident in the secondary electron images of the etched end-face, shown at greater magnification in Fig.11(c), correlate with the valleys AA' and BB' in the phosphorus concentration profile. A comparison of the silicon and phosphorus traces makes obvious the presence of a barrier layer.

6. CONCLUSION

Of the many techniques that have been developed to study the structural characteristics of practical MCVD fibres, the combination of near-field scanning and SEM examination proves to be a powerful analytical tool.

The study of etched fibre end-faces with the secondary electron mode of the SEM is an extremely sensitive method of observing small-scale structural characteristics and inhomogeneities. In some instances this approach is too sensitive, as imperfections that do not significantly perturb the fibre refractive index profile may have the appearance of major irregularities in SEM micrographs. A limitation of this method is that quantitative information about the fibre refractive index profile cannot be produced.

Near-field scanning is a rapid and convenient technique for determining the refractive index profile. The automated scanning system described in this paper makes this technique even more attractive. As discussed in Section 4.2, limitations of near-field scanning include the fact that absolute values of the core and cladding refractive indices, or of the relative difference in these indices, must be obtained by a separate measurement. Furthermore, attempts to place physical interpretations upon the fine structure recorded in the near-field intensity plot may prove difficult or misleading.

SEM microprobe analysis complements both of the above-mentioned methods of optical fibre examination. In the MCVD fibre fabrication process it is the addition of different dopants, in various controlled concentrations, that is the key to establishing the optical transmission characteristics of the fibre, notably the refractive index profile. Because a microprobe analysis records dopant concentrations within a finished fibre, it is a measurement that can be related directly to specific aspects of the fabrication process. The glass refractive index depends not only upon dopant concentration, but also upon the thermal history of the material; in particular, upon the quenching of the fibre following the high temperature drawing process. However each manufacturer standardizes the procedures involved in the MCVD process for his own particular facility. Thus it is planned to extend the microprobe measurement, by empirical calibration, to allow a quantitative refractive index profile to be inferred from the plots of dopant concentration.

There are many possible causes of, and explanations for, the small-scale variations observed in any one of the fibre measurement techniques. The examples discussed in Section 5 serve to illustrate that the greatest understanding of the fibre structural characteristics can be obtained only by correlating results from all three methods. Two purposes are fulfilled by this correlation process. Firstly, it provides verification that a particular characteristic

TABLE 1 - MCVD Fabrication Data for AWA Optical Fibres

FIBRE IDENTIFICATION NUMBER	121	172	242
Fibre type	Step Index	Barrier Layer-Step Index	Barrier Layer-Step Index
Cladding material	SiO_2	SiO_2	SiO_2
Barrier layer dopant	-	B_2O_3	B_2O_3
Core dopant	P_2O_5	P_2O_5	P_2O_5
Number of barrier layers deposited	-	13	11
Number of core layers deposited	17	20	11
Number of collapse passes	6	3	3
Numerical aperture	0.14	0.20	0.22

observed by one method is indeed due to a physical property of the fibre rather than to some extraneous effect. Secondly, it ensures the most accurate interpretation and efficient utilization of the available data - both from an individual measurement and collectively from the three techniques.

This paper has focused attention upon the structural characteristics of MCVD fibres that cause the fibre properties, and particularly the refractive index profile, to depart from the ideal. These structural characteristics are inherent in the MCVD process and are not confined to fibres fabricated by any one manufacturer. Furthermore, it is generally found that these structural characteristics exert only a second order effect upon the fibre transmission performance, as indicated by the attenuation and bandwidth. The optical transmission properties of all three fibres discussed in this paper were such that the fibres were well suited to telecommunications applications. For example, the barrier layer step-index fibre 242 offers a large NA of 0.22, low ellipticity (<2%) of core and cladding, and a low attenuation of 3.4dB/km at a wavelength of 850nm.

In conclusion, the information obtained from these measurements is important in at least two areas. First, the systems engineer can use the data as inputs to obtain estimates of fibre bandwidth, attenuation and jointing loss. Second, quantitative information concerning the structural characteristics of the fibre provides feedback to the manufacturer and in this way facilitates the fabrication of fibres with improved properties and greater reproducability.

7. ACKNOWLEDGEMENTS

The authors are grateful to D. Nicol, C. Storey and F. Donaghy of AWA for supplying fibre samples and MCVD fabrication data. Valuable technical support was provided by P. Francis and G. Wood. G. Stone and P. Elliott are thanked for their contribution to the minicomputer control of the scanning system.

8. REFERENCES

1. Payne, D.N. and Gambling, W.A., "New Silica-Based Low-Loss Optical Fibre", Electron. Lett., July 1974, Vol.10, No.15, pp.289-290.

2. Horiguchi, M. and Osanai, H., "Spectral Losses of Low-OH-Content Optical Fibres", Electron. Lett., June 1976, Vol.12, No.12, pp.310-312.

3. Donaghy, F.A., Nicol, D.R. and Storey, C.H., "Advances in Optical Fibre Fabrication and Characterization", Proc. IREECON Intl., Melbourne, Aug. 1977, pp.299-301.

4. Miller, S.E., Marcatili, E.A.J. and Li, T., "Research Toward Optical-Fibre Transmission Systems. Part 1: The Transmission Medium", Proc. IEEE, Dec. 1973, Vol.61, No.12, pp.1703-1726.

5. Gloge, D. and Marcatili, E.A.J., "Multimode Theory of Graded-Core Fibres", Bell Syst. Tech. J., Nov. 1973, Vol.52, No.9, pp.1563-1578.

6. Nicol, D.R., "Low-Loss Optical Fibre Manufacturing Technology", Proc. IREE (Aust.), Jan/Feb. 1977, Vol.38, No.1, pp.403-407.

7. Gambling, W.A., Payne, D.N., Hammond, C.R. and Norman, S.R., "Optical Fibres Based on Phosphosilicate Glass", Proc. IEEE, June 1976, Vol.123, No.6, pp.570-576.

8. Nicol, D.R., "Manufacture of Optical Fibres", AWA Tech. Report. R76-59, Sept. 1976.

9. Nicol, D.R., "Manufacture of Optical Fibres", AWA Tech. Report R77-7, Feb. 1977.

10. French, W.G., Tasker, G.W. and Simpson, J.R., "Graded Index Fiber Waveguides with Borosilicate Composition : Fabrication Techniques", Appl. Opt., July 1976, Vol.15, No.7, pp.1803-1807.

11. Akamatsu, T., Okamaru, K. and Ueda, Y., "Fabrication of Graded-Index Fibers Without an Index Dip by Chemical Vapour Deposition Method", Appl. Phys. Lett., Oct. 1977, Vol.31, No.8, pp.515-517.

12. Presby, H.M., Standley, R.D., MacChesney, J.B. and O'Connor, P.B., "Material-Structure of Germanium-Doped Optical Fibres and Preforms", Bell Syst. Tech. J., Dec. 1975, Vol.54, No.10, pp.1681-1692.

13. Burrus, C.A. and Standley, R.D., "Viewing Refractive Index Profiles and Small-Scale Inhomogeneities in Glass Optical Fibres : Some Techniques", Appl. Opt., Oct. 1974, Vol.13, No.10, pp.2365-2369.

14. Gloge, D., Smith, P.W., Bisbee, D.L. and Chinnock, E.L., "Optical Fiber End Preparation for Low-Loss Splices", Bell Syst. Tech. J., Nov. 1973, Vol.52, No.9, pp.1579-1588.

15. Johansen, E., "Characterizing Optical Fibres Using a Scanning Electron Microscope", First Australian Workshop on Optical Communications, Sydney, March 1977.

16. Maissel, L.I. and Glang, R., "Handbook of Thin Film Technology", 1970, McGraw Hill, pp.11.43-11.44.

17. Burrus, C.A., Chinnock, E.L., Gloge, D., Holden, W.S., Li, T., Standley, R.D. and Keck, D.B., "Pulse Dispersion and Refractive Index Profiles of Some Low-Noise Multimode Optical Fibres", Proc. IEEE, Oct. 1973, Vol.61, No.10, pp.1498-1499.

18. Katsuyama, T., Suganuma, T., Ishida, K. and Toda, G., "Refractive Index Behaviour of SiO_2-P_2O_5 Glass in Optical Fiber Application", Optics Commun., April 1977, Vol.21, No.1, pp.182-184.

19. Sabine, P.V.H., "Refractive Index Profile Determination in Optical Waveguides", Aust. Tele. Res., May 1977, Vol.11, No.2, pp.3-13.

20. Payne, D.N., Sladen, F.M.E. and Adams, M.J., "Index Profile Determination in Graded Index Fibres", Proc. First European Conference on Optical Fibre Communication, Sept. 1975, pp.43-45.

21. Sladen, F.M.E., Payne, D.N. and Adams, M.J., "Determination of Optical Fibre Refractive Index Profiles by a Near-Field Scanning Technique", Appl. Phys. Lett., March 1976, Vol.28, No.5, pp.255-258.

22. Adams, M.J., Payne, D.N. and Sladen, F.M.E., "Length-Dependent Effects due to Leaky Modes on Multimode Graded-Index Optical Fibres", Opt. Commun., May 1976, Vol.17, No.2, pp.204-209.

23. Adams, M.J., Payne, D.N. and Sladen, F.M.E., "Correction Factors for the Determination of Optical-Fibre Refractive Index Profiles by the Near-Field Scanning Technique", Electron. Lett., May 1976, Vol.12, No.11, pp.281-283.

24. Arnaud, J.A. and Derosier, R.M., "Novel Technique for Measuring the Index Profile of Optical Fibres", Bell Syst. Tech. J., Dec. 1976, Vol.55, No.10, pp.1489-1508.

25. Costa, B. and Sordo, B., "Measurement of the Refractive Index Profile in Optical Fibres : Comparison Between Different Techniques", 2nd European Conference on Optical Fibre Transmission, Paris 1976.

26. Petermann, K., "Uncertainties of the Leaky Mode Correction for Near-Square-Law Optical Fibres", Electron. Lett., Aug. 1977, Vol.13, No.17, pp.513-514.

27. Bianciardi, E., Rizzoli, V. and Someda C.G., "Spatial Correlation of Field Intensity in Incoherently Illuminated Multimode Fibres", Electron. Lett., Jan. 1977, Vol.13, No.1, pp.25-26.

28. Sabine, P.V.H., "Near-Field Scanning Systems for Measuring the Refractive Index Profiles of Optical Waveguides", First Australian Workshop on Optical Communications, Sydney, March 1977.

29. Sabine, P.V.H., "A Near-Field Scanning System for Determining the Refractive Index Profiles of Multimode Optical Fibres", Telecom Australia, Res. Lab. Report No.7182, 1978.

30. Stone, G.O., "A System for Evaluation of High-Radiance Light-Emitting Diodes for Optical Fibre Sources", First Australian Workshop on Optical Communications, Sydney, March 1977.

31. Sabine, P.V.H. and Johansen, E., "Structural Characteristics of Optical Fibres Manufactured by a CVD Process", Proc. IREECON Intl., Melbourne, Aug. 1977, pp.302-304.

32. Gordon, K.S., Rawson, E.G. and Nafarrate, A.B., "Fiber-break Testing by Interferometry : A Comparison of Two Breaking Methods", Appl. Opt., April 1977, Vol.16, No.4, pp.818-819.

BIOGRAPHY

ED JOHANSEN received the Degree of Bachelor of Engineering with First Class Honours in 1970 from the University of Western Australia. He joined the Solid State and Quantum Electronics Section of the Research Laboratories of Telecom Australia in 1974. His current interests include the epitaxial growth of thin semiconductor films and specialized studies using the recently established Scanning Electron Microscope facility. The characterization of optical fibres using various imaging modes and microprobe techniques is one such study.

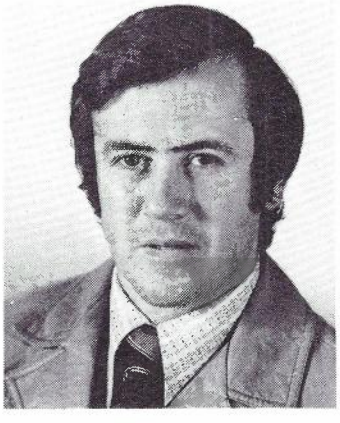

BIOGRAPHY

HARVEY SABINE received the degrees of B.Sc. and B.E., with first class honours, from the University of Adelaide in 1966 and 1968, respectively. The same University awarded him a Ph.D. in 1973 for research in the field of surface acoustic wave devices. In 1972 he joined the Solid State and Quantum Electronics Section of the Research Laboratories of Telecom Australia, where currently he holds the position of Senior Engineer. His present interests include laser sources and modulators, terminal devices for optical fibre communication links and components for integrated optical circuits.

Comparison of Rain Attenuation Predicted by Radar and Distrometer with Attenuation Measured with a Radiometer

P.V. LAATS[1]
Department of Administrative Services
A.D.P. Section
Canberra

R.C. BOSTON
School of Agriculture
La Trobe University
Melbourne

J.A. BENNETT[2]
Department of Electrical Engineering
Monash University
Melbourne

Reasonable agreement was found between predicted and measured attenuation. However, a very high degree of precision is required in the radar calibration. Besides establishing a statistical relation between attenuation and radar return, the distrometer can provide information about rain in the dead zone of the radar. For elevated paths, the neglect of this region can lead to serious error. At low attenuations there may be significant attenuation (0.5 to 1dB at 11GHz) due to drops too small to be observed by the distrometer or radar.

1. INTRODUCTION

If quantitative estimates of the attenuation of microwave radiation passing through a volume containing rain can be obtained from measurements of the radar return from the rain, this will greatly aid the gathering of data required for the design of a satellite communications system operating at microwave frequencies. Measurements at a single radar frequency can be used to estimate attenuation at any frequency of interest.

Also, by operating the radar in a scanning mode, a large number of different paths may be examined. This would make possible the investigation of the optimum location of earth stations and possible space diversity schemes. To the extent that different paths may be regarded as samples from the same statistical population, they may be used to increase the sample size and reduce the time required to obtain significant statistics.

There are, however, some uncertainties in the applicability of the theory and limited success has been reported in experiments designed to directly verify the relation between radar returned power and attenuation (Refs.1,2). An early attempt was made by Crane (Ref.3), McCormick (Ref.4), Strickland (Ref.5) and Joss et al. (Ref.6) reported good agreement but in each case the radar was not fully calibrated (see Section 3.2). Recently Goldhirsh has reported an experiment with the fully calibrated Wallops Island radar (Ref.7).

Because of the ambiguities between theory and measurements, and the potential value of calculating attenuation from radar measurements, an experimental verification of the technique was planned. Had the results of Goldhirsh been reported at that time, the experiment would still have been worth undertaking, as are further experiments today.

The experiment set up involved the radar at the same fixed azimuth and elevation as a radiometer located within some 20 m of the radar. This mode of operation simplified comparison of the radar derived attenuation with that measured with the radiometer operating in the sky temperature mode and gave good time resolution. A distrometer (Ref.8) was located near the radar so that the drop-size distribution could be sampled every 30 sec. The theoretical basis of the experiment is discussed in Section 2.

---

1. Formerly with the Bureau of Meteorology.
2. Formerly, Radio Research Board Fellow, Telecom Research Laboratories, Melbourne.

It was realized that the dead zone of the radar (about 3 km) would lead to some problems. These turned out to be more severe than anticipated. In order to fill in the gap caused by the dead zone, initially the radar return from the first valid range gate was extrapolated. It was found that generally this was not as successful as using the distrometer data. The results of both techniques are discussed in this paper.

2. THEORY

The theoretical basis of the relation between radar echo power and the attenuation of a microwave signal passing through the same rain filled region is indicated briefly here. More details will be found in (Ref.2) and papers referred to there, and in (Refs.9 and 10). A significant limitation is that nothing is learned about the bi-refractivity of the medium. However, the theory might be extended to deal with both modes and the use of a dual polarization radar.

2.1 Radar Backscatter

Suppose the number of drops of diameter D per unit increment in diameter, per unit volume, N_D is known. Then the backscatter cross section per unit volume can be calculated. At the frequencies used in meteorological radar, the Rayleigh theory is valid for backscatter. Hence, the ability of the drops to backscatter is usually measured in terms of the reflectivity factor

$$Z = \int_0^\infty N_D D^6 \, dD \quad . \qquad (1)$$

Z is often measured in units of $(mm)^6 m^{-3}$. Neglecting attenuation, the average power returned to the radar, $\bar{P}_r$ is given by (Ref.11)

$$\bar{P}_r = 1.31 \times 10^7 \, P_t \, \tau \frac{G^2 \theta \phi}{\lambda^2} \left| \frac{m^2 - 1}{m^2 + 1} \right|^2 \frac{Z}{r^2} \, . \qquad (2)$$

Here $\bar{P}_r$ is the average received power, P_t the transmitted power, λ the wave-length, τ the pulse length, G the antenna gain, and θ and ϕ the antenna 3 dB beam widths in radians. The reflectivity factor is expressed in $m^6 m^{-3}$, i.e. in m^3. The factor $|(m^2-1)/(m^2+1)|^2$ is usually taken as 0.93 for the 3 GHz to 10 GHz range. The numerical factor (units $m\ s^{-1}$) takes account of the fact that the antenna gain is not constant across the main lobe and of the effect of a pulse matched receiver.

In operating a calibrated radar, the only unknown on the right hand side of (2) is Z. Hence, if attenuation at the radar frequency may be neglected, measurements of the returned power received by the radar allow Z to be determined as a function of range and radar beam direction. Because of the noise-like character of the radar echo it is not possible to measure Z at a point in space and instant in time. It is necessary to average the received signal over time and or space (Refs.10,11,12). This limit on resolution is usually more severe than that imposed by antenna beam width, pulse length and repetition rate.

2.2 Attenuation

Knowing N_D, it is also possible to calculate the attenuation per kilometre or specific attenuation Y dB km^{-1}. The underlying idea is that, in the forward direction, the signals scattered by individual particles combine coherently (Ref.13). For example, we may write

$$Y = 0.4343 \int N_D C_D \, dD \qquad (3)$$

where C_D is the extinction cross section of drops of diameter D, and N_D is expressed per m^3. For spherical drops, C_D is found from the Mie theory.

In (3) C_D depends upon frequency, so that Y is also a function of frequency. The term extinction is used since energy is removed from the forward beam both by absorption by the rain drops and by scattering out the beam.

2.3 Relation between Attenuation and Z

It can be seen from (2) and (3) that for a given drop-size distribution, as characterized by N_D, Z and Y may be calculated. It is found that, in a particular storm, the drop-size distribution at the ground appears to depend mainly on rainfall rate. This should not be taken to imply a direct causal relationship. The drop-size distribution depends upon the microphysical processes going on, within the cloud, and as the drops fall. Given a distribution N_D the rainfall rate R can be calculated. The important point is that a plot of Z against R shows little scatter. There is thus a functional relationship between Z and R. In fact, this relationship is represented quite well by a power law. Similarly a plot of specific attenuation Y against Z shows little scatter. Again a functional relationship that may be represented by a power law, exists.

3. EXPERIMENTAL TECHNIQUE

3.1 Outline of Experiment

The nature of the experiment is indicated schematically in Fig.1. A meteorological radar was used to measure Z, or more strictly Z_e, using equation (2). A distrometer (Ref.8) was used to measure the drop size distribution at the ground. From the output of the distrometer specific attenuation Y, and reflectivity factor Z, were calculated. Thus the relation between Y and Z was established.

An RC 33 radar operating near 3 GHz was used. This frequency was chosen so that measurement of Z would not be corrupted by unknown attenuation. Details of the radar are listed in Table 1. The radar was operated in conjunction with a digital sampling and range gating system which performed

some signal processing (Ref.12). The range gates could be set at 0.6 or 1.2 km. In this experiment 1.2 km was used. The signal in each range gate was averaged over 2 s. This averaging overcomes signal fluctuation problems (Refs.2,11,12). The signal processing is discussed in a little more detail in Section 3.2.

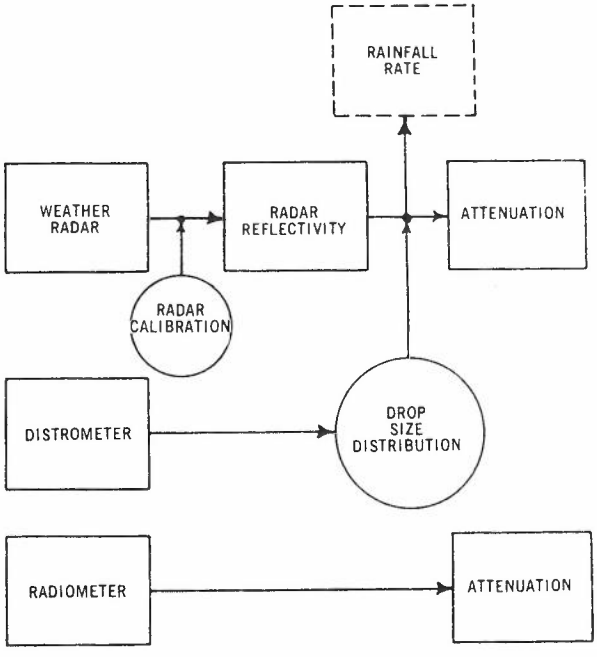

Fig.1 - A schematic outline of the experiment.

TABLE 1 - Details of Radar

Frequency		2.806 GHz
Pulse Length		0.7 sec
	or	2.1 sec
Pulse Repetition Rate		318 Hz
Peak Transmitted Power		450 Kw
Dish Diameter		3 m
3 dB Beam Width		
Horizontal		2.3^{o}
Vertical		2.5^{o}
Minimum Detectable Signal		-110 dBm
Overall Gain		35.6 dB
Polarization		Fixed Horizontal

TABLE 2 - Details of Radiometer

Frequency	11.07 GHz
Dish Diameter	1.219m
3 dB Beam Width (based on $58\lambda/D$)	1.29^{o}
Useful Range in Sky Noise Mode	0-10 dB

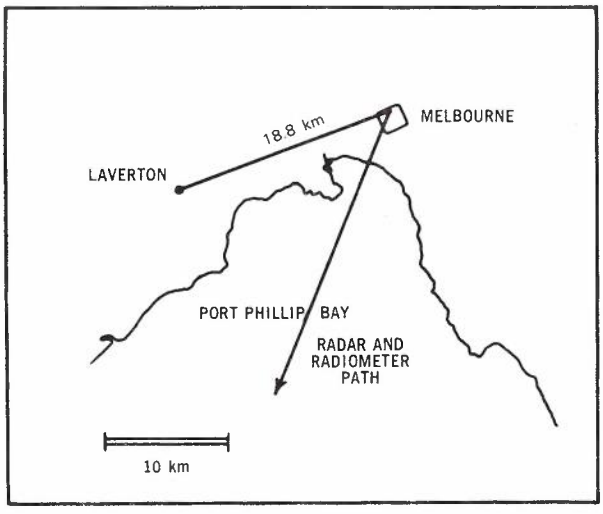

Fig.2 - A map showing the radiometer and radar path in plan and the 9 GHz link from the radar to Laverton.

The radiometer, (Table 2), measured attenuation near 11 GHz using the sky temperature mode, for comparison. The path examined by the radiometer has an elevation of 34^{o} and a bearing of 213^{o} (Fig.2).

The output of the distrometer was via paper tape. This was subsequently read to allow the necessary calculations to be carried out using a digital computer.

The output of the radiometer was by chart. This chart could be calibrated directly in terms of attenuation in dB and the radiometer output converted to a scale linear in dB, either manually or by computer. Later a second output from the radiometer was telemetered using FM transmission over a telephone line to the Telecom Research Laboratories at Clayton.

3.2 Required Accuracy of Radar Calibration

The returned average power, $\bar{P}_r$ can be written

$$\bar{P}_r = CZ \qquad (4)$$

where C is the radar calibration. From (2), C is not constant, but depends upon range r. However, frequently meteorological radars employ swept gain which automatically compensates for the $1/r^2$ dependence. This is the case with the RC 33 radar although it was found necessary to apply an additional correction at close range because of incomplete cancelling of the $1/r^2$ dependence of echo strength. From (4), we see that for a given $\bar{P}_r$,

$$\frac{\delta C}{C} = -\frac{\delta Z}{Z} . \qquad (5)$$

Now it is usually adequate (Refs.14,15) to write

$$Y = KZ^{\alpha} \qquad (6)$$

where, it appears, in all cases it has been found that $1 \leq \alpha \leq 0.5$. α falls to 0.5 at 100 GHz for a Laws-Parson drop size distribution (Ref.14). From (6)

$$\delta Y = \alpha K Z^{\alpha-1} \delta Z \qquad (7)$$

or

$$\frac{\delta Y}{Y} = \alpha \frac{\delta Z}{Z} \quad . \qquad (8)$$

Combining (5) and (8)

$$\frac{\delta Y}{Y} = -\alpha \frac{\delta C}{C} \qquad (9)$$

Thus

$$\frac{\delta Y}{Y} = -0.2303 \alpha \delta(\mathrm{CdB}) \qquad (10)$$

where δ(CdB) represents the dB error in the calibration. Thus a 1 dB error in calibration leads to an error in attenuation of between 23% and 12% depending on the value of α. In this experiment, we find $\alpha = 0.8379$. Thus a 1 dB error in calibration would lead to an error in attenuation of 20%. This was confirmed directly. It is believed the calibration of the Melbourne RC 33 radar is good to $\pm$ 2½ dB and this is approaching the best calibration achieved in any weather radar. On the other hand this error is mainly associated with an inability to establish an absolute calibration of the test signal generator (Ref.16). Thus, in any given experiment of reasonable duration, the error is not random but systematic. For example, Joss et al. (Ref.6) established the calibration of their radar by equating the measured Z at the closest range (about .5 km) to that calculated from a distrometer measurement on the ground. McCormick (Ref.4) and Strickland (Ref.5) calibrated their radars by comparing direct attenuation measurements with radar return calculated attenuation measurements, and then performed their comparison experiments on another day.

One other point arises. We have seen that a 1dB error in the measurement of the returned power gives a 20% error in the attenuation. However, the quantization step of the digital radar processing equipment is nominally 4.5dB. The situation might appear hopeless. However, Sirmans (Ref.12) estimated the residual variance of the averaged output to be about $\Delta P^2/9$ where ΔP is the quantization step or interval in dB. The variance due to quantization is $\Delta P^2/12$ (Ref.12). Since a digital output is available every 2 sec. it is possible to average 10 successive outputs (giving a sample every 20 sec) without sacrificing necessary resolution in time. This has the effect of further reducing the variance to about $\Delta P^2/90$ (i.e. an uncertainty of about 0.5dB) and also allows interpolation between digital levels. If a normal distribution of echo power in dB is assumed, it can be shown that it is possible to interpolate to a little worse than one tenth of the quantization interval, i.e. about 0.5dB. The residual variance acts like a dither signal allowing this improvement in resolution. If there was no (or very small) error associated with each of the ten samples, assuming stationarity, each would correspond to the same digital level and nothing would be gained by averaging. This procedure was followed in processing the radar output, the arithmetic being carried out to 0.1 of a level. All ten levels are observed to occur. That is, there was no obvious "graininess", the presence of which would have suggested the effective interpolation was to worse than one tenth of a level.

4. EXPERIMENTAL RESULTS

4.1 Radiometer

The radiometer derived attenuation for a Melbourne storm of 30 October 1975 is shown in Fig.3. This was quite a severe storm for Melbourne. A peak rainfall rate of 46 mm hr^{-1}

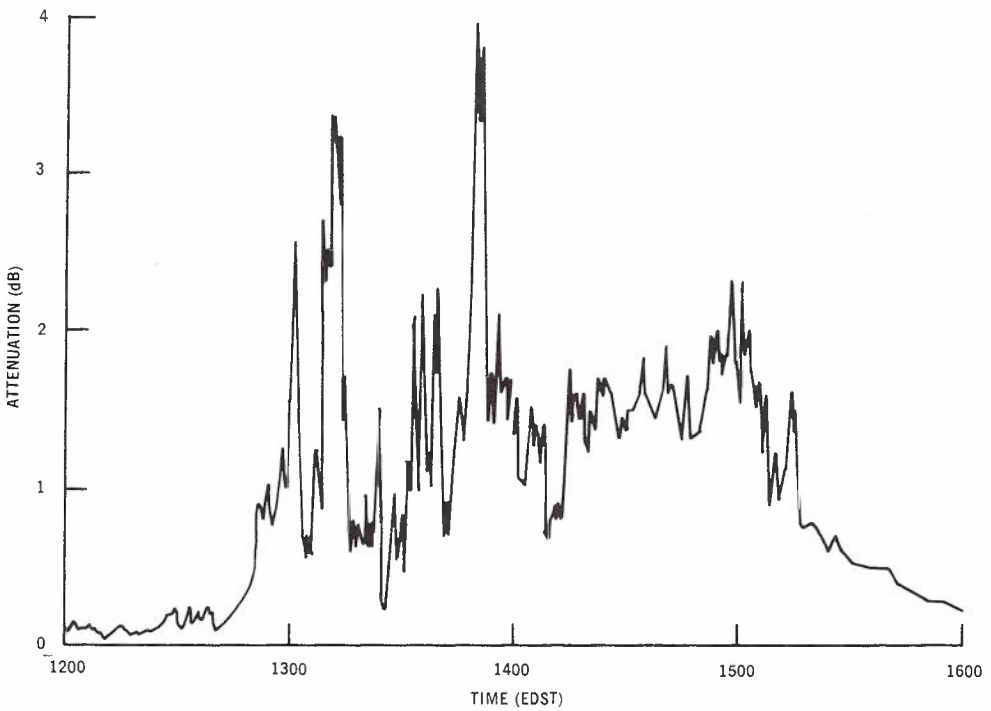

Fig.3 - 11 GHz attenuation, as deduced from the radiometer output.

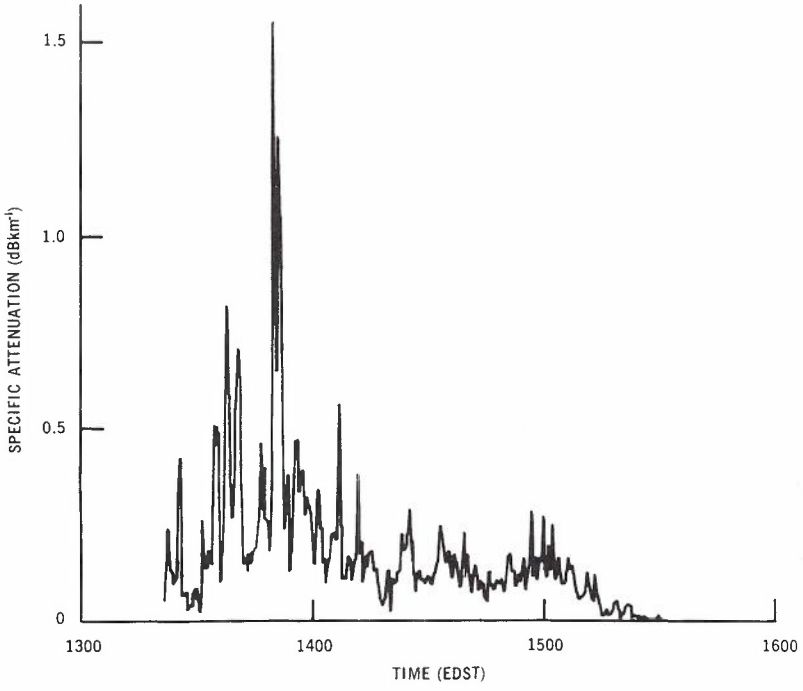

Fig.4 - Specific attenuation at 11 GHz as calculated from the distrometer output.

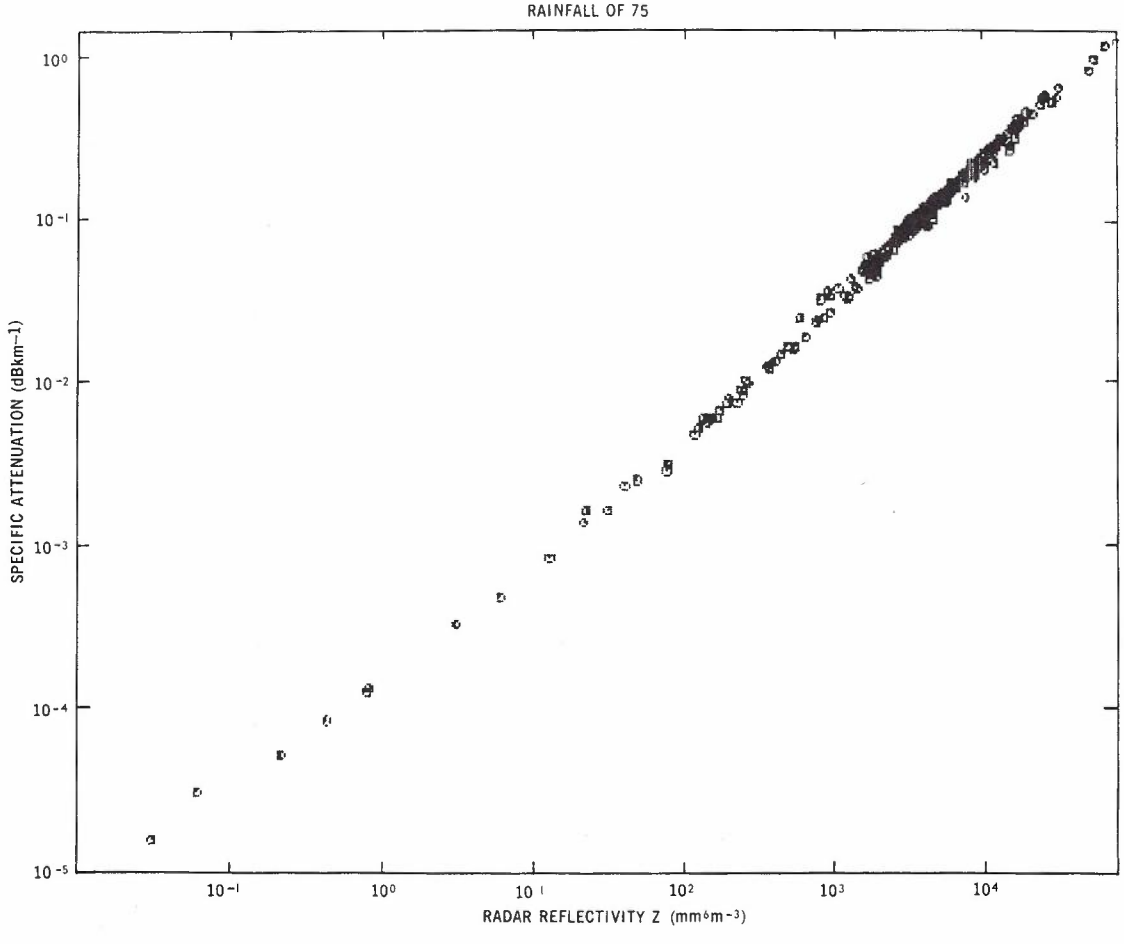

Fig.5 - Logarithmic regression of specific attenuation against reflectivity factor from distrometer output.

averaged over 30 seconds, was observed with the distrometer. In the 11 hours to 8 p.m. 24 mm of rain fell, causing minor flooding. Unfortunately, because the radar was used for other measurements several times during the storm, it is only possible to compare radar and radiometer derived attenuation for restricted periods.

4.2 Distrometer

From the distrometer output, the specific attenuation Y was calculated for each 30 second sample of the drop-size distribution. The result is shown in Fig.4. Comparing Figs.3 and 4 it can be seen that there is quite high correlation between 1330 and 1400 hours, corresponding to an effective path length of about 2.6 km. Around 1500 there is also a fairly high correlation, but corresponding to an effective path length of 9 km. The reflectivity factor Z was also calculated for each sample and Fig.5 shows a regression plot of log Y against log Z. It can be seen that there is some scatter about the regression line

$$Y = 0.0001311\ Z^{0.8329} \qquad (11)$$

At Z = 795 $mm^6 m^{-3}$, the spread is about 0.0262-0.0376 dB km^{-1}, and at Z = 13500 $mm^6 m^{-3}$, 0.221-0.265 dB km^{-1}. It is interesting to note that a much improved fit would be obtained by taking two straight line segments, as suggested by Boston (Ref.15).

4.3 Radar

The attenuation was calculated from the radar output using the formula

$$A = A_o + K \sum_{i=1} Z_i^{\alpha} \ell \qquad (12)$$

with K = 0.0001311, α = 0.8329. The gate length ℓ is 1.2 km. A_o represents the contribution from the radar dead zone which was not sampled. A_o was estimated in two ways, simple extrapolation from the first valid gate

$$A_o = KZ_1^{\alpha} \ell_o \qquad (13)$$

or using the distrometer derived attenuation

$$A_o = Y_{dist} \cdot \ell_o \cdot \qquad (14)$$

The length of the dead zone, ℓ_o is 3.0532 km.

The results of the two calculations are shown in Fig.6, compared with the radiometer result. The radar constant used included a 2 dB allowance for the effect of pulse matching. Nathanson & Smith (Ref.17) estimate an average contribution of 1.7 dB due to this effect. In earlier work using the calibrated radar for the study of Z - R relationships, this contribution was not included as it was judged to be insignificant in that application (Ref.18).

Early in the storm, the agreement is reasonable, particularly bearing in mind the fact that in order to obtain radiometer attenuation at 30 sec. intervals, it was necessary to read the chart output every 0.5 mm. However, late in the storm the radar-distrometer calculated attenuation consistently underestimates the radiometer measured attenuation.

5. DISCUSSION

Consider first the correlation between the radiometer measured attenuation and the specific attenuation, as calculated from the distrometer output. The correlation between 1330 and 1400 hours is not hard to understand, given that the effective path length is about 2.6 km. Most of the attenuation is apparently due to intense local rain and this is reasonably represented by the distrometer. On the other hand, around 1500 the correlation implies a fair degree of spatial correlation of the drop size distribution over about 9 km. The radar output shows a high correlation between the returns from the first three range gates near this time. Assuming the behaviour in the radar dead zone is the same, this suggests correlation over a distance of around 7 km. Thus a reasonably consistent picture emerges.

At these times the equivalent path length idea of Goldhirsh (Ref.19) may be useful for the frequency scaling of attenuation.

In considering the attenuation predicted using the radar, some consideration must be given to the radar dead zone. Suppose the effective scale size of a rain cell, measured along the beam, is greater than 3 km. If the cell straddles the dead zone, the specific attenuations at the distrometer and the first radar range gate will be closely the same. The attenuation calculated using the distrometer attenuation for the dead zone will agree closely with that calculated extrapolating from the first range gate. On the other hand, if the cell does not extend from the distrometer to the first range gate the specific attenuations will be different and there may be a large difference between the attenuation calculated using the two methods. However, the true result should be somewhere between the extremes. While one or the other of these two situations occur many times early in the storm, there are occasions when the two methods of calculation agree, but fail to predict the radiometer attenuation accurately. At other times there is a wide spread between the result obtained using the distrometer attenuation and the extrapolation of the first range gate, but the radiometer attenuation lies outside this range. Disagreement of this type would result if the effective cell size was less than 3 km, the length of the dead zone.

Early in the storm the agreement between calculated and measured attenuation is reasonable, with some uncertainties and discrepancies that appear to be associated with the radar dead zone. However, later in the storm the calculated attenuation consistently underestimates that measured with the radiometer. The error increases from about 0.5 dB at 1430 hours to 1 dB at 1500 hours. Near this time the distrometer specific attenuation suggested an effective path length of 9 km against 7 km suggested by the radar. This reduced path length would

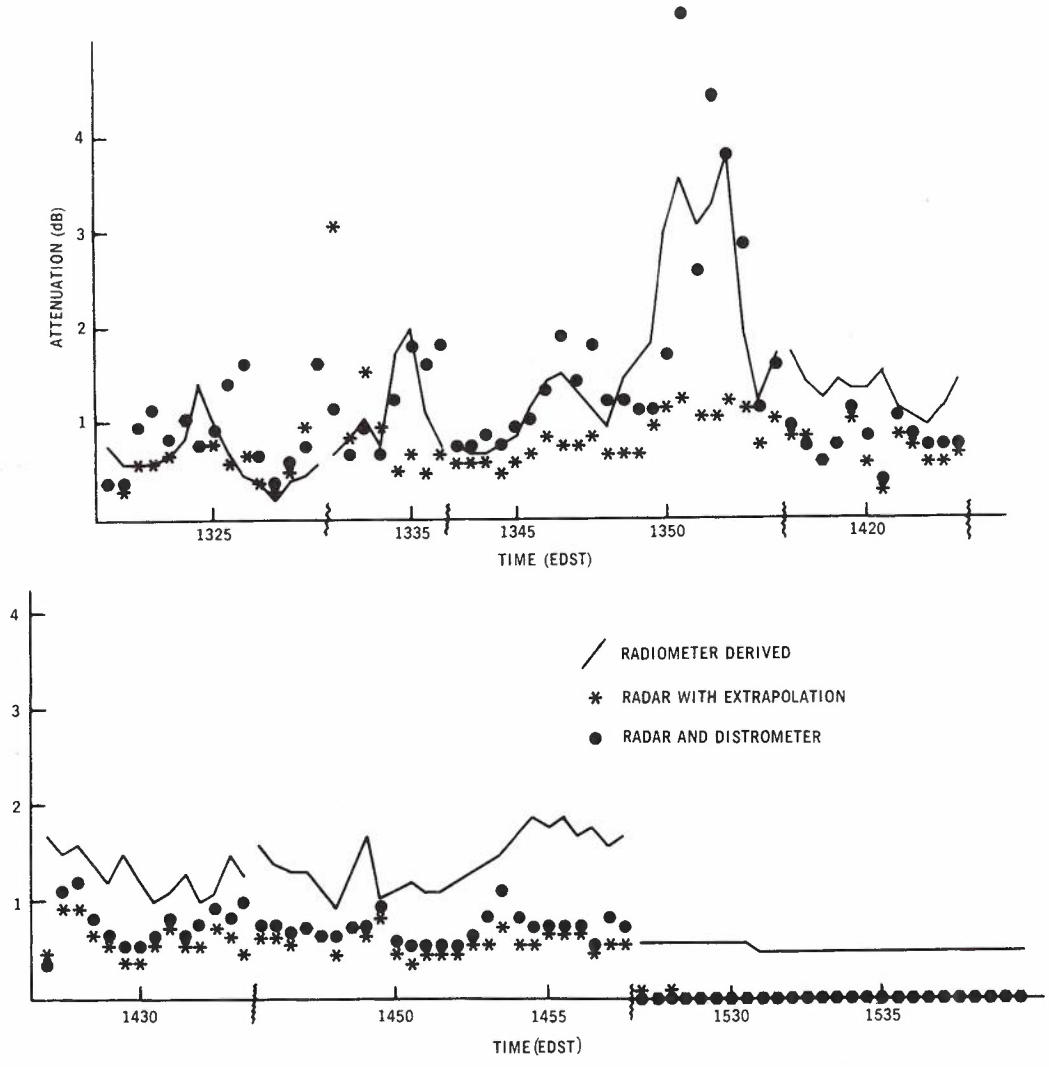

Fig.6 - Radiometer derived attenuation compared with attenuation calculated from the radar and distrometer.

lead to underestimating the attenuation by about 0.5 dB. This approach is of course less precise than calculating the attenuation using the radar return power. After 1530 hours there is steady attenuation of 0.9 dB although an insignificant amount of rain was recorded by the distrometer and no radar echoes were received.

It can be seen that, at these times, there is additional attenuation of from 0.5 to 1 dB. A possible reason for this additional attenuation is atmospheric water vapour. Table 3 gives surface atmospheric temperature and relative humidity. The corresponding specific attenuation, calculated by the method of Gunn and East (Ref.20) is also shown. A path length of around 30 km would be required to produce 0.5 dB of attenuation. Thus, atmospheric water vapour is not a plausible explanation of the additional attenuation. Moreover, the specific attenuation due to water vapour, rather than increasing, actually falls during the storm, mainly due to the fall in air temperature and the corresponding fall in absolute humidity.

TABLE 3 - Attenuation Due to Humidity

TIME EDST	TEMPERATURE ^{o}C	RELATIVE HUMIDITY %	SPECIFIC ATTENUATION 10^{-2}dB km^{-1}
600	19	83	1.58
700	19	83	1.58
800	20	80	1.53
900	20	74	1.42
1000	20	73	1.40
1100	20	73	1.40
1200	17	83	1.27
1300	16	88	1.30
1330	15	94	1.31
1400	15	94	1.31
1500	15	98	1.36
1600	14	98	1.25

Cloud droplets also cause attenuation. Around 1530 hours it was observed that very dark cloud still filled the radiometer beam. The darkness is of course due to attenuation at optical wavelengths. From (Ref.20), a cloud of liquid water content of 1 gm^{-3}, a plausible value, contributes a specific attenuation of about 7.5×10^{-2} dB km^{-1}. A path length of 7 km would give 0.5 dB attenuation. This figure is based on the Rayleigh Theory. If drop growth continues in the cloud, but for some reason large drops are no longer generated, the population of very small raindrops and very large cloud droplets might grow. Also, drops at the small end of the rain drop classification may be held in the cloud by updraughts. Now for drops as small as 0.2 mm, the Rayleigh Theory underestimates the contribution to attenuation at 11 GHz (Ref.20). Thus the additional attenuation may be due to drops too small to be measured by the distrometer (0.35 mm diameter and smaller) or to cause radar echoes.

5.1 Additional Experimental Results

Fortunately, additional results are available which help to clarify the points raised in the discussion. Simultaneously with the experiment described in Section 3 and Fig.1, the Bureau of Meteorology engineering group was measuring attenuation at 9 GHz (8.940) on a terrestrial route terminating at the radar (Fig.2). The experimental result is shown in Fig.7. Unfortunately the resolution is not high. In Fig. 8, the specific attenuation from the distrometer output for this frequency is displayed. The measured attenuation over this path at 9 GHz and

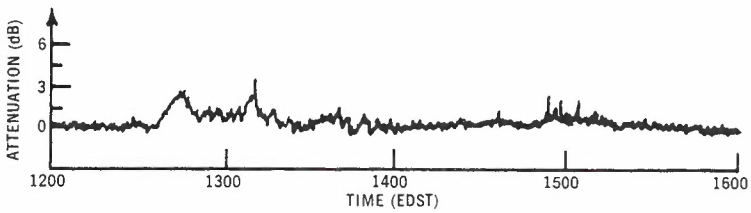

Fig.7 - 9 GHz attenuation over terrestrial path. (Tracing of original record).

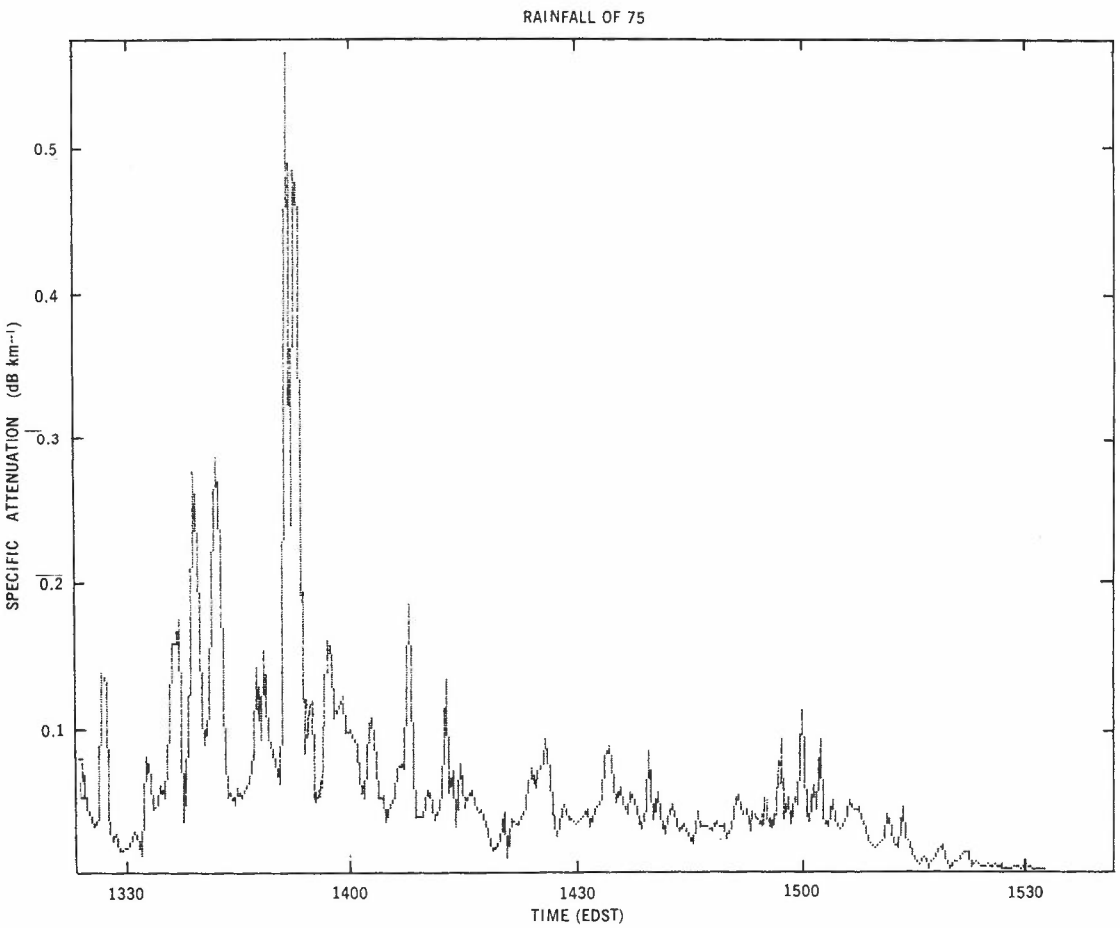

Fig.8 - Specific attenuation at 9 GHz, as calculated from the distrometer output.

the radiometer attenuation at 11 GHz show a general correlation.

In the period 1300 to 1400, comparison of the terrestrial route attenuation and the distrometer specific attenuation suggest an effective path length of about 6 km. Bearing in mind the geometry of the two paths, this is consistent with the radiometer effective path length of 2.6 km. In this period there is also a fair degree of correlation between attenuation on the two paths. Most of the attenuation appears to be due to a relatively uniform localized rain. The measurements suggest the time dependence of attenuation is mainly due to time variations in the rain rather than spatial movement of rain cells.

Near 1500 there is again quite high correlation between the various attenuation figures. For the 9 GHz terrestrial path, an effective path length of 30 km is suggested. If the rain falling at the distrometer were assumed to fall uniformly along the path, the attenuation would be underestimated by about 0.5 dB. Near this time the attenuation appears to be due to widespread rain fairly uniform in space. There may also be a contribution due to very small drops.

After 1530 there is again attenuation of about 0.5 dB, which drops measured by the distrometer are quite inadequate to explain.

6. CONCLUSION

We conclude that meteorological radar, when combined with simultaneous distrometer measurements is useful in gathering data on microwave attenuation by rain. The distrometer, besides establishing a statistical relation between specific attenuation Y and radar reflectivity factor Z, also yields information about the time dependence of one contribution to the total attenuation. However, there are times when there is 0.5 to 1 dB attenuation due to drops that can not be measured with the distrometer, nor observed with a 3 GHz radar.

A high degree of precision in the radar calibration is required if quantitative results are to be obtained. This experiment was far from definitive, not only because of the small amount of data, but also because of uncertainties associated with the radar dead zone. If this could be reduced to 0.5 km, as in the experiment of Joss et al (Ref.6), use of simultaneous distrometer measurements would be expected to lead to satisfactory results. Alternatively, if the radar is scanned in range, azimuth, and elevation, along a remote path (Ref.7) the dead zone problem can be avoided. However, the time needed to carry out the scan will result in loss of time resolution. Another possibility is the use of a bistatic radar system. If the transmitter and receiver were only a short distance apart it would not be necessary to scan in order to calculate attenuation along a path from the radar site. However, the path in the region near the radar would not be well defined.

Differences in the beamwidths of the radar and radiometer may lead to differences in the attenuation because of the nonuniform spatial distribution of raindrops.

The experiment yielded some evidence in support of the equivalent path length concept of Goldhirsh (Ref.19).

7. ACKNOWLEDGEMENT

We are grateful to a number of colleagues for advice and assistance - in particular, at Telecom Australia Research Laboratories, A.J. Seyler (deceased), E.R. Craig, G.F. Jenkinson; at the Bureau of Meteorology, P.A. Barclay, A. West, S.C. Martin; at the Department of Physics, R.A.A.F. Academy, E.L. Unthank (now at State College Burwood).

The experimental phase of this work was carried out while one of us (J.A.B.) held a Radio Research Board Fellowship.

8. REFERENCES

1. Ippolito, L.J., "Millemeter Wave Propagation Measurements from an Orbiting Earth Satellite", IEE Conference Publication, Propagation of Radio Waves above 10 GHz, 1973, pp.104-107.

2. Bennett, J.A., "The Calculation of Microwave Attenuation by Rain from Radar Measurements", Telecom Australia Research Laboratories Report No.7072, Aug. 1976.

3. Crane, R.K., "Simultaneous Radar and Radiometric Measurements of Rain and Shower Structure", MIT Lincoln Laboratories, Lexington, Mass., U.S.A. Technical Note 1968-33, ASTIA Document AD-678079.

4. McCormick, K.S., "A Comparison of Precipitation Attenuation and Radar Backscatter along Earth-Space Paths", IEEE Trans. Antennas Propagat. Vol.AP-20, 1972, pp.747-755.

5. Strickland, J.I., "The Measurement of Slant Path Attenuation Using Radar, Radiometers, and a Satellite Beacon", J. Recherches Atmospherique, Vol.8, 1974, pp.347-358.

6. Joss, J., Cavalli, R. and Crane, R.K., "Good Agreement Between Theory and Experiment for Attenuation Data", J. Recherches Atmospherique, Vol.8, 1-2, 1974, pp.229-318.

7. Goldhirsh, J., "Attenuation of Propagation Through Rain for an Earth Satellite Path Correlated with Predicted Values Using Radar," IEEE Trans. Antennas Propagat. Vol.AP-24, No.6, Nov.1976, pp.800-806.

8. Joss, J., and Waldvogel, A., "Ein Spektrograph für Niederschlagstropfen mit Automatischer Auswertung", Pure and Applied Geophysics, Vol.68, 1967, pp.240-246.

9. Rogers, R.R., "Statistical Rain Storm Models: Their Theoretical and Physical Foundations", IEEE Trans. Antennas Propagat. Vol.AP-24, No.4, July 1976, pp.547-566.

10. Crane, R.K., "Prediction of the Effects of Rain on Satellite Communications Systems", Proc. IEEE, Vol.65, No.3, March 1977, pp.456-474.

11. Smith, P.L., Hardy, K.R. and Glover, K.M., "Applications of Radar to Meteorological Operations and Research", Proc. IEEE, Vol.62, No.6, 1976, pp.724-745.

12. Sirmans, D., "Digital Processing of Meteorological Radar Signals", Met. Study 25, Bur. Met. Australia, 1972.

13. Van De Hulst, H.C., "Light Scattering by Small Particles", John Wiley, New York, 1957.

14. Zawadzki, I.I. and Rogers, R.R., "ADA: An Instrument for Measuring Attenuation due to Rain over Slant Paths", Radio Sci. Vol.7, No.6, 1972, pp.619-624.

15. Boston, R.C., "Radar Attenuation and Reflectivity due to Size Distributed Hydrometers", J. Appl. Meteor. Vol.9, No.1, 1970, pp.188-191.

16. Barclay, P.A., and Unthank, E.L., "An Assessment of the Overall Gain of the Melbourne Weather Radar System", Proc. 12th Radar Met. Conf., Norman, Oaklahoma, 1966, pp.76-80.

17. Nathanson, F.E. and Smith, P.L., "A Modified Coefficient for the Weather Radar Equation", Proc. 15th Radar Met. Conf. Champaign, Urbana, Illinois, Oct.10-12, 1972, pp.228-230.

18. Barclay, P.A., "Digital Radar Areal Rainfall Measurements", Ph.D. Thesis, Physics Dept. (R.A.A.F. Academy) University of Melbourne, July, 1977.

19. Goldhirsh, J., "Prediction Methods for Rain Attenuation Statistics at Variable Path Angles and Frequencies Between 13 and 100 GHz", IEEE Trans. Antennas Propagat., Vol. AP-23, No.6, Nov.1975, pp.786-791.

20. Gunn, K.L.S., and East, T.W.R., "The Microwave Properties of Precipitation Particles", Q.J. Roy. Met. Soc. Vol.80, 1954, pp.522-545.

BIOGRAPHY

PETER LAATS was born in Melbourne on 28/11/50. He completed the Bachelor of Applied Science (Electronics) Degree at Melbourne University in 1972. His main interest is in Computer Science and he is currently studying for a Post Graduate Diploma in Information Science at the Canberra College of Advanced Education.

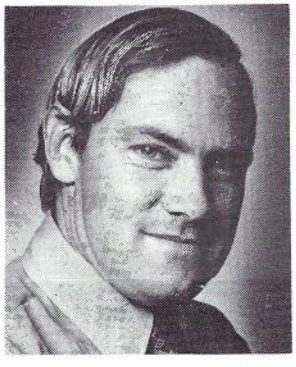

RAYMOND CHARLES BOSTON received his Secondary education at Camberwell High School, Melbourne, Victoria. He graduated with an Honours Degree from Melbourne University in 1964. In 1966 he took out a Master of Science Degree in Physiology at that University and in 1970 a Ph.D. in Physics. The course of study during his Ph.D. led him to investigate such diverse aspects of radar meteorology as bistatic radar systems, polarization diversity radar and Doppler radar. During this program he spent some 10 months with the well-known Stormy Weather Group at McGill University Montreal. Currently he is a Biometrician with the School of Agriculture at La Trobe University, Melbourne where his interest includes biomathematical modelling and experimental design. He has on two occasions worked as a Guest Scientist at the National Institutes of Health, Washington D.C., U.S.A.

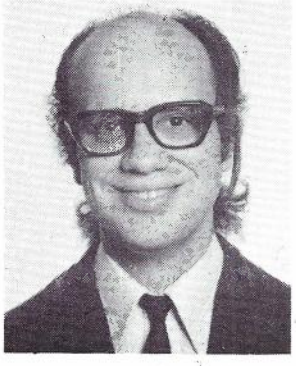

JOHN A. BENNETT was born in Adelaide, South Australia, on 9/2/42. He received the B.E. Degree in Electrical Engineering, and the B.Sc. and Ph.D. Degrees in Pyhsics, from the University of Melbourne, in 1964, 1965 and 1971, respectively. While working for the Ph.D. Degree, he also spent one year as a temporary Lecturer.

After completing the Doctoral Degree, he continued to carry out research on wave propagation and has published some two dozen papers in this area. He spent some time with the Institute of Earth and Planetary Physics at the University of Alberta, Edmonton, Canada as a Post Doctoral Fellow. He was then awarded an Alexander von Humboldt Fellowship which enabled him to carry out research at the Institute for Theoretical Physics of the University of Düsseldorf, Germany; and the Cavendish Laboratory, University of Cambridge, England. He returned to Australia as the first Radio Research Board Fellow to work at the Research Laboratories of Telecom Australia. He joined Monash University as a Lecturer in Electrical Engineering early in 1976. Dr. Bennett is a Member of the Australian CCIR National Study Group 4, a Fellow of the Australian Institute of Physics and a Member of the Institute of Electrical and Electronics Engineers.

Cumulants of PCM System Crosstalk in Multipair Cable

A.J. GIBBS
Telecom Australia Research Laboratories

PCM system engineering in multipair cable requires estimation of the upper skirts of the distribution of the total mean-square crosstalk interference at, typically, the 99% or 99.9% level. These can be estimated from the cumulants (mean, variance and third central moment) of the intersystem crosstalk. Expressions for the first three cumulants are derived in this paper, and their behaviour is discussed for typical cables and PCM regenerator characteristics.

1. INTRODUCTION

PCM system engineering in multipair cable requires estimation of the upper skirts of the distribution of the total mean-square crosstalk interference at, typically, the 99% or 99.9% levels. The total crosstalk interference is the sum of uncorrelated approximately lognormal component variates, and the approximate distribution of the total can be estimated from a knowledge of the first three cumulants (mean, variance, third central moment) of the component variates, (Refs.1-6). The component variates are of the form

$$v^2 = \int_0^\infty |X(f)|^2 P(f)df \qquad (1)$$

where X(f), the near end crosstalk (NEXT) or far end crosstalk (FEXT), is a stochastic process and P(f) is a deterministic function of the regenerator equalizer characteristic, the transfer function of the cable and the power spectral density of the regenerator output signal.

The FEXT case is relatively straightforward. The FEXT process is modelled by

$$|X(f)|^2 = k_F(f/f_o)^2 \qquad (2)$$

where k_F is a random variable with truncated lognormal distribution, (Refs.3,4). Thus the cumulants of v^2 are simply related to the cumulants of FEXT, and are not discussed further in this paper.

The NEXT case is less straightforward. The NEXT process is modelled by, (Refs.1,6),

$$X(f) = j2\pi f \int_0^\infty C(x)e^{-2\gamma x}dx \qquad (3)$$

where γ is the cable propagation constant and C(x) is the pair-to-pair unbalance process characterized by

(a) for a fixed pair combination C(x) is a zero mean normal process with covariance $E(C(x)C(y)) = k_1\delta(x-y)$.

(b) k_1 is a random variable over all pair combinations.

This model has been analysed to give the first two cumulants of v^2, (Ref.6), and the purpose of this paper is to derive the third cumulant and to illustrate some of the properties of the cumulants for typical cables and regenerator characteristics.

2. CUMULANTS OF 'NEXT' INTERFERENCE

Denoting the i-th cumulant of v^2 by κ_i, we have from (Ref.6):

$$\kappa_1 = E(k)I_m$$

$$\kappa_2 = E(k^2)I_v + \mu_2(k)I_m^2$$

where $\mu_2(.)$ denotes the second central moment (variance),

$$I_m = \int_0^\infty F^{2-x}P(f)df \quad ; \quad F = f/f_o \qquad (4)$$

$$I_v = \iint_0^\infty V(F_1,F_2)P(f_1)P(f_2)df_1df_2 \quad ; \quad F_i = f_i/f_o \qquad (5)$$

$$V(F_1,F_2) = \frac{4F_1^{2x}F_2^{2x}}{(F_1^x + F_2^x)^2 + \varepsilon(F_1 - F_2)^2} \qquad (6)$$

$$\gamma = \alpha + j\beta \approx \alpha_0 F^{\times} + 2\pi f_0 TF \qquad (7)$$

$$k = \frac{\pi^2 k_1 f_0^2}{\alpha_0} \quad ; \quad \varepsilon = (2\pi f_0 T/\alpha_0)^2, \qquad (8)$$

α_0 is the cable pair loss/unit length at f_0, $\times$ is the cable pair loss exponent (usually between 0.5 and 0.6),T is the cable pair time delay/ unit length and $\varepsilon \approx 200$ for paper insulated 0.64mm cable with f_0 = 1024kHz.

The third cumulant of v^2 is derived in Appendix I:

$$\kappa_3 = E(k^3) I_W + \mu_3(k) I_m^3$$

where $\mu_3(.)$ denotes the third central moment and

$$I_W = \iiint_0^{\infty} W(F_1,F_2,F_3) P(f_1) P(f_2) P(f_3) df_1 df_2 df_3 \qquad (9)$$

$$W(F_1,F_2,F_3) =$$

$$\frac{16F_1^2F_2^2F_3^2\{(F_1^{\times}+F_2^{\times})(F_2^{\times}+F_3^{\times})(F_3^{\times}+F_1^{\times})}{\{(F_1^{\times}+F_2^{\times})^2+\varepsilon(F_1-F_2)^2\}\{(F_2^{\times}+F_3^{\times})^2}$$

$$+\varepsilon\left|F_1^{\times}(F_2-F_3)^2+F_2^{\times}(F_3-F_1)^2+F_3^{\times}(F_1-F_2)^2\right|\}$$

$$+\varepsilon(F_2-F_3)^2\}\{(F_3^{\times}+F_1^{\times})^2+\varepsilon(F_3-F_1)^2\} \qquad (10)$$

Assuming that NEXT attenuation in dB has a truncated normal distribution with mean μ_0 at f_0, variance σ_0^2 and truncation factor c, then from Appendix II:

$$\kappa_1 = T(c,\sigma_0) 10^{0.1(0.115\sigma_0^2-\mu_0)} I_m \qquad (11)$$

$$\kappa_2 = \kappa_1^2 (\Delta_2 U_2(c,\sigma_0) 10^{0.023\sigma_0^2} - 1) \qquad (12)$$

$$\kappa_3 = \kappa_1^3 (\Delta_3 U_3(c,\sigma_0) 10^{0.069\sigma_0^2}$$

$$\frac{-3(1+\Delta_3)\, U_2(c,\sigma_0) 10^{0.023\sigma_0^2} + 2)}{2} \qquad (13)$$

where

$$\Delta_2 = \frac{1}{2}\left(1 + \frac{I_V}{I_m^2}\right) \quad ; \quad \Delta_3 = \frac{1}{3}\left(1 + \frac{I_W}{I_m^3}\right) \qquad (14)$$

$$T(c,\sigma) = \frac{\Phi(c - 0.23\sigma) - \Phi(-c - 0.23\sigma)}{\Phi(c) - \Phi(-c)}$$

$$\Phi(x) = \frac{1}{\sqrt{2\pi}} \int_{-\infty}^{\times} \exp(-t^2/2)\, dt$$

$$U_n(c,\sigma) = \frac{T(c,n\sigma)}{T^n(c,\sigma)}$$

3. BEHAVIOUR OF Δ_2 AND Δ_3

The factors Δ_2 and Δ_3 depend on the ratios I_V/I_m^2 and I_W/I_m^3, respectively, and are therefore functions of P(f), $V(F_1,F_2)$ and $W(F_1,F_2,F_3)$. P(f) is given by

$$P(f) = \frac{|D(f)|^2}{|G(f)|^2} P_0(f)$$

where D(f) is the Fourier Transform of the pulse shape at the regenerator decision point, G(f) is the transfer function of the cable pair, viz.,

$$G(f) = 10^{-0.1 A_0 F^{\times}}$$

where A_0 is the loss in dB at f_0 (here taken as half the PCM system clock rate), and $P_0(f)$ is the power spectral density of the transmitted pulse train (excluding the output pulse shape); V and W depend on the cable loss and time delay/unit length and the normalization frequency f_0 (see equations (6)-(10)).

Tables 1-4 show the behaviour of Δ_2 and Δ_3 for $14 \leq A_0 \leq 40$; $\times$ = 0.5, 0.6; D(f) either a Gaussian pulse with 3% intersymbol interference or a pulse with full cosine roll-off; ε = 200 or 330 (corresponding to 0.64mm or 0.9mm paper insulated pairs, respectively); and $P_0(f)$ either a HDB3 encoded random binary stream or a HDB3 encoded (ideal) "idle" binary stream from the PCM multiplex, i.e., a succession of 8 bit words of the form R1010101, where R is randomly 0 or 1 with equal probability.

The values of Δ_2 and Δ_3 show only a small variation with variation in A_0, with a tendency to increase with increasing A_0, to decrease with increasing ε and to increase with increasing $\times$. The most significant behaviour is that both Δ_2 and Δ_3 are greater for the idle power spectrum than for the random spectrum. This arises because the idle spectrum is highly concentrated at odd multiples of $f_0/4$, and the ratio $|D(f)/G(f)|^2$ peaks at approximately $3f_0/4$. Thus with the idle spectrum I_m, I_V and I_W are dominated by the spectrum lobe at $3f_0/4$, and I_V/I_m^2 approaches one and I_W/I_m^3 approaches two more closely than they do with the random spectrum, where no significant concentration occurs.

In fact, the values of Δ_2 and Δ_3 are bounded both above and below. They approach their lower bound as I_V and I_W approach zero, and attain their upper bound for $P_0(f)$ a single frequency line. Thus from equations (5), (6), (9), (10) and (14) we have

$$\frac{1}{2} < \Delta_2 \leq 1 \quad ; \quad \frac{1}{3} < \Delta_3 \leq 1 \qquad (15)$$

4. BEHAVIOUR OF CUMULANTS

The behaviour of κ_1 depends primarily on the behaviour of I_m, which has the property that I_m in dB varies approximately linearly with A_0, with little difference between the random and idle conditions, as shown in Figs. 1 and 2 (I_m normalized for unit height pulse at the regenerator decision point).

The behaviour of κ_2 and κ_3 is best described by considering the ratio $R_i = \kappa_i/\hat{\kappa}_i$, where $\hat{\kappa}_i$ corresponds to the case $\Delta_i = 1$. Thus R_i is the ratio of the "wide band" cumulant to the "sine wave" cumulant. It is interesting to note that $R_i \leq \Delta_i$, with equality only if $\Delta_i = 1$. This is simply shown:

$$\Delta_2 - R_2 = \frac{\kappa_1^2(1 - \Delta_2)}{\hat{\kappa}_2} \geq 0$$

because $\Delta_2 \leq 1$ and $\hat{\kappa}_2 \geq 0$;

$$\Delta_3 - R_3 = \frac{2\kappa_1^3(1 - \Delta_3)(0.75U_2 10^{0.023\sigma_0^2} - 1)}{\hat{\kappa}_3}$$

$$= \frac{2\kappa_1(1 - \Delta_3)\kappa_2^1}{\hat{\kappa}_3} \geq 0$$

because $\Delta_3 \leq 1$, $\hat{\kappa}_3 > 0$ for a truncated log-normal distribution, and κ_2^1 is a second cumulant with $\Delta_2 = 0.75$. Thus the wideband cumulants are reduced, which is a result of the smoothing of $|X(f)|^2$ by the integration in equation (1).

In typical cables $\sigma_0 \geq 7$, and for these values of σ_0 the first term in each cumulant dominates and we have $R_i \simeq \Delta_i$, with an error less than 10%.

The above results can be used to investigate the effect of different values of Δ_i on the estimation of the 99% or 99.9% points on the distribution of the total crosstalk interference. A complete discussion is outside the scope of this paper and only one example is given, viz., that

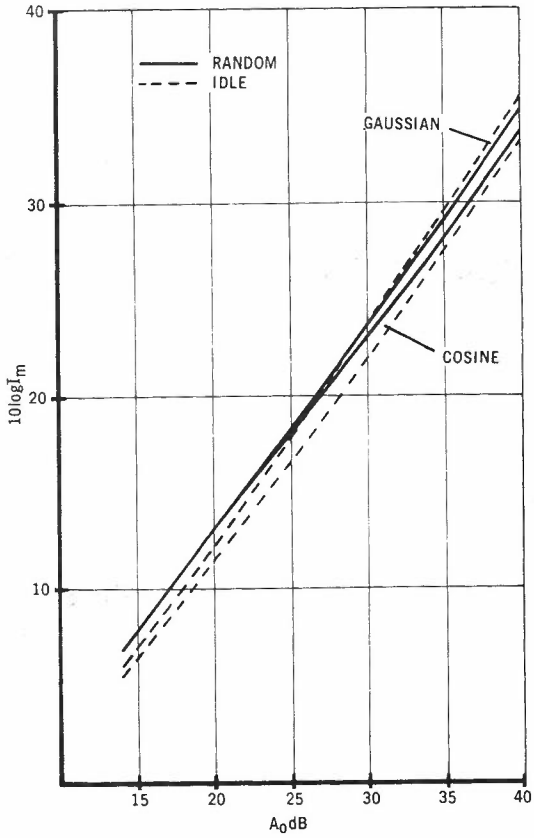

Fig. 1 I_m dB for $x = 0.5$

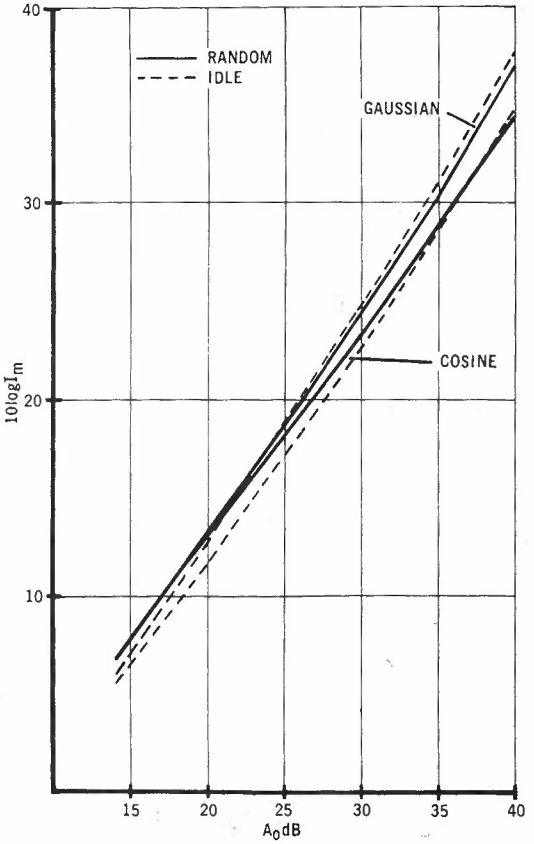

Fig. 2 I_m dB for $x = 0.5$

considered by Usher et.al. (Ref.5) of four groups of interferers with different means, variances, truncation factors, and number of interferers, N, from each group, as shown below:

N	μ_o	σ_o	c
6	73.6	5.5	2.75
15	76.4	7.8	3.15
64	77.5	9.6	2.91
53	80.2	8.3	3.6

Assuming $\Delta_i = 1$ the 99% and 99.9% points are -45.17dB and -44.12dB respectively, whereas using the Δ_i corresponding to a full cosine roll-off pulse and A_o = 34dB gives values of -45.64dB and -44.77dB. Thus the use of the wideband second and third cumulants results in a reduction of total interference at the 99% and 99.9% points of 0.5dB and 0.6dB respectively.

5. ACKNOWLEDGEMENT

The author thanks J. Semple and B. Smith for many helpful discussions, with particular thanks to J. Millott for calculating the numerical values of the cumulants.

6. REFERENCES

1. Cravis, H. and Crater, T.V., "Engineering of T1 Carrier Repeatered Lines", B.S.T.J., March 1963, pp.431-486.

2. Jacobson, B.B., "Cable Crosstalk Limits on Low Capacity PCM Systems", Elect. Comm., Vol.48, 1973, pp.98-107.

3. Bradley, S.D., "Crosstalk Considerations for a 48 Channel PCM Repeatered Line", IEEE Trans. on Comm., July 1975, pp.722-728.

4. Narayana Murthy, B.R., "Crosstalk Loss Requirements for PCM Transmission", IEEE Trans. on Comm., January 1976, pp.88-97.

TABLE 1 - Δ_2 and Δ_3 for Idle HDB3 Code and Gaussian Pulse

	ε=200				ε=330			
	x=0.5		x=0.6		x=0.5		x=0.6	
Δ_o	Δ_2	Δ_3	Δ_2	Δ_3	Δ_2	Δ_3	Δ_2	Δ_3
14	0.66	0.43	0.67	0.44	0.64	0.41	0.65	0.42
16	0.67	0.44	0.68	0.46	0.65	0.42	0.66	0.43
18	0.68	0.45	0.69	0.48	0.66	0.43	0.67	0.45
20	0.69	0.47	0.71	0.50	0.67	0.44	0.68	0.47
22	0.70	0.49	0.72	0.51	0.68	0.46	0.69	0.48
24	0.71	0.50	0.73	0.53	0.69	0.47	0.70	0.49
26	0.72	0.52	0.73	0.54	0.69	0.48	0.71	0.50
28	0.73	0.53	0.74	0.54	0.70	0.50	0.71	0.51
30	0.74	0.54	0.74	0.54	0.71	0.50	0.71	0.51
32	0.74	0.55	0.73	0.53	0.71	0.51	0.71	0.50
34	0.74	0.55	0.73	0.52	0.72	0.51	0.71	0.49
36	0.74	0.55	0.72	0.51	0.72	0.51	0.70	0.48
38	0.74	0.55	0.72	0.49	0.72	0.51	0.69	0.46
40	0.74	0.54	0.71	0.47	0.71	0.51	0.69	0.45

TABLE 2 - Δ_2 and Δ_3 for Random HDB3 Code and Gaussian Pulse

	ε=200				ε=330			
	x=0.5		x=0.6		x=0.5		x=0.6	
Δ_o	Δ_2	Δ_3	Δ_2	Δ_3	Δ_2	Δ_3	Δ_2	Δ_3
14	0.66	0.43	0.66	0.43	0.64	0.40	0.64	0.40
16	0.66	0.43	0.66	0.43	0.64	0.40	0.64	0.40
18	0.66	0.43	0.66	0.43	0.64	0.40	0.64	0.40
20	0.66	0.43	0.66	0.43	0.64	0.40	0.64	0.41
22	0.67	0.43	0.67	0.44	0.64	0.41	0.64	0.41
24	0.67	0.44	0.66	0.44	0.64	0.41	0.64	0.41
26	0.67	0.44	0.66	0.44	0.64	0.41	0.64	0.40
28	0.67	0.44	0.66	0.43	0.64	0.41	0.63	0.40
30	0.67	0.44	0.66	0.43	0.64	0.41	0.63	0.40
32	0.67	0.44	0.65	0.43	0.64	0.41	0.63	0.40
34	0.66	0.44	0.65	0.42	0.64	0.40	0.62	0.39
36	0.66	0.43	0.64	0.41	0.63	0.40	0.62	0.39
38	0.66	0.43	0.64	0.40	0.63	0.40	0.61	0.38
40	0.65	0.43	0.63	0.40	0.63	0.40	0.61	0.38

TABLE 3 - Δ_2 and Δ_3 for Idle HDB3 Code and 100% Cosine Roll-Off Pulse

	ε=200				ε=330			
	x=0.5		x=0.6		x=0.5		x=0.6	
Δ_o	Δ_2	Δ_3	Δ_2	Δ_3	Δ_2	Δ_3	Δ_2	Δ_3
14	0.65	0.41	0.65	0.41	0.62	0.39	0.63	0.39
16	0.65	0.41	0.65	0.42	0.63	0.39	0.63	0.40
18	0.65	0.42	0.66	0.43	0.63	0.40	0.64	0.41
20	0.66	0.43	0.67	0.45	0.64	0.40	0.65	0.42
22	0.67	0.44	0.69	0.47	0.65	0.41	0.66	0.44
24	0.68	0.45	0.70	0.49	0.65	0.43	0.68	0.46
26	0.69	0.47	0.72	0.51	0.67	0.44	0.69	0.48
28	0.70	0.49	0.74	0.54	0.68	0.46	0.71	0.50
30	0.71	0.51	0.75	0.56	0.69	0.47	0.72	0.52
32	0.73	0.53	0.77	0.59	0.70	0.49	0.74	0.54
34	0.74	0.55	0.78	0.61	0.71	0.51	0.75	0.57
36	0.75	0.57	0.79	0.63	0.72	0.52	0.76	0.58
38	0.76	0.59	0.80	0.65	0.73	0.54	0.77	0.60
40	0.78	0.60	0.82	0.67	0.74	0.56	0.78	0.62

TABLE 4 - Δ_2 and Δ_3 for Random HDB3 Code and 100% Cosine Roll-Off Pulse

	ε=200				ε=330			
	x=0.5		x=0.6		x=0.5		x=0.6	
Δ_o	Δ_2	Δ_3	Δ_2	Δ_3	Δ_2	Δ_3	Δ_2	Δ_3
14	0.68	0.45	0.68	0.45	0.65	0.41	0.65	0.41
16	0.68	0.45	0.68	0.45	0.65	0.41	0.65	0.41
18	0.68	0.45	0.68	0.45	0.65	0.41	0.65	0.42
20	0.68	0.45	0.69	0.46	0.65	0.42	0.65	0.42
22	0.69	0.46	0.69	0.46	0.65	0.42	0.66	0.42
24	0.69	0.46	0.69	0.46	0.66	0.42	0.66	0.43
26	0.69	0.46	0.69	0.47	0.66	0.42	0.66	0.43
28	0.69	0.46	0.70	0.47	0.66	0.43	0.66	0.43
30	0.69	0.47	0.70	0.47	0.66	0.43	0.67	0.43
32	0.70	0.47	0.70	0.48	0.66	0.43	0.67	0.44
34	0.70	0.47	0.71	0.48	0.67	0.43	0.67	0.44
36	0.70	0.48	0.71	0.49	0.67	0.43	0.68	0.44
38	0.70	0.48	0.71	0.49	0.67	0.44	0.68	0.45
40	0.71	0.48	0.72	0.49	0.67	0.44	0.68	0.45

5. Usher, E.S., Catchpole, R.J. and Beasley, M., "Analysis of Cable Crosstalk Data for Maximizing PCM System Application", 1978 Zurich International Symposium on Digital Communication, March 1978, pp.C3.1-C3.7.

6. Gibbs, A.J., "The Covariance of Near End Crosstalk and its Application to PCM System Engineering in Multipair Cable", IEEE Trans. on Comm., to be published.

7. Parzen, E., "Stochastic Processes", San Francisco, Holden-Day, 1962, p.58.

8. ibid., p.95.

BIOGRAPHY

ALAN J. GIBBS was born in Townsville, Queensland, and graduated from the University of Melbourne with a Bachelor of Engineering degree with honours in 1961.

Following graduation he joined the A.P.O. Research Laboratories, where he worked on the design of electrical networks with special emphasis on the use of digital computers. In 1966 he obtained the Degree of Master of Engineering for work in this area.

In 1967-1968 he studied at the University of Wisconsin, U.S.A., on a Public Service Board Scholarship, where he obtained the Degree of Doctor of Philosophy for work on digital signal processing. Since returning to the Research Laboratories, Dr. Gibbs has worked as Divisional Engineer of the Multichannel Systems Section, and currently is Head, Line and Data Systems Section, Transmission Systems Branch.

APPENDIX I

First some notation and basic relationships. The i-th central moment is denoted by $\mu_i(.)$ and the first three of these are equal to the first three cumulants κ_i, respectively. Subscripted variables denote the variable evaluated at the frequency f_i or $F_i = f_i/f_o$, as appropriate, e.g., $X_i = X(f_i)$. The i-th joint central moment is denoted by $J_i(.,.,...,.)$, and thus for

$$v^2 = \int_o^\infty |X(f)|^2 P(f)df \qquad (I.1)$$

$$\kappa_3 = \mu_3(v^2)$$

$$= \iiint_o^\infty J_3(|X_1|^2,|X_2|^2,|X_3|^2)P_1P_2P_3df_1df_2df_3 \qquad (I.2)$$

$$J_3(|X_1|^2,|X_2|^2,|X_3|^2)$$

$$= E(|X_1|^2|X_2|^2|X_3|^2) - E(|X_1|^2)E(|X_2|^2|X_3|^2)$$

$$- E(|X_2|^2)E(|X_3|^2|X_1|^2) - E(|X_3|^2)E(|X_1|^2|X_2|^2)$$

$$+ 2E(|X_1|^2)E(|X_2|^2)E(|X_3|^2) \qquad (I.3)$$

Finally, for variates X, Y, Z and conditional expectations on a specified value of a variate k, (Ref.7)

$$J_3(X,Y,Z) = E(J_3(X,Y,Z|k))$$

$$+ J_3(E(X|k),E(Y|k),E(Z|k)) \qquad (I.4)$$

From equation (3) we have

$$X(f) = j2\pi f\int_o^\infty C(x)e^{-2\gamma x}dx$$

where for a specified pair combination C(x) is a zero mean normal process with covariance $E(C(x)C(y)) = k_1\delta(x-y)$, and thus

$$\frac{E(|X_1|^2|X_2|^2|X_3|^2|k_1)}{64\pi^6 f_1^2 f_2^2 f_3^2}$$

$$= \iiiiint_o^\infty E(C(s)C(t)C(u)C(x)C(y)C(z)|k)\cdot\exp(-2\gamma_1 s$$

$$-2\gamma_1^* t-2\gamma_2 u-2\gamma_2^* x-2\gamma_3 y-2\gamma_3^* z)dsdtdudxdydz$$

where $\gamma_i = \alpha_i+j\beta_i$.

The expectation of the product of six zero mean normal variates is the sum of 15 terms, each term being the product of three covariances of three pairs of the six variates (Ref.8). Thus

$$\frac{E(|X_1|^2|X_2|^2|X_3|^2|k_1)}{\pi^6 f_1^2 f_2^2 f_3^2 k_1^3} = \frac{1}{\alpha_1\alpha_2\alpha_3}$$

$$+ \frac{4}{\alpha_1|\gamma_2+\gamma_3|^2} + \frac{4}{\alpha_1|\gamma_2+\gamma_3^*|^2}$$

$$+ \frac{4}{\alpha_2|\gamma_1+\gamma_3|^2} + \frac{4}{\alpha_2|\gamma_1+\gamma_3^*|^2}$$

$$+ \frac{4}{\alpha_3|\gamma_1+\gamma_2|^2} + \frac{4}{\alpha_3|\gamma_1+\gamma_2^*|^2}$$

$$+ \{\frac{8}{(\gamma_1+\gamma_2)(\gamma_1^*+\gamma_3)(\gamma_2^*+\gamma_3^*)}$$

$$+ \frac{8}{(\gamma_1^*+\gamma_2^*)(\gamma_1+\gamma_3^*)(\gamma_2+\gamma_3)}$$

$$+ \frac{8}{(\gamma_1^*+\gamma_2^*)(\gamma_1+\gamma_3)(\gamma_2+\gamma_3^*)}$$

$$+\frac{8}{(\gamma_1+\gamma_2)(\gamma_1^*+\gamma_3^*)(\gamma_2^*+\gamma_3)}$$

$$+\frac{8}{(\gamma_1^*+\gamma_2)(\gamma_1+\gamma_3)(\gamma_2^*+\gamma_3^*)}$$

$$+\frac{8}{(\gamma_1+\gamma_2^*)(\gamma_1^*+\gamma_3^*)(\gamma_2+\gamma_3)}$$

$$+\frac{8}{(\gamma_1+\gamma_2^*)(\gamma_1^*+\gamma_3)(\gamma_2+\gamma_3^*)}$$

$$+\frac{8}{(\gamma_1^*+\gamma_2)(\gamma_1+\gamma_3^*)(\gamma_2^*+\gamma_3)}\} \qquad (1.5)$$

From (Ref.6) we have

$$E(|X|^2|k_1) = \frac{\pi^2 f^2 k_1}{\alpha} \qquad (1.6)$$

$$E(|X_1|^2|X_2|^2|k_1) =$$

$$\pi^4 f_1^2 f_2^2 k_1^2\{\frac{1}{\alpha_1\alpha_2} + \frac{4}{|\gamma_1+\gamma_2|^2} + \frac{4}{|\gamma_1+\gamma_2^*|^2}\}$$

and using equation (1.3) we have

$$J_3(|X_1|^2,|X_2|^2,|X_3|^2|k_1) =$$

{last 8 terms of equation (1.5)}

Making approximations similar to those in (Refs.1,6), which hold over the frequency range 100kHz to 10 MHz, only the last two terms are significant, and using

$$\gamma_i = \alpha_o F_i^{\times} + j2\pi f_o T F_i \quad ; \quad k = \pi^2 f_o^2 k_1/\alpha_o \quad ;$$

$$\varepsilon = (2\pi f_o T/\alpha_o)^2$$

we have

$$J_3(|X_1|^2,|X_2|^2,|X_3|^2|k) = k^3 W(F_1,F_2,F_3)$$

$$= \frac{16F_1^2F_2^2F_3^2k^3\{(F_1^{\times}+F_2^{\times})(F_2^{\times}+F_3^{\times})(F_3^{\times}+F_1^{\times})}{\{(F_1^{\times}+F_2^{\times})^2+\varepsilon(F_1-F_2)^2\}\{(F_2^{\times}+F_3^{\times})^2+\varepsilon(F_2-F_3)^2\}}$$

$$\frac{+\varepsilon[F_1^{\times}(F_2-F_3)^2+F_2^{\times}(F_1-F_3)^2+F_3^{\times}(F_1-F_2)^2]\}}{\{(F_3^{\times}+F_1^{\times})^2+\varepsilon(F_3-F_1)^2\}} \qquad (1.7)$$

together with, from (Ref.6),

$$J_2(|X_1|^2,|X_2|^2|k)$$

$$= k^2V(F_1,F_2) = \frac{4k^2F_1^2F_2^2}{(F_1^{\times}+F_2^{\times})^2+\varepsilon(F_1-F_2)^2} \qquad (1.8)$$

$$E(|X|^2|k) = kF^{2-x} \qquad (1.9)$$

These approximations are consistent with those in (Ref.1) where it is shown that for a specified pair combination, i.e., for specified k_1 or k, $|X(f)|^2$ is (approximately) exponentially distributed. Thus we should have:

$$E(|X|^2|k) = kF^{2-x} \quad ; \quad \mu_2(|X|^2|k) = k^2F^{2(2-x)} \quad ;$$

$$\mu_3(|X|^2|k) = 2k^3F^{3(2-x)} \quad ;$$

which are consistent with equations (1.9), (1.8) and (1.7), viz.,

$$\mu_2(|X|^2|k)=k^2V(F,F) \text{ and } \mu_3(|X|^2|k)=k^3W(F,F,F).$$

Turning to equations (1.4), (1.7) and (1.9) we have

$$J_3(|X_1|^2,|X_2|^2,|X_3|^2) =$$

$$E(k^3)W(F_1,F_2,F_3)+\mu_3(k)F_1^{2-x}F_2^{2-x}F_3^{2-x} \qquad (1.10)$$

and for completeness, from (Ref.6)

$$J_2(|X_1|^2,|X_2|^2) = E(k^2)V(F_1,F_2)+\mu_2(k)F_1^{2-x}F_2^{2-x} \qquad (I.11)$$

$$E(|X|^2) = E(k)F^{2-x} \qquad (I.12)$$

Finally, using equation (I.2) and (Ref.6) we have

$$\kappa_1 = E(k)I_m \qquad (I.13)$$

$$\kappa_2 = E(k^2)I_v + \mu_2(k)I_m^2 \qquad (I.14)$$

$$\kappa_3 = E(k^3)I_w + \mu_3(k)I_m^3 \qquad (I.15)$$

$$I_m = \int_0^\infty F^{2-x}P(f)df \quad ;$$

$$I_v = \iint_0^\infty V(F_1,F_2)P_1P_2df_1df_2 \quad ;$$

$$I_w = \iiint_0^\infty W(F_1,F_2,F_3)P_1P_2P_3df_1df_2df_3 \qquad (I.16)$$

APPENDIX II

NEXT loss in dB in multipair cable over the frequency range 100kHz to 10MHz has a mean which varies with frequency at approximately 15dB/decade and an approximately constant variance. Thus we assume that

$$E(-10\log|X(f)|^2) = E(L(f)) = \mu_o-10(2-x)\log F$$

where x is the cable pair loss exponent, μ_o is the mean NEXT loss at f_o, and

$$\mu_2(L(f)) = \sigma_o^2 .$$

Assuming that NEXT loss has a truncated normal distribution, with truncation factor c, we have (Ref.5)

$$E(|X|^2) = T(c,\sigma_o)10^{0.1(0.115\sigma_o^2-\mu_o)}F^{2-x} = K_1F^{2-x} \qquad (II.1)$$

$$\mu_2(|X|^2) = K_1^2(U_2(c,\sigma_o)10^{0.023\sigma_o^2}-1)F^{2(2-x)} \qquad (II.2)$$

$$\mu_3(|X|^2) = K_1^3(U_3(c,\sigma_o)10^{0.069\sigma_o^2} -3U_2(c,\sigma_o)10^{0.023\sigma_o^2}+2)F^{3(2-x)} \qquad (II.3)$$

where

$$T(c,\sigma) = \frac{\Phi(c-\lambda\sigma) - \Phi(-c-\lambda\sigma)}{\Phi(c) - \Phi(-c)} \quad ; \quad \lambda = (10\log e)^{-1}$$

$$\Phi(x) = \frac{1}{\sqrt{2\pi}}\int_{-\infty}^{x}\exp(-t^2/2)dt$$

$$U_n(c,\sigma) = \frac{T(c,n\sigma)}{T^n(c,\sigma)}$$

Turning now to equations (I.12), (I.11) and (I.10), with $F_1 = F_2 = F_3 = F$ we have

$$E(|X|^2) = E(k)F^{2-x}$$

$$\mu_2(|X|^2) = (2E(k^2) - E^2(k))F^{2(2-x)}$$

$$\mu_3(|X|^2) = (3E(k^3) - 3E(k)E(k^2) + 2E^3(k))F^{3(2-x)}$$

Equating these with equations (II.1), (II.2) and (II.3) we have

$$E(k) = K_1$$

$$E(k^2) = \frac{T(c,2\sigma_o)}{2} 10^{0.2(0.23\sigma_o^2-\mu_o)}$$

$$\mu(k^2) = K_1^2\left(\frac{U_2(c,\sigma_o)}{2} 10^{0.023\sigma_o^2} - 1\right)$$

$$E(k^3) = K_1^3\left(\frac{U_3(c,\sigma_o)}{3} 10^{0.069\sigma_o^2}\right.$$

$$\left. - \frac{U_2(c,\sigma_o)}{2} 10^{0.023\sigma_o^2}\right)$$

$$\mu_3(k) = K_1^3\left(\frac{U_3(c,\sigma_o)}{3} 10^{0.069\sigma_o^2}\right.$$

$$\left. - 2U_2(c,\sigma_o) 10^{0.023\sigma_o^2} + 2\right)$$

Substituting these into equations (I.13), (I.14) and (I.15) we have

$$\kappa_1 = T(c,\sigma_o) 10^{0.1(0.115\sigma_o^2-\mu_o)} I_m$$

$$\kappa_2 = \kappa_1^2(\Delta_2 U_2(c,\sigma_o) 10^{0.023\sigma_o^2} - 1)$$

$$\kappa_3 = \kappa_1^3(\Delta_3 U_3(c,\sigma_o) 10^{0.069\sigma_o^2}$$

$$\left. - \frac{3(1+\Delta_3)}{2} U_2(c,\sigma_o) 10^{0.023\sigma_o^2} + 2\right)$$

where

$$\Delta_2 = \frac{1}{2}\left(1 + \frac{I_v}{I_m^2}\right) \quad ; \quad \Delta_3 = \frac{1}{3}\left(1 + \frac{I_w}{I_m^3}\right)$$

Errata ATR Vol. 12 Number 1

The following errors appeared in the paper Suppression of Limit Cycle Oscillations by P. Rashidi and R.E. Bogner. Fig. 1 Extreme top: U_n should be u_n

Fig. 4 In all five lables of the lines, the symbol A should have been a.

Fig. 5 Horizontal axis: S should be s.

ATR AUSTRALIAN TELECOMMUNICATION RESEARCH

ISSN 0001-2777

VOLUME 12, NUMBER 2,
1978

Contents*

*Abbreviated Titles